# Genome engineering to expand applications of human T-cell immunotherapy

Alexandra E. Grier

A dissertation

submitted in partial fulfillment of the

requirements for the degree of

Doctor of Philosophy

University of Washington

2017

Reading Committee:

Andrew M. Scharenberg, Chair

Michael C. Jensen

Philip D. Greenberg

Program Authorized to Offer Degree:

Immunology

University of Washington

**Abstract**

Genome engineering to expand applications of human T-cell immunotherapy

Alexandra E. Grier

Chair of the Supervisory Committee:
Andrew M. Scharenberg, MD
Departments of Pediatrics and Immunology

Adoptive T-cell therapy, particularly chimeric antigen receptor (CAR) therapy, is a revolutionary and quickly-evolving means of treating cancer patients who can no longer be helped by standard therapies. In multiple clinical trials, including our own at Seattle Children's Hospital, αCD19 CAR therapy for B-cell leukemia and lymphoma has achieved a complete remission rate of >90%. Unfortunately, in its present form, CAR therapy has had limited success against solid tumors. It is also not currently an option for patients who lack sufficient numbers of their own T-cells due to their disease or prior treatments. Thus, genome engineering strategies to overcome these limitations could be of great benefit to patients. We chose a two-pronged approach to achieve this goal: knock-out of the endogenous TCR and multiplex knock-out of the T-cell inhibitory checkpoints PD-1, Tim3, Lag3, and TIGIT. Knocking out these inhibitory checkpoint proteins specifically in the CAR T-cells will maintain the synergistic effects

recently seen in combination monoclonal antibody therapy without the serious, sometimes fatal, immune-mediated side effects seen with systemic antibody therapy.

To this end, we first developed a linear mRNA expression vector with a long, encoded poly(A) tail to allow transient delivery of nucleases such as TALENs or CRISPR to primary human cells in a consistent, clinically applicable, and scalable fashion. We then used IVT mRNA made from this vector to deliver a TALEN pair targeting the TCR$\alpha$ locus to $\alpha$CD19 CAR T-cells, and demonstrated that removal of the endogenous TCR does not hinder CAR T-cell function *in vitro* or *in vivo* in a murine xenograft tumor model. Knockout of the endogenous TCR will facilitate production of an allogeneic CAR T-cell product to be used as a bridge to HSCT in patients who cannot receive autologous CAR therapy. Removal of the endogenous TCR will also add a measure of safety when creating CAR T-cells lacking inhibitory checkpoint proteins by preventing GvHD while retaining anti-tumor effects. These technologies and methods may allow a wider variety of patients to benefit from the recent advances in CAR T-cell therapy.

**Acknowledgements**

I would first like to thank my mentors Andy Scharenberg and Mike Jensen, who have been amazingly supportive, patient, energetic, and enthusiastic mentors with a never-ending well of optimism. They have an uncanny sense of when to challenge me and when to let me figure things out on my own, all while maintaining unwavering belief in my abilities. They have taught me how to think like a scientist, communicate, and take risks in my work.

They have each brought together a group of exceptionally bright, caring, and motivated lab members who have taught me so much. I owe special thanks to several members of each lab. Lisa, Adam, and Cindy are sources of endless knowledge, mentorship, enthusiasm, and seamless teamwork. Kamila provided support, encouragement, advice, mentorship, and a spirit of adventure both in and out of the lab throughout these years. Kyle taught me how to think through problems, design experiments, streamline my work, challenge myself, and most importantly willingly joined me in the depths of pEVL voodoo and led me out alive. Ryan and Tyler turned the lab into a fun and lively environment while working hard, lending a helping hand, and making sure that I didn't take myself or life too seriously. Sarah and Abbie brought me into the lab and introduced me to the world of genome engineering with encouragement, insight, and enthusiasm, and never hesitated to answer my endless stream of questions. Jaya was always willing to assist me with any problem that came up and provided company during many late nights in the lab. Mei is one of the most helpful, caring, and selfless people I have ever met. Finally, the rest of the Rawlenberg and Jensen labs have been invaluable sources of advice, camaraderie, support, and fun.

My thesis committee members Paul Nghiem, Marion Pepper, and Phil Greenberg have provided helpful insight and guidance throughout my time in the lab as well as the benefit of their wisdom and experience as I shape my own career. I am also thankful to the MSTP directors and administration, especially Marcie Buckner, Maureen Holstad, and Mary Claire King for their advice, guidance, dedication, and enthusiasm. The Barbo family have provided important financial support and a sense of family through the ARCS Fellowship. Mark Pellegrino, Marsha Altschuler, and Lois Banta sparked my love of science, genetics, and teaching many years ago and started me down the path to where I am today. I am also incredibly grateful to my MSTP, graduate school, and medical school colleagues. I can't imagine surviving the past eight years without them.

And finally, I would especially like to thank my family: my parents, Phil and Ella, and my brother and sister-in-law Andrew and Robyn, as well as my extended family in the US and Russia. They spared no time, effort, or love to encourage me in scholarly, musical, or athletic pursuits. They allowed me to dream big, go for my goals, and helped me back up when I fell short, no matter how busy they were or how many miles were between us. Andrew and Robyn paved the way and guided me through the ups and downs of graduate school by demonstrating the perseverance, curiosity, work ethic, and resilience needed to emerge mostly intact. I want to thank my family from the bottom of my heart for their unending love, guidance, hard work, and passion throughout my life.

# 1. Introduction

## 1.1 Immunotherapy: harnessing the immune system to fight disease

Over the past forty years, the development of chemotherapy, radiation therapy, and stem cell transplants have transformed cancer from a uniformly fatal diagnosis to one that may be successfully treated in many patients. Unfortunately, some patients do not respond to these therapies, and while others respond initially, they later relapse. Until recently, there were no other options for these patients. However, over the past two decades, the understanding of anti-tumor mechanisms of the immune system has advanced to the point that the immune system is now increasingly harnessed as a weapon to combat cancer, leading to the rise of a new field of oncology: immuno-oncology. Although the idea of cancer immunotherapy dates back to William Coley's work in the late 19$^{th}$ century, and modern efforts in the field can be traced back as far as 40 years, it is only in the past few years that high response rates have been achieved in multiple types of cancer.[1–6]

## 1.2 CAR T-cell immunotherapy: a revolution in hematologic tumor therapy

Some of the most exciting results in immunotherapy have come from the recent trials of **c**himeric **a**ntigen **r**eceptor T-cells (CAR T-cells). In CAR T-cell therapy, immune cells are isolated from a patient and reprogrammed *in vitro* via genome engineering to target tumor cells. They are then infused into the patient, thus activating the body's anti-tumor activity against cancerous cells that have mutated to avoid it.

The initial highly successful use of CAR T-cell therapy has been against leukemias and lymphomas from the B-cell lineage.[7–9] These cancers possess several properties that make

them relatively straight-forward to treat with CAR T-cell therapy. First, because they are found in the blood and lymph nodes where T-cells naturally reside, they are accessible via simple intravenous infusion and do not require any special trafficking of the CAR T-cells. Second, patients can survive (at least in the short term) without B-cells,[8] which allows the targeting of all B-cells rather than trying to differentiate cancerous B-cells from their healthy counterparts. Third, since interactions with B-cells naturally help T-cells survive and function, CAR T-cells that are attacking B-cells are supported by this interaction.

CAR T-cell therapy used to treat B-cell leukemias and lymphomas are directed against CD19 (and more recently CD22), which are expressed at high levels on B-cells and B-cell-derived tumors. The CAR itself is composed of a recognition domain, derived from the $V_H$ and $V_L$ sequences of a monoclonal antibody specific for CD19,[10] fused to a transmembrane domain, the CD3ζ signaling domain, and at least one costimulatory signaling domain, typically CD28 or 4-1BB (**Figure 1.1a and c**).[7,11–14] This creates a population of cells specifically targeting CD19, with the normal activation pathway in T-cells enhanced for increased activity. The CAR is introduced into T-cells via lentiviral transduction (**Figure 1.1c**) and the modified T-cells are expanded *ex vivo* before being infused into the patient, often after lymphodepletion (**Figure 1.1b**). The development of CD19 CAR T-cell therapies has illuminated multiple elements of CAR T-cell design that must be optimized for each target antigen, which will be extremely helpful in developing CAR T-cell therapy against additional types of tumors.[11,12,15,16]

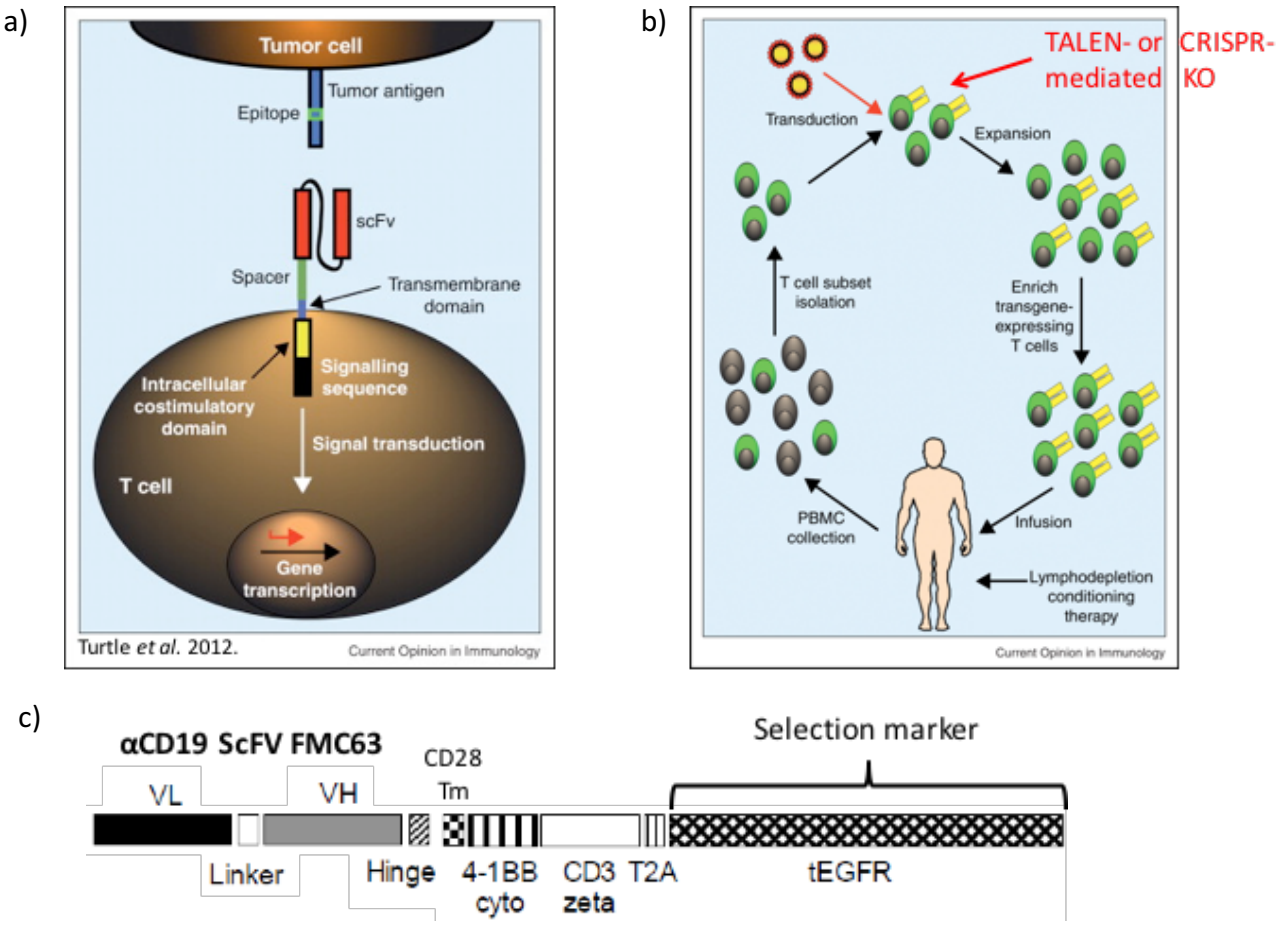


Turtle et al. 2012.

**Figure 1.1. Schematics of CAR therapy. a)** A T-cell with a CAR expressed on its surface interacting with the target antigen on a tumor cell. Recognition of the target antigen by the CAR induces activation of the T-cell to kill the tumor cell. **b)** Standard procedure for production of and treatment with an autologous CAR T-cell product. Additional gene editing can be done at the time of lentiviral transduction of the CAR construct via TALENs or CRISPR/Cas9. **c)** Construct encoding the CD19 second generation CAR used in these studies. The selection marker EGFRt is a truncated EGF receptor which lacks the intracellular signaling domain but retains binding capacity for the FDA-approved mAb cetuximab and can therefore be used as an expression, selection, or suicide marker.

The earliest attempts using CAR T-cells clinically (with the CD3ζ chain as the only signaling moiety) demonstrated that short-term persistence and limited expansion were possible. Further iterations achieved long-term persistence of CAR T-cells in patients, but did not eradicate tumors in most patients.[3,17] Since then, with advancements in the design of CARs,

the inclusion of co-stimulatory domains, and improvements in clinical protocols, the complete response rate for otherwise untreatable B-cell leukemia has begun to approach 90%.[2] The complete response rate in lymphomas is lower but still impressive at ~40%, depending on the subtype of lymphoma and the details of the treatment regimen.[18]

### 1.3 Challenges in extending CAR T-cell technology to solid tumors

Given the impressive remission rates achieved in hematopoietic cancers, there is considerable interest in expanding this technology to treat solid tumors. However, there are significant challenges to applying CAR T-cell therapy to solid tumors, including difficulty trafficking the cells into solid tumors, the lack of specificity of tumor-associated antigens, and the survival and sustained activity of the CAR T-cells in the immunosuppressive tumor microenvironment.[19,20] As discussed above and in contrast to solid tumors**,** CD19 CAR T-cells benefit from several features of their B-cell targets that other CAR T-cells will not: B-cells express multiple T-cell co-stimulatory molecules, can be depleted in patients via CD19 with limited off-tissue effects, and patients can be maintained with IVIG therapy when healthy B-cells are depleted.[21] In addition, B-cell derived leukemias and lymphomas generally lack the immunosuppressive microenvironment that is present in solid tumors, and which is thought to be an important barrier to any type of immunotherapeutic approach to treating these tumors.

Most solid tumors develop an immunosuppressive microenvironment which acts to inhibit the anti-cancer immune response. Nonspecific factors such as hypoxia, acidity, low levels of glucose and other nutrients, and high levels of lactate and other waste products make solid tumors hostile environments for T-cell survival and function.[22–26] Regulatory/anti-

inflammatory adaptations and mutations are present, including Tregs, myeloid-derived suppressor cells, and suppressive cytokines such as IL-10 and TGFβ. These specific immunomodulatory factors quell activated T-cells and dampen the immune response.[22,23] Solid tumors have also been shown to create barriers to T-cell trafficking, such as FasL expression in the tumor vasculature.[19] Finally, many tumor cells express ligands that interact with inhibitory receptors on T-cells, such as PD-1, Tim3, TIGIT, and Lag3.[24–28]

Therefore, it may be necessary to manipulate many of these barriers for CAR T-cell therapy to be successful against solid tumors. A compelling clue for a place to start comes from recent clinical trials of monoclonal antibodies (mAbs) targeting T-cell inhibitory checkpoints. In these trials, treatment of non-small cell lung carcinoma (NSCLC), renal cell carcinoma (RCC), and metastatic melanoma patients with PD-1- or PD-L1-blocking mAbs increased survival and led to durable responses in a subset of patients.[29–32] For instance, survival rates in metastatic melanoma have doubled from 16% with traditional treatment modalities to 34%, a tremendous increase in a cancer previously considered nearly incurable.[29] Additional clinical trials are underway with anti-Tim3 and anti-Lag3 mAbs.

Importantly, combinations of checkpoint inhibitors seem to act synergistically to increase overall efficacy: in a trial combining a PD-1 blocking mAb with a CTLA-4 blocking mAb in melanoma, the combination led to an improved 58% response rate, compared to 44% and 19% for the individual mAbs.[33] Unfortunately, these combination mAb treatments also have synergistic toxicities. In the αPD-1 and αCTLA-4 melanoma trial, grade 3 or 4 treatment-related adverse events, such as hepatotoxicity and colitis, occurred in 55% of patients receiving the combination treatment, but only 16% and 27% of patients receiving the individual

treatments.[33,34] This will make it essential to develop targeted rather than systemic delivery systems for combination checkpoint blockade in the treatment of solid tumors. It is also becoming clear that a patient's response to immune checkpoint blockade correlates to the mutational burden of that patient's tumors (i.e. the number of T-cell neoantigens present), which will improve identification of patients that may benefit from checkpoint blockade.[35]

The impressive success of the first checkpoint blockade trials has driven a burst in the number of checkpoint blockade targets being studied. A large percentage of these, including CTLA-4, PD-1, Tim3, Lag3, TIGIT, and BTLA, are members of the immunoglobulin super family (IgSF) and contain immunoreceptor tyrosine-inhibitory motifs (ITIMs) and/or immunoreceptor tyrosine switch motifs (ITSMs) that can recruit phosphatases such as SHP-1 and SHP-2 to dampen signaling downstream of the immune synapse.

**1.3.i PD-1**

PD-1 is part of the immunoglobulin superfamily (IgSF), and is an important mediator of immune tolerance. It contains both ITIM and ITSM domains in its cytoplasmic tail. PD-1 is not expressed on naïve T-cells, and its expression on T-cells is upregulated by antigenic signaling as well as exposure to many cytokines of the interleukin-2 common gamma chain (IL-2$\gamma$C) family.[36] PD-1 has two ligands: PD-L1 and PD-L2. PD-L1 is constitutively expressed on many hematopoietic and tumor cells at low levels, and is upregulated in the presence of IFN$\gamma$ and activation of the PI3K or MAPK signaling pathways.[37–39] In contrast, PD-L2 is only expressed on macrophages, dendritic cells,[40] and some solid tumor cells. After PD-1/ligand binding, the intracellular tail of PD-1 becomes phosphorylated, allowing binding of SHP-1 and/or SHP-2 to

the ITSM domain, thereby inhibiting signaling downstream of the immune synapse, especially PI3K/AKT activation.[41]

PD-1 is essential for peripheral tolerance and is expressed by exhausted T-cells.[42] The importance of PD-1 in regulating the immune response is evident in murine models, as mice that lack PD-1 develop multiple types of autoimmunity. However, in cancer murine models, blockade of the PD-1 pathway in mice leads to lymphocyte expansion and reduction in tumor growth.[43,44] Interaction of PD-1 with its ligands in the solid tumor microenvironment suppress the immune response through T-cell anergy, exhaustion, and apoptosis.[43,45] Based on these results in mouse models, clinical trials blocking the PD-1 axis with mAbs were started in humans afflicted with a variety of solid cancers, including melanoma, NSCLC, RCC, head and neck squamous cell carcinoma, and urothelial carcinoma,[46] as well as non-Hodgkin's lymphoma. So far, two PD-1-blocking mAbs have gained FDA approval, nivolumab and pembrolizumab. In addition, atezolizumab, avelumab, and durvalumab, which all target PD-L1, have also recently been approved. Multiple others are still in clinical trials.

The first FDA approvals for PD-1 inhibitors were in metastatic melanoma, an aggressive and deadly disease with a 16% five-year-survival rate and a median survival of 5 months using conventional therapy.[30] In a phase III trial of patients with metastatic melanoma who were no longer responding to conventional therapy, nivolumab had a 40% response rate with a 73% one-year survival rate.[30] In a different trial of nivolumab, the five-year survival was 34%, with a median survival of 17 months.[29] In a trial using pembrolizumab, the overall survival rate after three years was 40%, and the median overall survival was 24 months.[48]

In patients with recurrent NSCLC without EGFR or ALK mutations, pembrolizumab was approved as a first-line treatment, but only for patients whose tumors cells are more than 50% PD-L1+. Patients in this group had a 45% response rate and a median overall survival of ~16 months.[47] Nivolumab gained approval as a second-line treatment, but was approved regardless of the patient's PD-L1 status. Nivolumab had a higher response rate at ~20% (compared with standard treatment at ~10%), and increased overall survival by 3 months.[50] Pembrolizumab recently also gained FDA approval for head and neck squamous cell carcinoma. The breadth/wide variety of cancers now being treated with these mAbs suggests that the PD-1/PD-L1 axis may be an important immune resistance mechanism in even more types of solid tumors not yet tested.

However, the variation in response rate, durability, and importance of PD-L1 status with the different PD-1 mAbs suggests that there is still much we don't understand about blockade of this pathway. Though both pembrolizumab and nivolumab are both humanized IgG4 mAbs that block the binding of PD-1 to PD-L1 and PD-L2, they have distinct binding sites on PD-1.[48,49] It is not known if this difference in their binding sites is responsible for their variable responses, but using a genetic knock-out rather than antibody blocking may nullify these differences.

Excitingly, there is also evidence that PD-1 blockade may be successful as an adjuvant to CAR immunotherapy. A recent case report detailed a patient with diffuse large B-cell lymphoma whose tumors were still growing after CD19 CAR T-cell therapy. Pembrolizumab was added to the CAR T-cell therapy, and resulted in tumor regression, CAR T-cell expansion, and decreased expression of PD-1 and Eomes by the CAR T-cells.[50]

### 1.3.ii TIGIT

TIGIT (T-cell immunoglobulin and immunoreceptor tyrosine-based inhibitory motif) is another co-inhibitory molecule that is part of the IgSF, and contains two ITIM domains in its cytoplasmic tail. It is expressed on activated CD4 and CD8 effector T-cells, as well as activated Tregs and memory T cells.[51–54] TIGIT binds to the Ig-like molecules CD155 (PVR) and CD112 expressed on APCs or tumor cells with high affinity,[54] outcompeting the activating molecules CD226 and CD96 for binding to CD155, and thereby blocking T-cell co-activation. TIGIT also plays a cell-intrinsic role in dampening T-cell activation, as evidenced by T-cell inhibition in culture with agonistic TIGIT antibodies but no other cells.[52,55] In both the cell-extrinsic and -intrinsic pathways, the engagement of TIGIT by ligands or monoclonal antibodies inhibits T-cell proliferation and pro-inflammatory cytokine production.[54,55]

TIGIT's expression is associated with the expression of PD1 and Tim3 on CD4+ T cells in murine tumor models,[56,57] and was also found to be co-expressed with PD1 and CTLA4 on CD8 tumor infiltrating lymphocytes (TILs) in the solid tumors of patients with lung and kidney carcinomas.[57] Promisingly, blocking monoclonal antibodies against both TIGIT and PD1, but not against either one in isolation, were necessary for tumor rejection and long-term protection against relapse in two syngeneic mouse tumor models.[57]

### 1.3.iii Lag3

Another co-inhibitory member of the IgSF found on T-cells is Lag3 (lymphocyte activation gene 3). Lag3 plays a role in negatively regulating cellular proliferation, activation, and homeostasis of T cells.[58] It is similar in structure and sequence to CD4 in both mice and

humans, and is expressed on activated T-cells and NK cells. Its canonical ligand is MHC class II, though more recent evidence also suggests that it binds to Gal3.[59] Upon ligation, Lag3 associates with the TCR/CD3 complex and inhibits the downstream calcium response. It is known that the T-cell homeostatic functions of Lag3 are dependent on a conserved KIEELE motif in its cytoplasmic tail, but the exact mechanisms by which Lag3 functions have not been completely elucidated.

Though Lag3 has been shown to help maintain CD8 T cells in a tolerogenic state,[60] Lag3-deficient mice do not develop spontaneous autoimmunity. If allowed to age, however, Lag3-deficient mice do show an expansion of both the CD4 and CD8 T-cell compartments.[61] In a chronic LCMV infection model, Lag3 was co-expressed with PD1 on exhausted T-cells.[42] Additionally, CD8+ TILs that were specific for NY-ESO-1 were negatively regulated by Lag3 and PD-1 in an ovarian cancer model.[62] Anti-Lag3 mAbs are currently in clinical trials for both hematologic and solid tumors.

**1.3.iv Tim3**

Yet another ITIM-containing member of the IgSF that plays a negative regulatory role on T-cells is Tim3 (T-cell Ig and mucin domain 3). Tim3 is expressed upon activation on subsets of CD4+ and CD8+ cells in humans;[26,27,63,64] in mice, expression is limited to activated Th1 cells only.[63] Its expression can also be induced by pro-inflammatory cytokines independent of antigenic stimulation.[64] The ligand for Tim3 is disputed, as evidence exists for both Gal9 and CEACAM1.[63,65–69] Regardless, following ligand binding, Tim3 recruits SHP2 via its ITIM to repress TCR signaling.

Tim3 is increasingly being recognized to play an important role in the immune response to tumors, especially in concert with other checkpoint molecules. In human melanoma patients and mouse models, PD1+ Tim3+ dual positive TILs are the most exhausted and dysfunctional as well as the most abundant TILs.[27] They are unable to secrete IL-2, TNF, or IFNγ and are not able to proliferate.[27,70] Correspondingly, dual blockade of PD1 and Tim3 with monoclonal antibodies in mice increases tumor rejection in a solid tumor model and reverses T-cell exhaustion in a chronic infection model. Recently, it was shown that in some human patients with lung adenocarcinoma who were treated with αPD-1 therapy but developed resistance and subsequent disease progression, there was a specific increase in Tim3 expression on T-cells compared to patients who did not receive αPD-1.[71]

**1.4 Risks of Immune checkpoint blockade**

While checkpoint blockade mAb therapies are certainly beneficial to some patients, they are not without side effects. The same checkpoint inhibitors used by tumor cells to defend against TILs are also used by healthy cells to defend against autoimmune T-cell attack. For this reason, patients prone to autoimmunity due to genetics or family history were excluded from the clinical trials. Now that PD-1/PD-L1 blockade is FDA-approved and available clinically, a wider variety of patients are receiving these treatments, including those with a predisposition to autoimmunity as well as patients who are post-allogeneic hematopoietic stem cell transplant (HSCT) and are at risk for GVHD. Shortly after mAb checkpoint blockade was FDA-approved, it was reported that six adult patients receiving a PD-1 mAb therapy for melanoma developed autoimmune diabetes following the PD-1 mAb therapy,[72] confirming the fear that systemic

checkpoint blockade using antibodies could lead to a break in peripheral tolerance. Immune-related adverse events have also been reported involving the skin, liver, gastrointestinal, thyroid, and nervous systems.[73] While it could be argued that an autoimmune disease is a small price to pay if the mAb therapy saves the patient's life, it was unfortunately recently reported that multiple post-allogeneic HSCT patients who received PD-1 mAb blockade therapy developed fatal graft versus host disease (GvHD) shortly after receiving systemic checkpoint PD-1 blockade.[74]

**1.5 Genome engineering: A safer avenue for multiplex immune checkpoint blockade**

The synergism of blocking multiple checkpoints apparent in recent studies will certainly be important since only approximately one-third of patients that received PD-1/PD-L1 blocking antibodies responded to the treatment. However, this also means blocking multiple pathways involved in peripheral tolerance, and therefore increasing the likelihood and severity of autoimmune reactions. For this reason, it would be beneficial to restrict checkpoint blockade to T-cells that can only recognize tumor antigens, rather than the systemic distribution resulting from mAb treatment.

This can be accomplished by using targeted genome editing to eliminate both the endogenous TCR and checkpoint protein expression on CAR T-cells or other engineered T-cells that are restricted to tumor-specific antigens. Knock-out of the checkpoint proteins should increase proliferation, cytokine production, and cytolytic activity toward any cell that the T-cell can target, whether it is a tumor cell or a healthy cell, and may also prevent or delay T-cell exhaustion. In the case of tumor cells, this is exactly the intended outcome. But in healthy

cells, this attack would cause autoimmune injury since the ligands that tumor cells have usurped to evade the immune system are normally expressed on healthy tissues to downregulate the activity of rogue T-cells that escape negative selection. By eliminating the endogenous TCR that allows T-cells to "see" other cells, we can restrict the cytolytic activity of these aggressive T-cells to target cells that are recognized by the CAR, such as tumor cells.

Multiple platforms are now available to accomplish high-efficiency, multiplexed knock-out and knock-in in primary human T-cells in a clinically relevant, scalable manner. To safely edit patient T cells, a gene editing platform with high specificity and engineerability towards a desired target is necessary. The two platforms we focused on are transcription activator-like effector nucleases (TALENs)[75] and clustered regularly interspaced short palindromic repeats (CRISPR/Cas9).[76] TALENs are noteworthy for their high specificity and modular nature, but they are not able to efficiently cleave highly-methylated loci. CRISPR/Cas9-based nucleases are not blocked by methylation and are easily engineered towards almost any DNA target of interest, but their off-target cleavage profiles are presently less well understood than for TALENs.[77].The DNA binding component of TALENs consist of 15-20 tandem repeats of 34 amino acids, each of which specifies binding to a particular nucleotide of DNA via the identity of the $12^{th}$ and $13^{th}$ amino acids in the repeat (**Figure 1.2**). The DNA binding domain is fused to a Fok1 cleavage domain to create the double-stranded break. However, Fok1 must dimerize to induce cleavage, so TALENs are introduced in pairs that bind with precise spacing to allow Fok1 dimerization. This requirement for paired binding increases the overall specificity of the TALEN pair, making it even safer for use in patients.

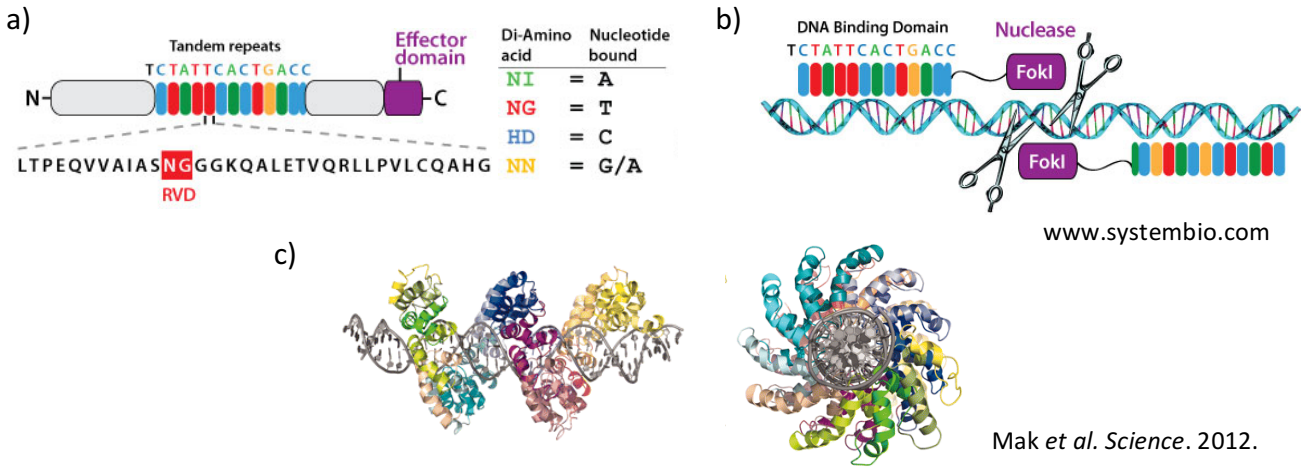


**Figure 1.2. Transcription activator like effector nucleases (TALENs). a)** Nucleotide binding by TALENs is determined by the identity of the 12$^{th}$ and 13$^{th}$ amino acid di-residue in each 34-amino acid repeat. The modularity and 1:1 nature of this binding make TALENs an easily engineerable platform. **b)** DNA cleavage of TALENs is carried out by an endonuclease such as Fok1. Because Fok1 must form a homodimer to cleave DNA, TALENs are introduced in pairs that bind to the DNA with precise spacing. This increases the overall DNA specificity and minimizes off-target cutting. **c)** Crystal structure of a TALEN DNA binding domain bound to DNA. The different colors denote different repeats. The DNA contact is made by the 12$^{th}$ and 13$^{th}$ amino acid di-residue of each repeat.

The CRISPR/Cas9 platform is comprised of the Cas9 nuclease (here we use *Sp*Cas9 from *Streptococcus pyogenes*), and a synthetic guide that targets Cas9 to the locus of interest. This synthetic guide has a 20nt sequence of homology to the DNA sequence of interest, followed by NCC (NGG in the genomic DNA - known as the protospacer adjacent motif, PAM), followed by the transactivating RNA (tracrRNA) that binds to the Cas9 nuclease (**Figure 1.3**). Synthetic guides can be delivered as RNA, chemically modified RNA, or RNP complexes; or as DNA via plasmid transfection or viral vector transduction.

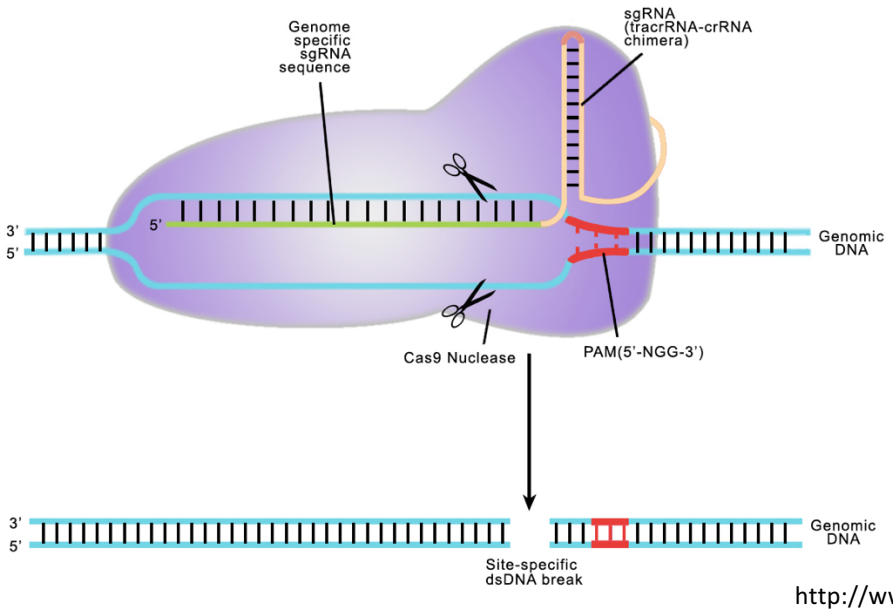


http://www.genecopoeia.com

**Figure 1.3. DNA recognition and cleavage by CRISPR/Cas9.** The CRISPR-Cas9 system is made up of two components, the Cas9 nuclease and the CRISPR RNA, which itself is made up of the guide RNA sequence that dimerizes to genomic DNA, and the tracrRNA that binds to Cas9. Together, the guide and tracrRNA are termed the synthetic guide RNA (sgRNA), and direct the Cas9 nuclease, which has no intrinsic cleavage or binding specificity, to cleave a specific genomic target. The Cas9 nuclease leaves blunt DNA breaks, which can then be resolved via several different DNA repair pathways. Importantly, the guide RNA target is bound by the protospacer adjacent motif (PAM), which for SpCas9 has the sequence NGG. Most guide RNA sequences are 18-20 base pairs in length.

Alternative genome engineering platforms include homing endonucleases (HEs), megaTALs (MTs), and zinc-finger nucleases (ZFNs).[78–82] Each of these are highly valuable in specific contexts, but were not the most efficient tools in this setting. Although HEs, MTs, and ZFNs have high on-target specificities and low rates of off-target cleavage, they require large amounts of upfront design and re-design to increase activity at the intended target. Thus, for research purposes, these are time- and cost-prohibitive.

Following creation of a double-strand break by a nuclease, the cell's own DNA repair machinery is activated to resolve the break.[83,84] These endogenous pathways can be manipulated/utilized to achieve introduction of a novel genetic element or deletion of a gene. The two main pathways of DNA double strand break repair are classical non-homologous end joining (cNHEJ) and homologous recombination (HR) (Figure 1.4). There are also 'backup' repair pathways that cells can utilize if NHEJ or HR cannot be activated or completed, including alternative non-homologous end joining (alt-NHEJ) and single-strand annealing.[85,86] Both alt-NHEJ and SSA always result in loss of genetic information by deletion, and are thus not the optimal repair pathway choices for endogenous cell processes.

Treatment with an exogenous endonuclease without a repair template will usually result in DNA repair via cNHEJ.[87] cNHEJ can seamlessly repair double-stranded DNA breaks, but can also leave small insertions or deletions, known as indels. These can create frameshifts in the resulting ORF, causing gene knock-outs. The indel spectrum varies widely depending on the endonuclease type: for example, TALENs tend to leave larger deletions, while the CRISPR-Cas9 system tends to leave mostly +1 and -1 insertions/deletions.[88–90]

To introduce a knock-in gene or a genetic segment, homologous recombination (HR) must be activated. This DNA repair pathway is most active in dividing cells in S/G2 phase, when proteins involved in HR are upregulated and a homologous DNA template is present. By this mechanism, an exogenous gene template may be used not only for introduction of a gene, but also for gene repair. The desired repair template is delivered to coincide with expression of the nuclease, and the cell's HR machinery uses this exogenous DNA to copy information into the native genome. There is some evidence that the type of endonuclease used to create the

double-strand break may impact the efficiency of HR,[91,92] where a 3' overhang is preferable to a 5' overhang.

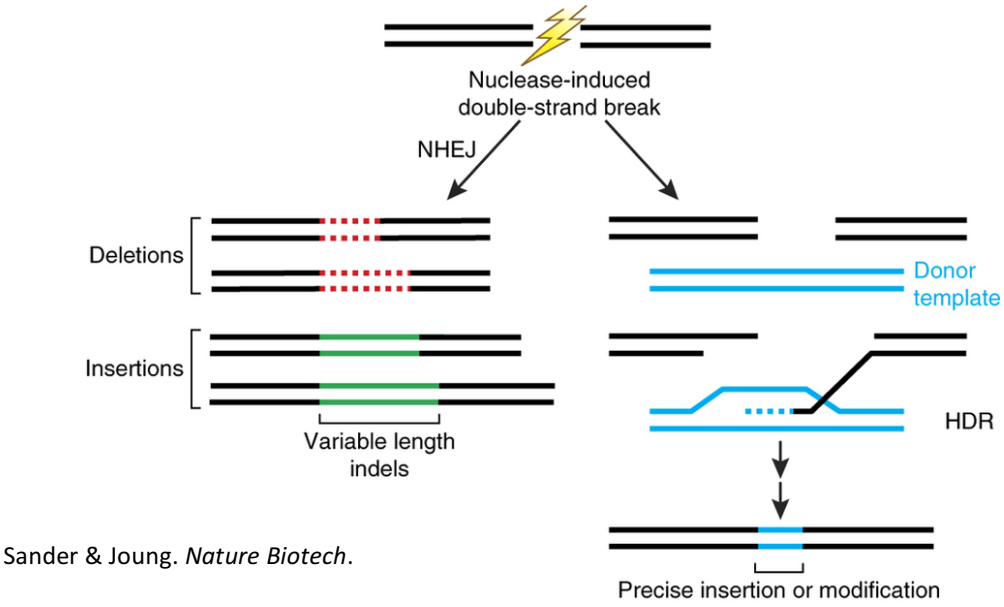


**Figure 1.4. Major DNA repair pathways activated after a double-stranded break.** After a DNA break is induced by one of the genome engineering platforms, the cell's native DNA repair pathways quickly resolve the break. If the break is resolved by the cNHEJ pathway, small indels are often produced. If repair instead proceeds via the HR pathway and a donor template is also introduced to the cell, targeted insertion or repair using the donor template can occur.

### 1.6 Project summary

I have developed methods for multiplexed TALEN- and CRISPR-based editing of T-cell inhibitory checkpoints, with the goal of increasing the efficacy of CAR T-cells in a solid tumor microenvironment. This required first the development of clinically relevant and scalable methods for the engineering of primary human T-cells. Our initial engineering goal was knock-out of the endogenous TCR$\alpha$ locus as a safeguard against autoimmunity and GvHD. In addition to restricting T-cell activation and cytotoxicity to cells expressing the target antigen, ablation of the endogenous TCR also opens the possibility of allogeneic CAR therapy in patients for whom

autologous therapy is not an option. Healthy and plentiful T-cells isolated from a parent, sibling, or unrelated donor engineered to express a CAR but not an endogenous TCR could provide at least short-term tumor regression and control as a bridge to a definitive therapy without the risk of GvHD. Once we achieved efficient knock-out at the TCR$\alpha$ locus using both TALENs and CRISPR/Cas9, we evaluated the growth, cytokine production, and cytolytic function of the TCR-deficient CAR T-cells and determined that they perform at least as well as TCR-sufficient CAR T-cells in both *in vitro* and *in vivo* applications.

We next explored the ability of this technology to knock out multiple T-cell inhibitory checkpoint proteins, whose loci are more difficult to engineer because of their highly-methylated nature. Due to this highly methylated status, TALENs were not efficient in achieving bi-allelic knock-out at PD-1. However, CRISPR/Cas9 is more tolerant of DNA methylation, and efficiently knocked out PD-1, Tim3, Lag3, and TIGIT individually in a bi-allelic manner. Therefore, this is the platform we chose for the development of multiplexing approaches to knock out all of these genes in a single population of T-cells.

In the approach developed over the course of my thesis work, we chose to use AAV6 to deliver CRISPR guides to human T-cells.[91] AAV6 is the serotype of AAV that transduces human T-cells at the highest efficiency with the lowest toxicity.[91] In addition to delivering the Cas9 via mRNA electroporation, we also include mRNA encoding additional "helper proteins" from adenovirus serotype 5 (Ad5) in the electroporation. These proteins act to increase the effective guide dosage by enhancing AAV transduction and to alter the DNA repair environment of the cell (Figure 1.5).[89] If gene knock-in is desired rather than gene knock-out, this approach is compatible with delivery of the donor template for homologous recombination via AAV6.

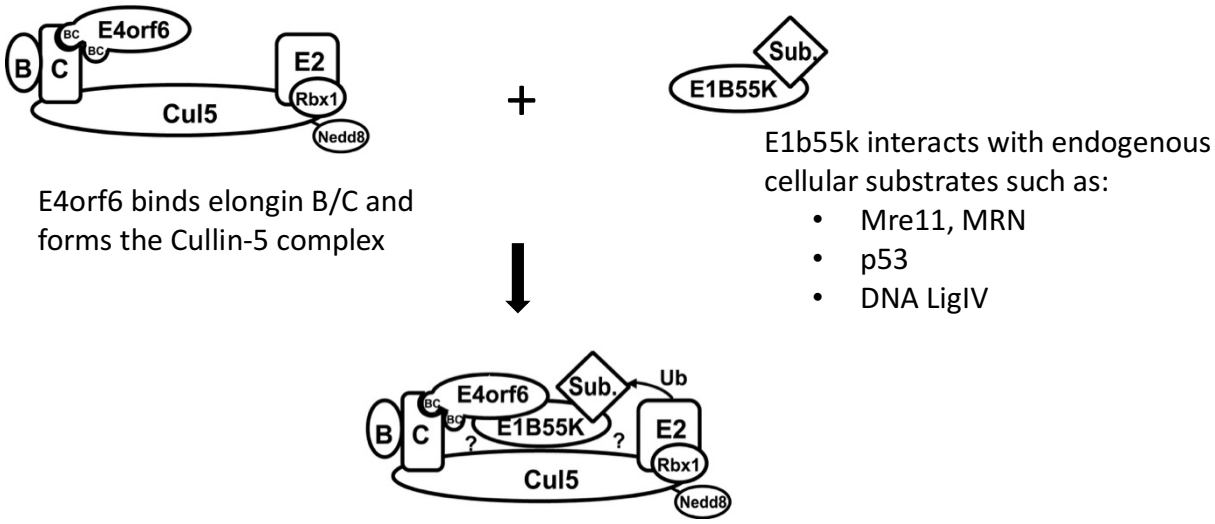


**Figure 1.5. The Ad5 E1b55-E4orf6 protein complex functions to degrade endogenous cellular components.** Viral E4orf6 binds to the endogenous cullin 5 complex, which functions to ubiquitinate different proteins for degradation. E1b55k, meanwhile, binds various cellular substrates, including p53, MRN, and DNA Ligase IV, and then binds to E4orf6. Once E1b55k and E4orf6 form a complex, this brings the E1b55k-bound substrates in proximity to be ubiquitinated and degraded. In this way, the Ad5 protein complex is able to degrade various cellular components and promote viral propagation.

Using this method, we successfully multiplexed knock outs of TCR$\alpha$, PD-1, Tim3, Lag3, and TIGIT without affecting the baseline phenotype or growth of the T-cells. In the future, we plan to test these multiplexed knock-out CAR T-cells for activity against solid tumors, using an orthotopic tumor model of neuroblastoma in mice.

# 2. Development of a scalable mRNA expression vector with a long, encoded poly(A) tail for transient protein expression in clinical applications

## 2.1 Introduction

To realize our goal of genome editing in primary human T-cells on a clinical scale, we first had to choose a delivery platform for the nucleases that would be safe for patients, scalable, consistent, reproducible, and non-antigenic for the immune system. To address safety, we wanted to preclude the possibility of integration or long-term protein production, which made introduction by mRNA electroporation an attractive candidate. Due to the labile nature of mRNA stability, protein expression from mRNA is transient, and it has no mechanism for integration. It is also possible to synthesize mRNA by *in vitro* transcription (IVT) in such a way that it is extremely similar to native mRNA, and therefore will have no- or low-antigenicity when introduced into immune cells. mRNA production by IVT is relatively simple and can be scaled by at least six orders of magnitude in volume. This allows small experiments with positive results to be scaled up to clinical manufacturing size without further optimization.

For these reasons, IVT mRNA has emerged as an important modality of transient heterologous protein expression for therapeutic applications,[93–97] and electroporation of IVT mRNA is presently being employed in translational applications, both *in vivo* and *ex vivo*. For example, IVT mRNA is used for *in vivo* expression of antigenic proteins in dendritic cells for cancer and infectious disease vaccine purposes as well as for *ex vivo* expression of nucleases for gene editing in primary hematopoietic stem cells and T-cells.[97–106]

A fundamental goal in any IVT mRNA application is to obtain maximally efficient protein expression. High expression efficiency reduces costs by directly reducing the quantity of mRNA

necessary for a given level of expression, and may also reduce potential mRNA antigenicity due to the reduced exposure of a patient's cells to a foreign nucleic acid. Numerous determinants of mRNA expression efficiency have been identified, including the nature of the 5' cap, the efficiency of capping, nature of 5' and 3' UTR's, codon optimization of protein coding sequence, presence of miRNA target sequences in the protein coding sequence and UTR's, and the length of the polyadenosine (poly(A)) tail.[107] Of these determinants, the length of the poly(A) tail is most problematic to optimize. Although poly(A) tail length is known to be one of the most important physiological determinants of translational efficiency and mRNA stability,[108–110] and therefore of total protein synthesis, existing technologies did not allow for production of IVT mRNA with defined length poly(A) tails in the physiological range of a newly synthesized tail (approximately 250 nucleotides).

To this end, we developed a novel method for generation of homopolymeric tracts of arbitrary length and content, and demonstrated that a previously described linear plasmid, pJazz,[111] can incorporate poly(A) tracts up to approximately 500 base pairs in length. Further, we modified pJazz by removing extraneous BsaI sites while incorporating a unique BsaI site downstream from the poly(A) tract. BsaI is a type IIs restriction enzyme that cuts upstream of its recognition sequence, allowing the mRNA to end in free adenine residues (or in any other residues we choose). Together, these modifications produced a template for IVT that was named p(Extended Variable Length) (pEVL). It is a linear plasmid that allows for facile generation of IVT mRNAs with defined, extended poly(A) tails using standard T7 phage RNA polymerase chemistry.

The pJazz linear plasmid system upon which we built pEVL was developed for cloning of highly repetitive DNA from bacterial genomes.[111] pJazz is derived from the coliphage N15, which has a linear dsDNA genome, and encodes the phage genes necessary for maintenance of the linear structure within the plasmid. The linear DNA is created by cleavage with a phage enzyme, protelomerase (TelN), which generates closed hairpin DNA ends and maintains them during replication.[111] Replication is primed by a phage-derived replication protein (RepA) encoded on the plasmid.[111]

Though traditional cloning and propagation methods can be used successfully with pEVL, several changes were necessary to achieve maximal efficiency. An electrocompetent *E. coli* host strain that contains the TelN gene (in addition to the TelN gene included in the plasmid), called BigEasy TSA, is commercially available and increases transformation efficiency. Recovery of DNA from plasmid purification is increased by the use of arabinose for copy number induction in liquid culture, the use of terrific broth (TB) as the liquid culture media, and isopropanol precipitation by centrifugation for plasmid recovery after elution from column clarification.

## 2.2 Homopolymeric poly(A) tracts of 175 base pairs or longer are extremely unstable in circular plasmids

Adapted from Grier AE, Burleigh S, Sahni J, Clough CA, Cardot V, Choe DC, Krutein MC, Rawlings DJ, Jensen MC, Scharenberg AM, and Jacoby K. pEVL: A Linear Plasmid for Generating mRNA IVT Templates with Extended Encoded Poly(A) Sequences. *Mol Ther Nucleic Acids*. 2016 Apr 19;5:e306.

Although there are frequent testaments in the life science literature to the instability of repetitive DNA and extended homopolymeric tracts in circular plasmids,[97,107] we were unable to find any published data that describe the robustness of the phenomena. To illustrate the

difficulties in cloning and propagating extended homopolymeric tracts, we attempted to ligate inserts containing 70, 172, and 325 base pair homopolymeric poly(A) tracts respectively into a standard circular cloning vector plasmid designated pWNY **(Figure 2.1)**. To assess the stability of the inserts, we transformed the plasmids into *E. coli* and grew them overnight at 25°C on selective media, and performed PCR across the inserts using DNA obtained from individual bacterial colonies. After analysis by gel electrophoresis, the resulting PCR products resolved primarily into bands of two different sizes **(Figure 2.1)**. In **Figure 2.1**, those products reflecting expected insert sizes are represented by open circles, and products representing substantially shortened sizes are represented by closed circles. Although small poly(A) tracts of 70 bp are stable throughout the standard ligation/transformation process (all maintained their correct length), poly(A) tracts of 172 bp shortened one-third of the time, and longer tracts of 325 bp appear to be extremely unstable, with substantial shortening of the tract occurring without exception.

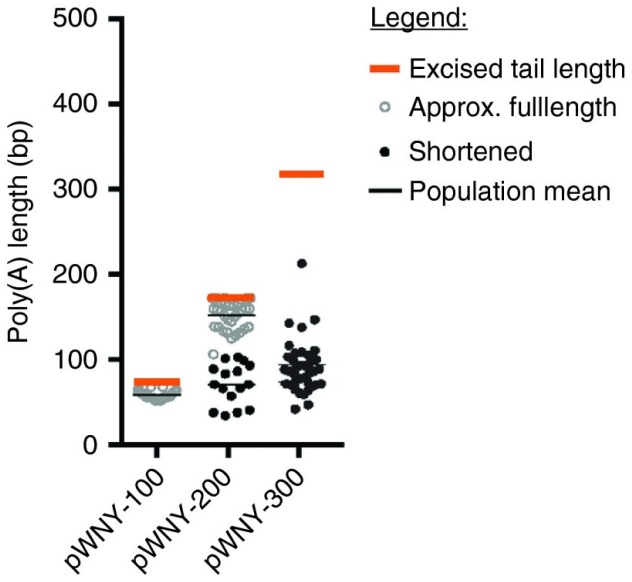

**Figure 2.1. Shortening of poly(A) tracts upon cloning into standard circular plasmid cloning vector at 25°C**. BFP-poly(A) tract inserts of 70, 172, and 325 base pairs bounded by restriction enzyme sites DraIII and SwaI were generated via restriction enzyme digest from the linear plasmid cloning vectors BFP-pEVL-100, BFP-pEVL-200, and BFP-pEVL-300. The inserts were ligated into a circular cloning vector, designated pWNY, and the resulting plasmids were transformed into *Escherichia coli* using standard methods and grown at 25°C. Individual colonies were amplified by PCR using primers flanking the poly(A) tract, and the length of the poly(A) tract was estimated based on the resulting band size. Typically, a band was obtained either near the expected size, or at a smaller size, reflecting shortening of the poly(A) tract during transformation. Colonies were scored for whether the poly(A) tract fragment was approximately of the expected size (open circle), or was substantially shortened (closed circle). BFP, blue fluorescent protein; pEVL, p(Extended Variable Length); poly(A), polyadenosine.

## 2.3 Homopolymeric poly(A) tracts up to approximately 500 base pairs can be incorporated into pJazz

Adapted from Grier AE *et al*. 2016. *Mol Ther Nucleic Acids*.

pJazz is a bacteriophage N15-based linear plasmid system that is reportedly superior in the propagation of genomic DNA from organisms with highly repetitive genomes,[111] but has not been previously reported to support the cloning or propagation of homopolymeric polynucleotide tracts. To determine whether pJazz was capable of cloning or propagating poly(A) tracts, we performed an *in vitro* ligation of chemically synthesized DNA oligonucleotides to generate a population of annealed double stranded poly(A/T) polynucleotides of varied lengths, gel purified those polynucleotides with lengths between approximately 100 to 850 base pairs, and attempted to ligate this population of oligonucleotide into a derivative of pJazz-OK with a custom MCS containing a BsaI site (pJazz-OK-MCS, **Figure 2.2A, top**). This ligation reaction led to the isolation of pJazz-OK-MCS derivatives containing c.a. 70 base pair, c.a. 172 base pair, and c.a. 325 base pair poly(A) tracts (**Figure 2.2A, bottom**) as assessed by gel electrophoresis.

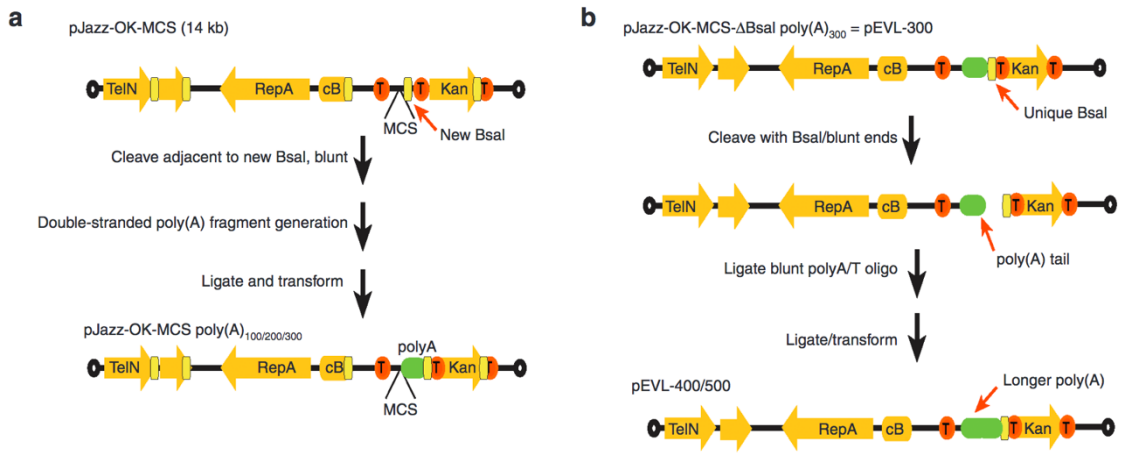


**Figure 2.2. Generation of pEVL: a linear plasmid vector for generation of mRNA with extended encoded poly(A) tracts.** (**a**) Schematic of pJazz and conversion to pEVL. The plasmids are shown with orange arrows denoting genes, red circles with T's denoting transcriptional terminators, open circles denoting terminal hairpin loops, yellow blocks denoting BsaI sites, and green blocks denoting the poly(A) tail. (**b**) Schematic of pEVL and method used for generation of extended poly(A) tracts in pEVL.

To determine the potential for pJazz to stably propagate further extended poly(A) tracts, we developed a method for generation of extended poly(A) tracts of arbitrary length (**Figure 2.2B**). As schematized in **Figure 2.2**, adaptation of pJazz for facile generation of extended poly(A) tracts required its modification such that it possessed a unique target site for the type IIS restriction enzyme BsaI. The BsaI site 3' to the poly(A) tract is central to the method we developed for iterative cloning of blunt end poly(A/T) oligonucleotides to allow extension of the poly(A/T) tract to a length greater than 300 base pairs. Therefore, this method required the removal of 4 BsaI sites in pJazz-OK-MCS to render the BsaI site at the end of the poly(A) tract unique, allowing BsaI, a type IIS restriction enzyme, to cleave only within the poly(A) tract. This plasmid was designated pJazz-OK-MCS-ΔBsaI (**Figure 2.2B, top**). Cloning of previously generated 70, 172, and 325 base pair tracts into pJazz-OK-MCS-ΔBsaI generated pEVL-100, pEVL-200 and pEVL-300 respectively, and subsequent cloning of a similarly generated blunt-

ended poly(A) polynucleotide population into BsaI-digested/blunted pEVL-300 resulted in incorporation of additional 100 and 200 base pair tracts of poly(A) at the end of the pEVL-300 poly(A) tract, thus allowing the isolation of pEVL-400 and pEVL-500 with poly(A) tracts of 425 bp and 525 bp, respectively (**Figure 2.2B, bottom**).

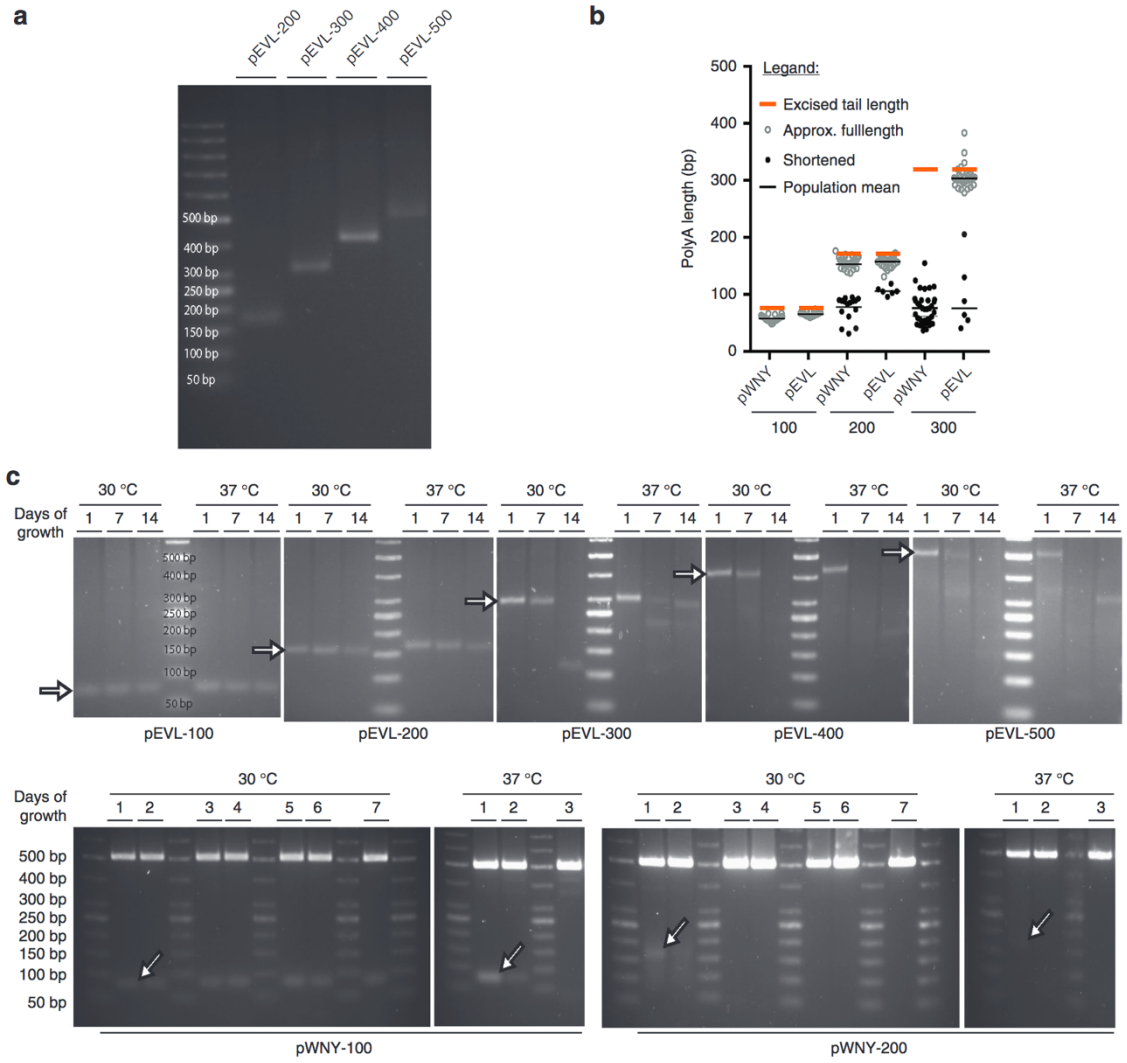


**Figure 2.3. Characterization of poly(A) tract stability in pEVL.** (**a**) Stability of the encoded poly(A) tracts following overnight induction of pEVL for template preparation. BFP-pEVL-200 through 500 were grown overnight with induction at 30°C and then maxiprepped. Each maxiprepped sample was digested with BsiWI and BsaI to release the poly(A) tail fragment from the rest of the plasmid. The tail length was

determined by gel electrophoresis with comparison to a known molecular weight standard. (**b**) Shortening of poly(A) tracts upon cloning into standard circular or linear plasmid cloning vectors at 30°C. BFP followed by poly(A) tract inserts of 70, 172, and 325 base pairs bounded by restriction enzyme sites DraIII and SwaI were generated via restriction enzyme digest from the linear plasmid cloning vectors pEVL-100, pEVL-200, and pEVL-300. The inserts were ligated into the circular cloning vector pWNY or subcloned into pEVL and transformed via electroporation. Transformed bacteria were grown with ampicillin (pWNY) or kanamycin (pEVL) selection at 30°C. Individual colonies were amplified by PCR using primers flanking the poly(A) tract, and the length of the poly(A) tract was determined based on the resulting band size as in **Figure 2.1.** Typically, a band was obtained at the expected size, or a smaller size, reflecting shortening of the poly(A) tract during transformation. Colonies were scored for whether the poly(A) tract fragment was approximately of the expected size (open circle), or was substantially shortened (closed circle). (**c**) Stability of encoded poly(A) tracts under extended propagation conditions. To test the stability of the poly(A) tail under stringent propagation conditions, pEVL 100 through 500 were grown for 2 weeks at 30°C and 37°C with reseeding into fresh media at a 1:1000 dilution every 24 hours. At days 0, 6, and 13, each sample was similarly reseeded into induction media and grown overnight before being miniprepped. Parallel analysis was performed with the circular vectors described in (**b**), in which the poly(A) tract fragment was sub-cloned into a circular vector (pWNY). As these are already high-copy plasmids, no inducing agent was added to the cultures. For the circular vectors, samples were miniprepped daily for 7 days. For both pEVL and the circular vectors, the tail length of the induced minipreps was determined by gel elctrophoresis as described above. The expected tail band size for each construct is indicated with an arrow.

Practically, we have found that inserts possessing up to around 300 base pair poly(A) sequences are easily sub-cloned into pEVL (**Figure 2.3A, Figure 2.3B**). In contrast to pWNY, where 172 bp poly(A) tracts remained full-length two-thirds of the time and 325 bp tracts were not able to be sub-cloned at all without substantial shortening, in pEVL, 172 bp and 325 bp tracts remained full-length 84% of the time (**Figure 2.3B**). Moreover, these tracts are also highly stable during extended propagation through at least a week of serial liquid culture at 30°C (**Figure 2.3C**). Consequently, these tracts are maintained during expansion, banking as a glycerol stock, and re-expansion as demonstrated by DNA sequencing in both directions across the pEVL300 poly(A) tail (**Figure 2.4)**. In contrast, we have noted a tendency for the pEVL-500 poly(A) tract to shorten during cloning, although we have always been able to identify clones possessing inserts with a poly(A) tract of the original size. Similarly, extended propagation of

pEVL-500 also shows a tendency for the poly(A) tract to shorten over time (**Figure 2.3C**), however, it is sufficiently stable for growth and generation of mRNA with templates with the expected poly(A) length.

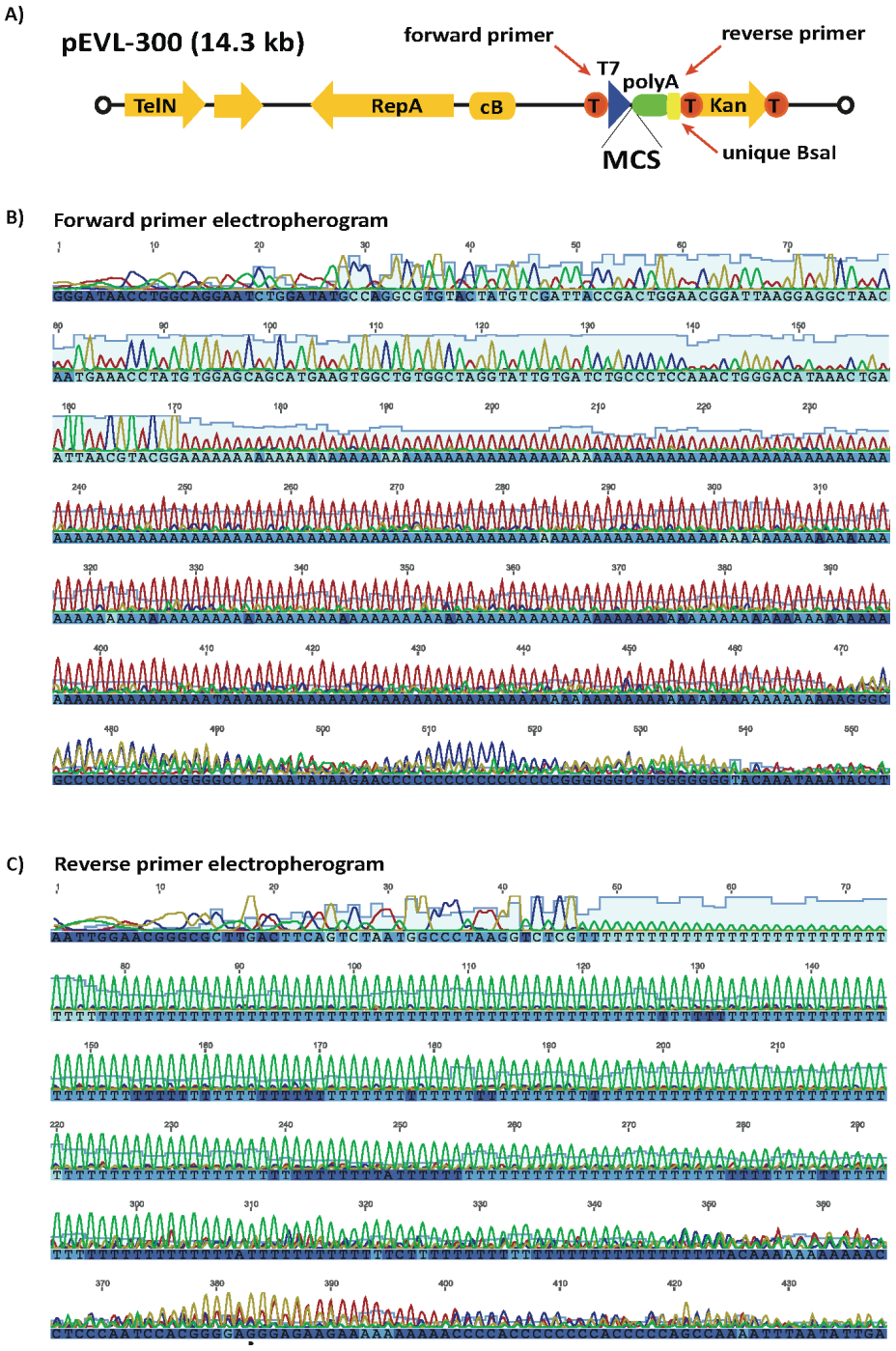

**Figure 2.4. Sequencing electropherograms covering the poly(A) tract in pEVL-300.** Forward and reverse sequencing electropherograms generated using standard sanger sequencing chemistry over the poly(A) template in pEVL-300, demonstrating the existence of a homopolymeric tract of at least 300 base pairs. Note that with a homopolymeric tract of this size, clear 3' boundaries are not expected due to polymerase slippage, thus explaining the gradual diminishment of the sequence and convoluted appearance of the processed electropherogram around the end of the tract.

## 2.4 mRNA incorporating extended polyA tails generated from pEVL templates exhibits superior translation properties

Adapted from Grier AE *et al*. 2016. *Mol Ther Nucleic Acids*.

As our goal for developing a means of propagating extended poly(A) tracts was for the purpose of generating IVT mRNA with extended poly(A) tails, we validated pEVL's capacity to function as a template for generating IVT mRNA by cloning a blue fluorescent protein (mTagBFP2) IVT cassette upstream from the poly(A) tracts in pEVL-100/200/300/400/500. We generated IVT mRNA using the BsaI-cleaved pEVL derivatives BFP-pEVL-100 through BFP-pEVL-500 as the IVT mRNA templates, and ARCA capping chemistry. The resulting mRNA was of the predicted size for each pEVL derivative and highly uniform (**Figure 2.5A, left panel**) compared to enzymatically polyadenylated RNAs (**Figure 2.5A, right panel**, see also Holtkamp *et al*.[97]). Enzymatically polyadenylated mRNAs have poly(A) tails varying in length from ~60 to 500 bases, depending on the amount of EPAP used, the amount of time given for the polyadenylation reaction, and the construct size and composition. Importantly, it is difficult to create a consistent tail length across multiple production batches of mRNA, even with standardized protocols.[97] In addition, enzymatically-added poly(A) tails are not of one homogenous length; the population always contains substantially shortened and lengthened tails, producing a smeared appearance on an RNA gel (**Figure 2.5**).

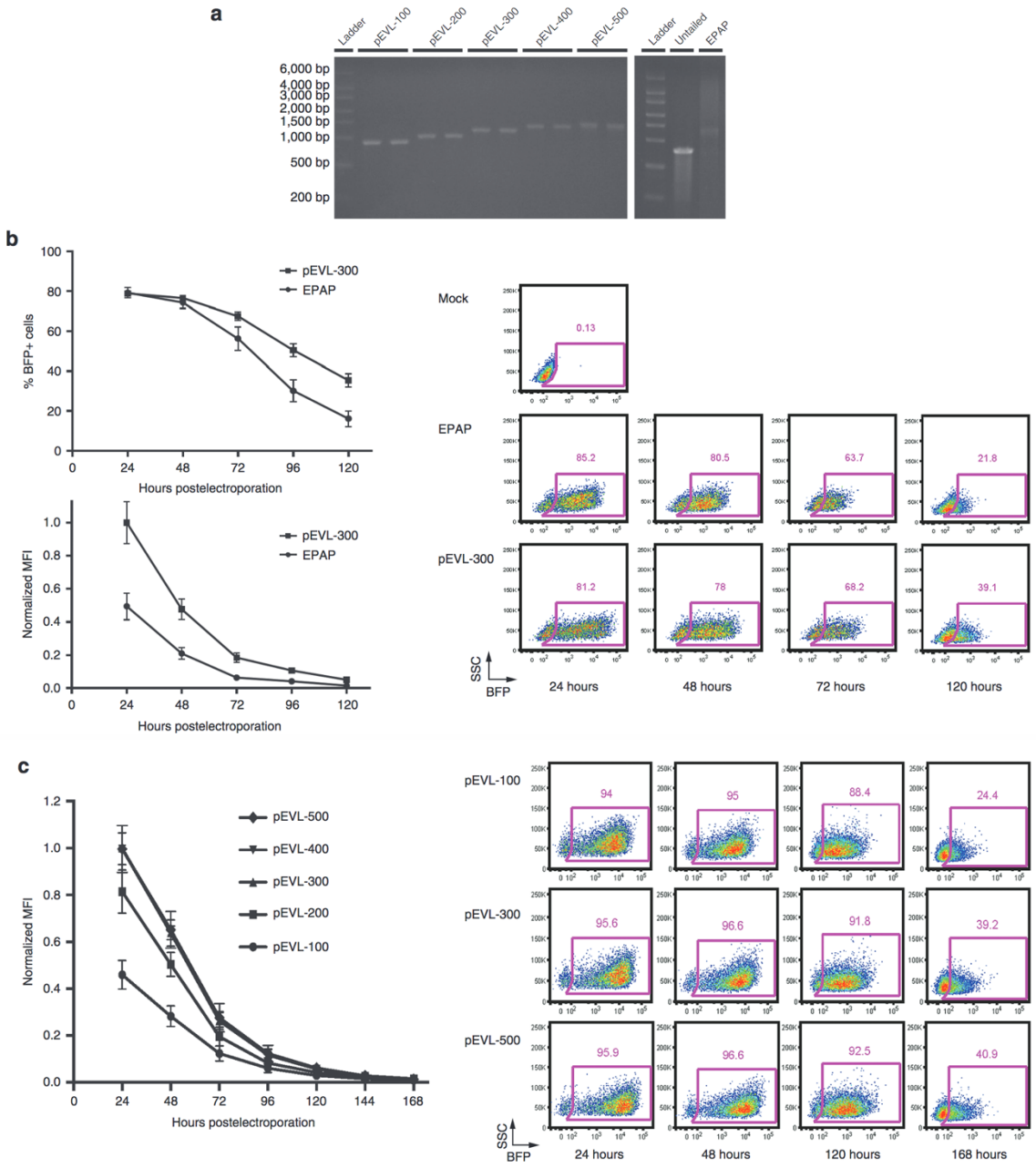


**Figure 2.5. Generation and characterization of mRNA from pEVL-encoded templates**. (**a**) IVT mRNA encoding blue fluorescent protein (mTagBFP2) generated from pWNY with enzymatic tailing and pEVL-100 through pEVL-500. BFP-pEVL-100 to 500 were digested with XbaI and BsaI, and pWNY with ScaI and BsiWI, to generate template for IVT. IVT was carried out with antireverse cap analog capping, and for pWNY, enzymatic tailing with EPAP. After purification, 200 ng of each transcript was imaged via gel electrophoresis on the FlashGel system. Typically, pEVL produces a single band of defined length,

whereas pWNY with enzymatic tailing produces transcripts of a more heterogenous length. (**b**) Relative potency of mRNA encoding BFP generated from a circular plasmid vector with enzymatic polyadenylation or from pEVL-300 and representative flow plots. 1 μg of IVT mRNA from the indicated template was electroporated into prestimulated primary human T cells. After a 24-hour cold shock at 30 °C, the cells were analyzed each day for 5 days by flow cytometry for the percentage of cells expressing BFP as well as the mean fluorescence intensity (MFI) of the BFP in BFP+ cells. Flow plots are shown as side scatter (SSC) versus BFP. (**c**) Relative potency of mRNA encoding BFP generated from pEVL-100 through pEVL-500 and representative flow plots. Equimolar amounts of IVT mRNA from BFP-pEVL-100 to 500 were electroporated into prestimulated primary human T cells. After an initial 24-hour cold shock at 30 °C, the cells were grown at 37 °C for 6 more days. Every 24 hours after electroporation, the percentage of cells expressing BFP and the BFI MFI of the BFP+ cells was analyzed by flow cytometry. Flow plots are shown as side scatter (SSC) versus BFP. BFP, blue fluorescent protein; IVT, *in vitro* transcribed; pEVL, p(Extended Variable Length).

We validated the potency of the mRNA produced from pEVL by comparing BFP expression following electroporation of mRNAs generated through enzymatic polyadenylation and from pEVL-300 into primary human T-cells (**Figure 2.5B**). We defined potency as mean fluorescence intensity (MFI) of BFP-positive cells following electroporation with equal molar amounts of mRNA. We observed a striking enhancement of potency, as assessed by differences in BFP mean fluorescence intensity at 24 hours to 5 days post-electroporation, for mRNA generated from pEVL-300 versus enzymatically polyadenylated mRNA. Furthermore, analyses comparing BFP expression driven by mRNA generated from pEVL-100 through pEVL-500 over a period of 7 days (**Figure 2.5C**) confirmed the above observations – pEVL-100 and pEVL-200 derived mRNA possessing poly(A) tail lengths of 70 base pairs and 172 base pairs, respectively, exhibited reduced potency versus mRNA derived from pEVL-300, pEVL-400, or pEVL-500, possessing poly(A) tail lengths of approximately 325, 425 and 525 base pairs, respectively. However, we were not able to detect significant potency differences among pEVL-derived mRNAs possessing encoded poly(A) tracts of 300 base pairs or greater. We did not detect any differences in toxicity between pEVL and enzymatically polyadenylated mRNA, as determined

by cell viability in the flow cytometric analysis 24 hours after electroporation.

### 2.5. Alternative 3' termini can be incorporated at the end of the poly(A) tail if desired and affect the stability of the mRNA

Adapted from Grier AE *et al*. 2016. *Mol Ther Nucleic Acids*.

Previous work has used cellular RNA sequencing to identify correlations between RNA length and the presence of single or double uridine or guanine residues on mRNA 3' termini.[112–114] Since the pEVL system allows one to specify the bases present at the 3' terminus of the IVT template using the unique BsaI site in a similar fashion to extension of the poly(A) tract, we chose to validate these correlations by generating mRNA from templates with termini encoding single or double uridine or guanine bases. We then evaluated their capacity to produce fluorescent protein following transfection into primary human T-cells (**Figure 2.6**). We consistently observed that mRNAs possessing uridine bases at or near the 3' end (U or UU) exhibited reduced potency (both reduced total magnitude and duration of expression) relative to a standard poly(A) tail of identical length, while those bearing guanine bases at or near the 3' termini (G or GG) drove BFP expression that was similar to standard poly(A) tails.

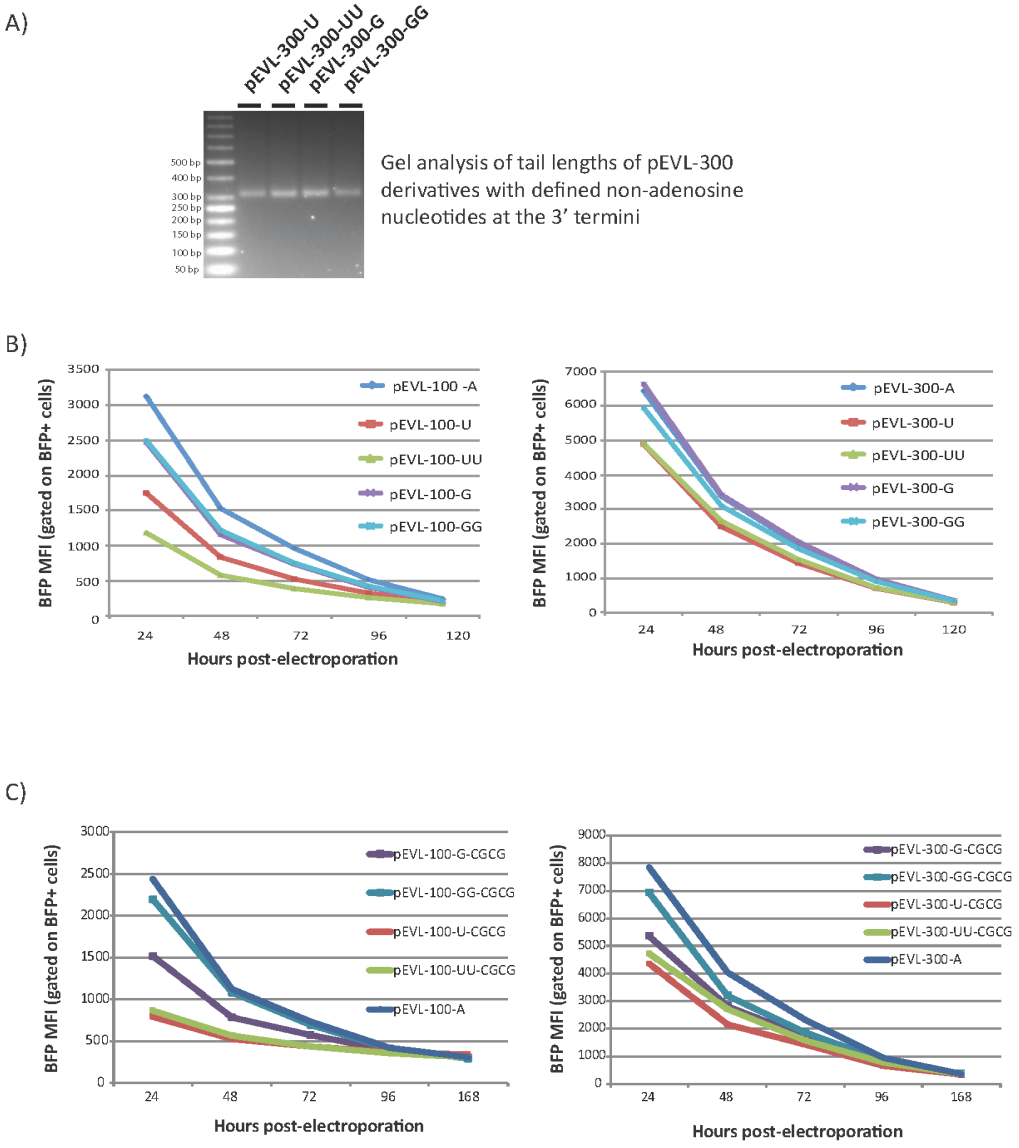


**Figure 2.6. Potency of mRNA generated from pEVL-300 variants with encoded terminal U, UU, G, or GG residues.** BFP-pEVL-100 and -300 variants were created with encoded poly(A) tracts to produce mRNA with -U, -UU, -G, or -GG residues at the 3' end, as well as these same four combinations of U and G residues followed by -CGCG, following BsaI digestion of the template. mRNA was transcribed from these pEVL variants, and 0.5 µg was transfected into primary human T-cells. Cells were incubated at 30°C for the first 24 hours after electroporation and then moved to 37°C. BFP fluorescence was monitored by flow cytometry over a five-day period. A) Representative gel showing tail lengths of plasmids with specified nucleotides at the end of the poly(A) tail. B) Plots represent relative MFI versus time for each variant mRNA with the indicated specified residue at the 3' end. C) Plots represent relative MFI versus time for each variant mRNA with the indicated specified residue at the 3' end followed by -CGCG.

Collectively, these data support the concept that use of pEVL mRNAs with longer, homogenous poly(A) tails are more efficacious for gene expression compared to mRNA with shorter poly(A) tails made by traditional means.

## 2.6 Materials and Methods

*Creation of pJazz-OK-MCS-pA-100, -200, and -300:*

We prepared pJazz-OK blunt (Lucigen, Middleton, WI) for insertion of a polyA tail by inserting an MCS comprising multiple blunt and sticky-ended RE sites as well as a terminal BsaI site [DraIII-FspI-BsiWI-NheI-BsaI] was ligated into pJazz-OK blunt to create pJazz-OK-MCS. pJazz-OK-MCS was digested with NheI (NEB, Ipswich, MA), blunted, and dephosphorylated with Calf Intestinal Alkaline Phosphatase (CIP, NEB). We then created a long poly(A) tail by annealing oligos of 200 T's and 50 A's at an equimolar ratio. The annealed oligos were treated with a single cocktail of T4 polymerase (NEB), Klenow fragment (NEB), and T4 PNK (NEB) to trim flaps, fill gaps, and create blunt, phosphorylated ends. The resulting mixture was run on a 3% agarose gel and fragments in the range of c.a. 200-800bp were gel extracted. After purification, these fragments were ligated into pJazz-OK-MCS with T4 DNA ligase (NEB) at room temperature for 2 hours. Resulting colonies were screened for poly(A) insert length by colony PCR as described below. Colonies with inserts of appropriate length were sequenced to screen for correct orientation of the insert. This process resulted in the identification of plasmids with poly(A) lengths of 70, 172, and 325 bp; these constructs were named pJazz-OK-MCS-pA-100, -200, and -300, respectively. The tail lengths were determined by gel electrophoresis as described below.

*Tail length screening by colony PCR:*

To screen large numbers of colonies and identify ones with the desired tail length after cloning and bacterial transformation, bacterial colonies were resuspended in water and used as template in a PCR reaction with primers that bind at the 3' end of the upstream ORF (for mTagBFP2 5'-cgcaaacgctaaaactacc-3') and in the pEVL vector just 3' of the tail (5'-tcagttctatgtaccagcaagg-3'). The resulting PCR products were run on a 1% agarose gel, stained with ethidium bromide, and imaged on a GelDoc XR+ imaging system (Bio-Rad, Hercules, CA).

*Determination of tail length by gel electrophoresis:*

To determine the length of the poly(A) tract without relying on polymerase-base methods, pEVL is transformed by electroporation into BigEasy TSA *E. coli* (Lucigen) and grown overnight with induction at 30°C in TB+Kan+10% arabinose media and then either miniprepped or maxiprepped. Minipreps are done with the QIAPrep Spin Miniprep kit (Qiagen, Valencia, CA) with doubled amounts of buffers P1, P2, and N3. Maxipreps are done with the NucleoBond Xtra Maxi kit (Macherey-Nagel, Bethlehem, PA), using the manufacturer's instructions for low-copy plamids (differs from the standard protocol namely in using 8-12 mL resuspension, lysis, and neutralization buffers per gram of pellet weight). For each miniprepped or maxiprepped pEVL plasmid, 2 μg is digested with BsiWI and BsaI. These restriction enzymes cut at the 5' and 3' ends of the poly(A) tract, respectively. The digested plasmid is run on a 3% agarose gel with 1-2 μL of GeneRuler 50 bp DNA ladder and post-stained with GelStar Nucleic Acid Stain. It is

then imaged on a GelDoc XR+ imaging system and the tail length is determined by comparison to the ladder using Quantity One 1-D Analysis Software (Bio-Rad).

*Creation of pJazz-OK-MCS-ΔBsaI:*

To create longer tails, it was necessary to mutate the 4 BsaI sites native to pJazz-OK to allow for unique digestion at the BsaI site directly 5' to and that cleaves within the poly(A). One site was removed by Gibson assembly using Gibson Assembly Master Mix (NEB) and designed with the NEBuilder tool (NEB). The remaining 3 sites were removed by restriction digest of a fragment containing the BsaI site to be mutated as well as a pair of flanking RE sites, blunting and ligation of this fragment into pUC57 digested with EcoRV (NEB), site-directed mutagenesis of the BsaI site, and then sub-cloning the mutated fragment back into pJazz-OK-MCS using the included flanking RE sites. This plasmid was designated pJazz-OK-MCS-ΔBsaI.

*Creation of pEVL series plasmids:*

Once all native BsaI sites were removed, the fragment containing the poly(A) tail from pJazz-OK-MCS-pA-100, -200, and -300 was cloned into pJazz-OK-MCS-ΔBsaI, creating pEVL-100, -200, and -300. pEVL-300 was then digested with BsaI, blunted with Klenow fragment, de-phosphorylated with CIP, and ligated with additional blunt double stranded poly(A) fragment prepared as above. Screening as above resulted in plasmids with 425 and 525bp p(A) tails; these were designated pEVL-400 and pEVL-500.

*Production of IVT mRNA:*

For the BFP construct, an insert containing a T7 promoter, Kozak sequence, and the mTagBFP2 [115] ORF was cloned into pWNY or pEVL-100 through pEVL-500. The sequence of the T7 promoter/spacer/Kozak sequence is: TAATACGACTCACTATAGGGAGAgcggccgctttttcagcaagattaaGCCGCCACCATGGCG. The BFP pEVL constructs were digested with BsaI (NEB or Thermo Scientific) to create a template with a terminal poly(A) tail. Templates were simultaneously digested with at a site upstream of the T7 (XbaI or SpeI, NEB or Thermo Scientific) to reduce the overall size of the template-containing fragment and enhance purification. pWNY constructs were linearized at the BsiWI at the end of the ORF, and with a second enzyme (typically ScaI or DraIII, NEB or Thermo Scientific) to ensure complete linearization. After checking the completeness of the digest on a 1% agarose gel, the digested DNA was purified on a silica column and eluted in water or 10 mM Tris. IVT with ARCA capping was carried out using the mMessage mMachine T7 Ultra kit (Life Technologies, Carlsbad, CA) per the manufacturer's directions with 200-1 000 ng of the T7 to poly(A) template fragment; IVT reactions were routinely extended to 150 min. Additional DNAse and/or incubation time was used to counterbalance any increased amount of template DNA in the reaction (e.g. double DNAse or double incubation time for double template). For pEVL constructs, the reaction was cleaned up after DNAse treatment using the RNeasy Mini kit (Qiagen) following the manufacturer's directions. For pWNY constructs, the enzymatic tailing step of the mMessage mMachine T7 Ultra kit was carried out for 1 hr according to the manufacturer's instructions before RNA clean-up by the same method as above. RNA quality was determined by NanoDrop spectrophotometry (Thermo Scientific) and gel analysis with the

FlashGel RNA system (Lonza). All mRNA was aliquoted in single use aliquots and stored at -80°C.

*mRNA electroporation of primary human T-cells:*

Freshly isolated primary human T-cells were stimulated with αCD3/αCD28 microbeads (Dynal, Thermo Scientific) in RPMI with 10-20% FBS, 2.5% HEPES, and 1% L-glut or Glutamax (Thermo Scientific). For isolated pan T-cells, IL-2 (Chiron, Emeryville, CA) and IL-15 (Miltenyi, San Diego, CA) at final concentrations of 5 ng/mL IL-2 and 1 ng/mL IL-15 were added. For isolated CD4+ T-cells, IL-2, IL-7 (Peprotech, Rocky Hill, NJ), and IL-15 were added at final concentrations of 50 ng/mL IL-2, 5 ng/mL IL-7, 5 ng/mL IL-15, and 2-mercaptoethanol (Sigma-Aldrich, St. Louis, MO) was added at a final concentration of 55 µM. After 48-72 hours, the stimulation beads were removed, and the T-cells were rested for 1-16 hours in complete media with cytokines. If the initial stimulation was carried out for more than 48 hours, half of the media was replaced with fresh media with cytokines at 48 hours post-stimulation. After resting, the T-cells were washed in PBS and resuspended at $3x10^7$ cells/mL in Neon Electroporation system Buffer T (Life Technologies) with 0.25-2 µg mRNA per 300,000 cells. Electroporation was carried out in a 10 µl tip on the Neon electroporation system (Life Technologies) at 1400V, 10ms, and 3 pulses. Immediately following electroporation, cells were resuspended in complete T-cell media with cytokines (as above). Cells were either placed in a 37°C incubator or in a 30°C incubator for 24 hrs and then moved to a 37°C incubator. A cold-shock step of this nature has been observed to increase the amount of protein per cell for the period when the mRNA is present [116–119].

*Flow Cytometry:*

Expression of the encoded protein was assayed by flow cytometry at 24-168 hours post-electroporation on an LSRII flow cytometer (BD Biosciences, San Jose, CA). Data was analyzed using FlowJo software (Treestar, Ashland, OR). Cells were gated on live singlet cells based on the forward and side scatter.

*Evaluation of transformation-associated tail shortening:*

BFP-pEVL100, 200, and 300 were digested with DraIII (which cuts 5' of BFP) and SwaI (which cuts ~75bp 3' of poly(A)/BsaI site). This fragment was gel purified and ligated back into pEVL digested with DraIII and SwaI as well as into pWNY digested with DraIII and SmaI. Following ligation, the ligase was heat-killed the pEVL and pWNY products were transformed by electroporation into BigEasyTSA electrocompetent cells (Lucigen) and Top10 electrocompetent cells (Life Technologies) respectively. After recovery at 30°C for 1 hr in SOC, aliquots of each transformation were plated in triplicate on kanamycin (kan) plates and grown at 25°C (72 hrs), 30°C (24 hrs), or 37°C (18 hrs). Colonies were screened for tail length by colony PCR as described above. For ligations of the 325 bp tail into pWNY, we were unable to recover any clones with full-length tail. To confirm that the poly(A) tail lengths determined by colony PCR were not biased by PCR polymerase slippage, tail lengths were also determined by gel electrophoresis, as described above. These digests confirmed that the poly(A) tail lengths determined by colony PCR are accurate.

*Evaluation of propagation-associated tail shortening:*

Colonies grown for 18 hours at 30°C after transformation of intact pEVL-200 to -500 in BigEasy TSA (Lucigen, Middleton, WI) *E. coli* were immediately screened for tail length by colony PCR. Colonies with the correct tail lengths were seeded into 4 aliquots of 1mL TB+Kan and grown overnight, 2 at 30°C and 2 at 37°C. At each temperature, 1 aliquot was grown under arabinose induction and 1 without. After 24 hours, 1 µl of each culture without arabinose was seeded into another 1 mL of TB+Kan without induction. This was carried out for 2 weeks. At the time of seeding each day, another 1 µL was seeded into a 1 mL culture of TB+Kan+arabinose. Each induced culture was spun down and the pellet was frozen after 24 hours of growth. At the end of 2 weeks, all of the frozen induced pellets were miniprepped (Qiagen) and the tail length was determined by gel electrophoresis as described above.

*Generation of pEVL-100 and -300 with poly(A) 3' termini -U, -UU, -G, and -GG*

Pairs of oligos containing a -AAAA overhang, the desired 3' termini, a BsaI site (yellow highlight below), and an -AAT were ordered from IDT, annealed at a 1:1 molar ratio, and phosphorylated with PNK. An example of an annealed oligo pair to introduce a GG (red highlight) 3' terminus is shown below.

```
Sense          AAAAGGCGAGACCGGCC
Anti-sense         CCGCTCTGGCCGGAAT
```

To prepare pEVL for insertion of the annealed oligo pair, pEVL-100 and -300 were digested with BsaI and Bsu36I (NEB), dephosphorylated with CIP, and purified with the DNA Clean & Concentrate-5 kit (ZymoResearch, Irvine, CA). The annealed oligo pairs were ligated into the

prepared pEVL-100 and -300. The resulting plasmids were electroporated into BigEasy TSA *E. coli* (Lucigen) and plated with kanamycin selection. After overnight growth at 30°C, colonies were picked into water and PCR'd with primers flanking the poly(A) tail. The resulting PCR products were treated with Exonuclease I (Thermo Scientific) and Antarctic Phosphatase (Thermo Scientific), and sequenced to find colonies with the desired poly(A) tail 3'end modifications. These colonies were also screened by colony PCR as described above to choose colonies that also retain a full-length poly(A) tail. The colonies that passed both of these screening tests were then grown with induction overnight at 30°C and maxiprepped. The tail length was additionally checked by gel electrophoresis as described above.

# 3. Gene editing via mRNA-mediated delivery of TALENs and CRISPR/Cas9

## 3.1 Introduction

Once we had developed the pEVL system to make high quality, homogenous, and repeatable batches of IVT mRNA, we wanted to apply this technology to a gene editing application: disruption of the TCRα locus in primary human T-cells to create CAR T-cells lacking the endogenous TCR. Though the ability of autologous CD19 CAR T-cells to eradicate lymphoma and leukemia has been shown in both adults and children,[7,8,120–123] not all patients are candidates for autologous therapy. Allogeneic CAR T-cell therapy could benefit many of these patients, but GvHD is a major concern, and one that could be abrogated by removal of the endogenous TCR.

Many infants (whose T-cells are notoriously difficult to expand *ex vivo*), patients with too few T-cells after conventional chemotherapy, and patients whose T-cells don't expand sufficiently *ex vivo* for any number of reasons, are currently not candidates for CAR T-cell therapy because it is not possible to make autologous products for them. Some of these patients have an extremely high leukemic burden which cannot be reduced with conventional chemotherapy and radiation to low enough levels to allow HSCT. For all of these patients, CAR T-cell therapy with TCR-deficient allogeneic CAR T-cells may be a bridge to treatment that would allow them to survive long enough, be healthy enough, and reduce their leukemic burden enough to receive HSCT as a definitive therapy, even though the allogeneic CAR T-cells would eventually be rejected.

In addition, even when HSCT is possible, relapse after HSCT is a major problem in the treatment of B-cell ALL, and these patients tend to have a poor prognosis.[124] Being able to

augment the GvL effect seen in allogeneic HSCT without increasing the risk of GvHD will significantly improve the outcomes for these patients.[124] An innovative approach to achieve this goal is to manufacture CAR T-cells that lack the endogenous TCR from the HSCT donor's cells. These cells could then be infused after HSCT to attack any leukemic cells that survive the initial treatment, but would not be able to recognize the recipient's cells as foreign to cause GvHD. The TCR knock-out technology could also be applied to other T-cell based immunotherapies such as TCR gene transfer,[125] and may also be an important first step towards understanding the requirements for allogeneic CAR T-cell therapy.

### 3.2 TALEN mRNA generated from pEVL templates exhibits superior knock-out efficiency in human T-cells

Adapted from Grier AE *et al*. 2016. *Mol Ther Nucleic Acids*.

To evaluate the performance of pEVL-derived IVT mRNA in disrupting the endogenous TCR locus in primary human T-cells, ORFs encoding TALENs targeting the TCRα constant region locus were cloned into pEVL-300 and used for IVT mRNA production in parallel with production of TALEN mRNA from a standard circular plasmid. Following electroporation of pEVL-derived TALEN mRNA into primary human T-cells, we observed that rates of CD3 loss, which occur following disruption of the TCRα gene due to the necessity for TCRα holoreceptor/CD3 interaction to support surface expression of CD3, were consistently higher than with equal microgram amounts of enzymatically polyadenylated mRNA generated in parallel (**Figure 3.1**).

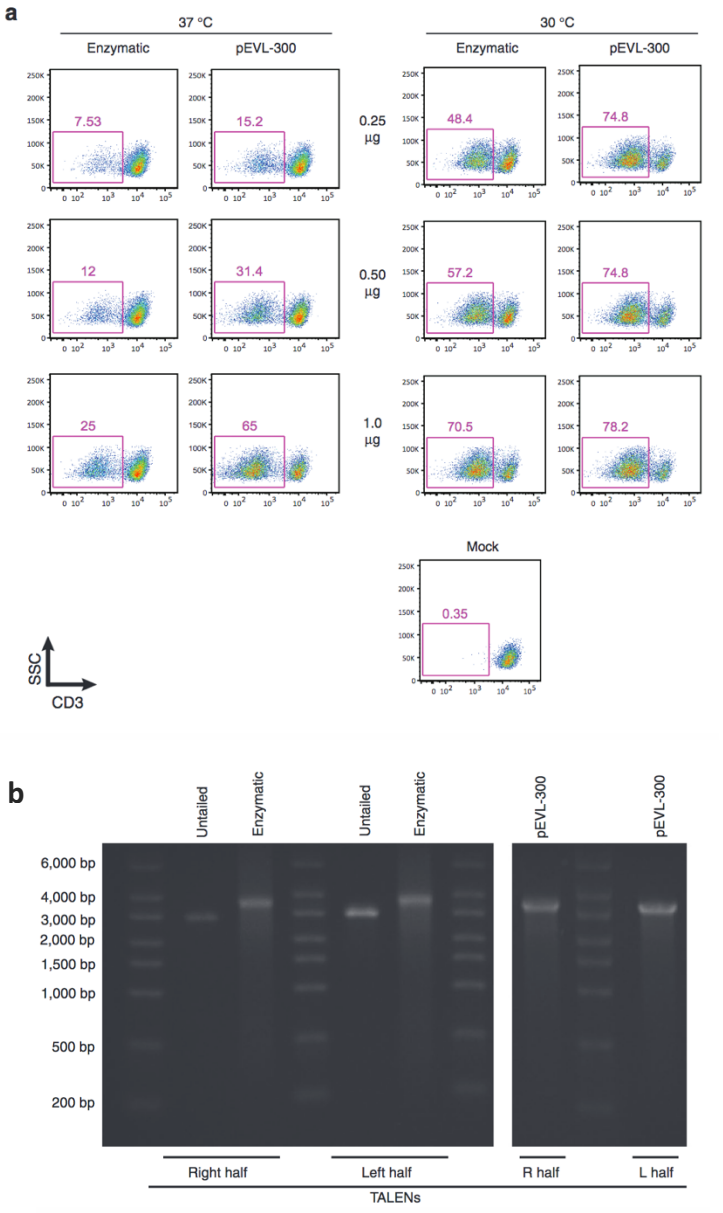


**Figure 3.1 TALEN-mediated TCR knock-out in primary human T-cells using pEVL-encoded mRNA. (a)** pEVL-mediated editing of the TCRα locus with TALEN mRNAs in primary human T-cells. TALENs targeting the constant region of the TCRα locus were each cloned into pEVL-300. After IVT mRNA production, the indicated amounts of mRNA encoding each TALEN half were electroporated into pre-stimulated primary human T-cells. In the left panel, cells were incubated at 37°C immediately following electroporation. In the right panel, cells were incubated at 30°C for 24 hours to increase nuclease protein accumulation after electroporation and then moved to 37°C. At 72 hours post-electroporation, successful TCR knock-out was assayed by flow cytometry for a loss of CD3 expression. **(b)** Representative RNA FlashGels

showing the mRNA transcripts for the left half and right half of the TCRα TALENS produced via enzymatic tailing and from pEVL-300.

This is consistent with the general observation that increased expression of gene editing nucleases results in higher rates of target site modification.[126] In comparing TCRα TALEN-mediated knock-out using enzymatically polyadenylated or pEVL-300 derived mRNA, we found a dose-dependent response of pEVL-derived mRNA that led to substantially higher gene knock-out than enzymatically polyadenylated mRNA (**Fig. 3.1A, left panel**). When the T-cells were incubated at 30°C for 24 hours after electroporation,[127] we again found that we could achieve substantially higher levels of TCR knock-out using pEVL-300 derived mRNA and that highest levels of knock-out were achieved with a quarter the amount of pEVL-derived mRNA compared to enzymatically tailed mRNA (**Fig. 3.1A, right panel**).

### 3.3 Cas9 mRNA generated from pEVL templates exhibits superior CRISPR knock-out efficiency in human T-cells

Adapted from Grier AE *et al*. 2016. *Mol Ther Nucleic Acids*.

As a second evaluation of the performance of pEVL-derived mRNA for gene editing applications, we used CRISPR/Cas9 as an alternative means of deleting the TCR **(Figure 3.2)**. Although TALENs bind and cleave well at the TCRα locus, and have low rates of off-target cleavage, they cannot bind well to 5'-methylated cytosines, which are present in many highly-regulated loci.[128] CRISPR/Cas9, on the other hand, may have higher rates of off-target cleavage, but is not sensitive to methylation.[129] Because of these reciprocal features, we wanted to be

sure that the pEVL system could support the efficient expression of both TALENs and CRISPR/Cas9.

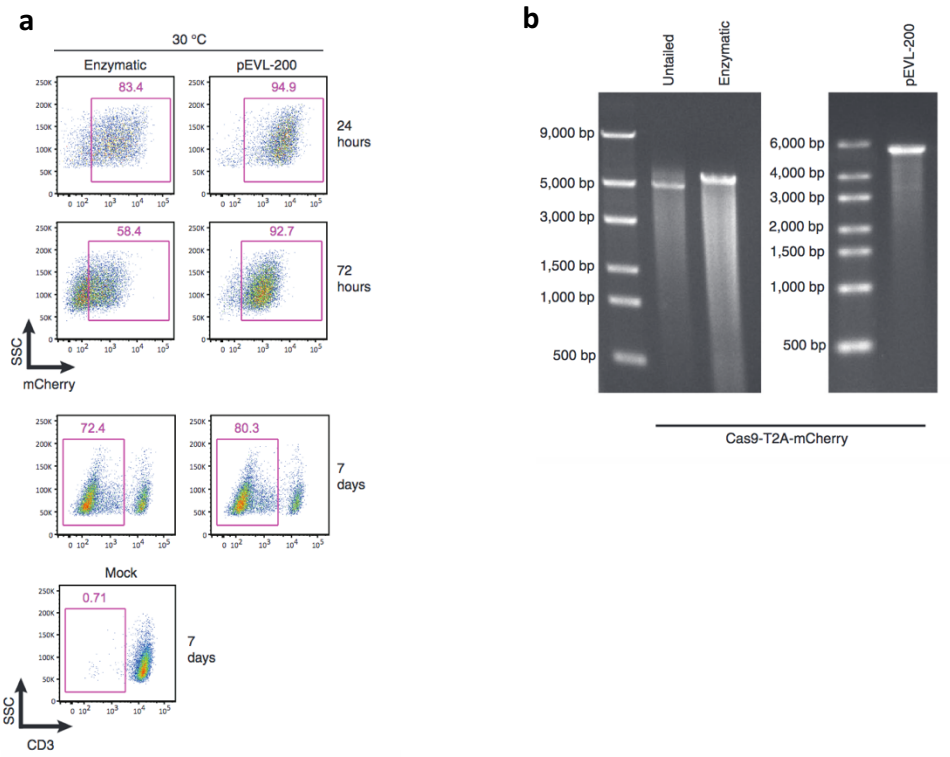


**Figure 3.2 CRISPR/Cas9-mediated TCR knock-out in primary human T-cells using pEVL-encoded mRNA.** **(a)** pEVL-mediated editing of the TCRα locus with CRISPR/Cas9 in primary human T-cells. A Cas9-T2A-mCherry construct was cloned into pEVL-200. After IVT mRNA production, Cas9 was electroporated into pre-stimulated primary human CD4+ T-cells. 3 hours post-electroporation, a CRISPR guide targeting the TCRα constant region was delivered via AAV6 transduction. After electroporation, the cells were incubated at 30°C for 24 hours before being moved to 37°C. At 24 and 72 hours post-electroporation, Cas9 electroporation efficiency was determined by FACS analysis of mCherry fluorescence. After 7 days, successful TCR knock-out was assayed by flow cytometry for a loss of CD3 expression. **(b)** Representative RNA FlashGels showing the mRNA transcripts for Cas9-T2A-mCherry produced via enzymatic tailing and from pEVL-200.

To this end, we cloned the spCas9 nuclease linked by a ribosomal skip sequence (T2A)[130,131] to mCherry into either a circular plasmid vector or pEVL-200, and used mRNAs derived from these vectors to express Cas9 and mCherry in primary human CD4+ T-cells. In our

CRISPR/Cas9 system, after mRNA electroporation of Cas9, we deliver the guide RNA (in this case targeting the TCR$\alpha$ constant region) by transducing the T-cells with an adeno-associated vector (AAV).[132] In using this mRNA that coded for a fluorophore-coupled nuclease, we observed that pEVL-derived mRNA (Cas9-T2A-mCherry) produced populations with a tighter distribution of fluorescence and higher average fluorescence compared to enzymatically polyadenylated mRNA (**Figure 3.2A, top panel**), and that this correlated with an enhanced efficiency of CRISPR/Cas9-mediated gene knock-out (**Figure 3.2A, bottom panel**).

Collectively, these data support the concept that efficiency of nuclease expression is an important determinant of the cleavage activity observed for a nuclease at a genomic target site in a living cell,[126] and that use of mRNA with longer, homogenous poly(A) tails increases the efficiency of gene editing compared to mRNA with standard enzymatic polyadenylation.

### 3.4 Effective guide dosage in CRISPR/Cas9-mediated knock-out can be increased by the addition of "helper proteins" from Adenovirus 5

Adapted from Gwiazda KS, Grier AE, Sahni J, Burleigh SM, Martin U, Yang JG, Popp NA, Krutein MC, Khan IF, Jacoby K, Jensen MC, Rawlings DJ, Scharenberg AM. High Efficiency CRISPR/Cas9-mediated Gene Editing in Primary Human T-cells Using Mutant Adenoviral E4orf6/E1b55k "Helper" Proteins. *Mol Ther*. 2016 Sep 29;24(9):1570-80.

Although the rates of knock-out we achieved at the TCRα locus with the CRISPR/Cas9 system were high enough to proceed with applications that only require a single knock-out, we wanted to increase the knock-out efficiency even further for several reasons. First, the TCRα locus is unique in that one of the alleles is silenced during T-cell development, which artificially inflates the knock-out efficiency seen by flow cytometry since a monoallelic knock-out may be enough to abrogate surface expression of the TCR. Using this system at other loci may require higher levels of DNA cleavage to see the same knock-out percentage by flow cytometry.

Second, one advantage that CRISPR/Cas9 has over TALENs is the ability to multiplex several knock-outs in the same cell populations. Multiplexing with TALENs requires additional mRNA to be electroporated into the cells for each locus, which negatively affects cell viability, but using CRISPR/Cas9, multiple guides can be delivered on a single AAV vector.

To achieve knock-out at multiple loci in each cell across a population, the overall rates of biallelic knock-out at each locus must be maximized. In our mRNA/AAV delivery system for CRISPR/Cas9, the efficiency of AAV transduction is a key limiting factor. This is known to be subject to restriction at the cell entry stage by surface receptor expression binding properties of the capsid,[133–135] and by multiple mechanisms following cell entry.[136–140] It has been previously shown that expression of E4orf6 and E1b55k proteins from adenoviral serotype 5 (Ad5) is effective at relieving post-entry restrictions on AAV expression in cell lines, among them genome concatamerization by DNA damage response proteins, activation of cell cycle DNA damage checkpoints, and pro-apoptotic DNA damage signaling.[136–140] Since our system already involved electroporation of Cas9 mRNA, we decided to deliver the Ad5 E4orf6/E1b55k to T-cells as mRNAs in the same electroporation step as the Cas9, with the goal of transiently relieving post-entry restriction of AAV-based expression (Figure 3.3). We found that following mRNA-based co-expression of E4orf6/E1b55k in primary T-cells (but not either protein alone; data not shown), we observed a four-log increase in GFP mean fluorescence intensity (MFI), and an 8-fold increase in GFP expression, driven from an AAV vector encoding a promoter/GFP cassette (Figure 3.3A, left and bottom panels), without compromising the rate of cell expansion (Figure 3.3B).

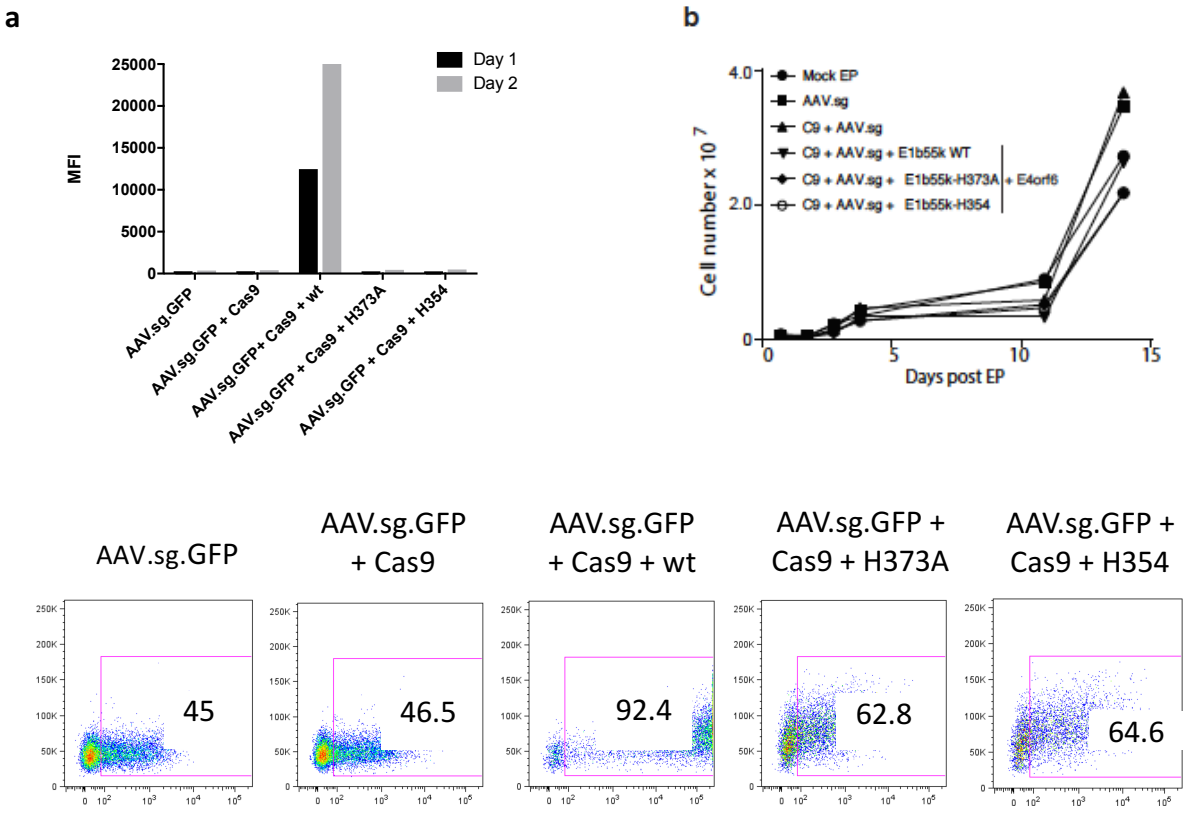


**Figure 3.3 Enhanced AAV-mediated gene expression in primary human T-cells using adenoviral E4orf6/E1b55k proteins to relieve post-entry AAV restriction mechanisms. (a)** AAV-mediated GFP expression following relief of post-entry AAV restriction by E4orf6/E1b55k. Primary CD4+ T-cells were electroporated with mRNA encoding adenoviral serotype 5 E4orf6/E1b55k (0.33 μg each), rested for 2-4 hours, then transduced with AAV driving GFP expression. Cells were placed in culture for the indicated periods of time, following which the cells were collected and analyzed for GFP expression by flow cytometry. **(b)** Expansion of cell populations following the indicated exposure to E4orf6/E1b55k mRNA transfection and AAV transduction, following the same protocol as described in (a).

The ability of E4orf6/E1b55k proteins to enhance AAV expression in cultured cell models has been reported to depend on their capacity to target the Mre11/Rad51/NBS1 DNA repair complex (MRN) for degradation, thus allowing incoming AAV genomes to escape intra-nuclear detection and silencing.[139,141–143] To determine if this same mechanism applied to primary human T-cells, for which there is little published data as a substrate for AAV transduction, we

compared AAV-driven gene expression alone or following transient expression of wild type E4orf6/E1b55k proteins or E4orf6/E1b55k-H373A and E4orf6/E1b55k-H354 mutants (**Figure 3.3A**). Both of these mutants has been shown to have largely lost the capacity for inducing degradation of MRN, whilst fully preserving other functions of wild type E4orf6/E1b55k.[143] As assessed by GFP MFI, these E1b55k mutants were markedly less efficient at relieving post-entry restrictions on AAV expression than WT E4orf6/E1b55k. However, replicate experiments using the E1b55k-H373A mutant, analyzed at a smaller scale, demonstrated that E4orf6/E1b55k-H373A expression was able to support a level of GFP expression significantly greater (1.58±0.09-fold at 96 hours) than that observed in the absence of helper protein expression. This is consistent with the idea that E1b55k-H373A possesses a residual capacity to relieve post-entry transduction or expression restrictions (**Figure 3.4**).

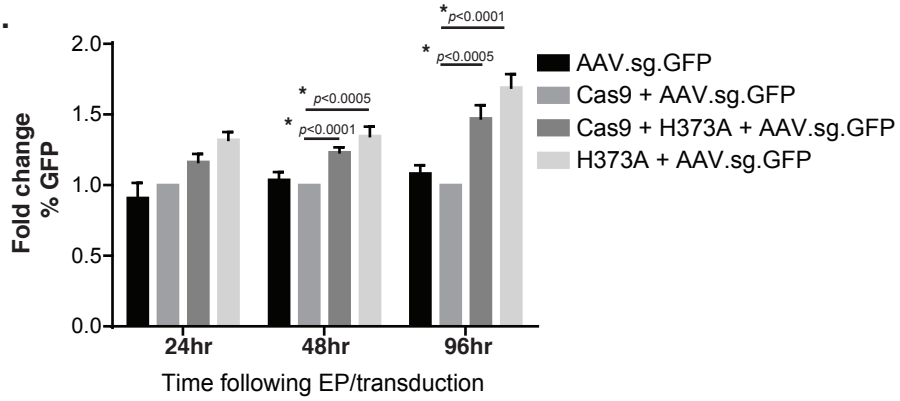


**Figure 3.4 Effect of E4orf6/E1b55k mutants on AAV-driven GFP expression.** Primary CD4+ or CD3+ human T-cells were electroporated with mRNA encoding Cas9-2A-mCherry proteins (1μg) and either WT or the indicated E4orf6/E1b55k mutants (0.03ug each), rested for 2-4 hours, and transduced with AAV driving guide expression and GFP. Cells were placed in culture for the indicated periods of time, following which the cells were collected and analyzed for GFP expression by flow cytometry and quantified. Graph represents n=5-6 independent experiments.

### 3.5 H373A and H354 mutant E4orf6/E1b55k expression enhance CRISPR-mediated knock-out in primary human T-cells

Adapted from Gwiazda KS *et al.* 2016. *Mol Ther*.

Based on the capacity of E4orf6/E1b55k proteins to enhance AAV-driven GFP expression in the analyses above, we hypothesized that their transient expression would similarly enhance the level and/or duration of guide RNA expression from a polIII-driven U6 promoter/guide RNA cassette incorporated into an AAV genome, and thus potentially enhance Cas9-mediated gene disruption efficiency by the mRNA/AAV system. To test this hypothesis, we expressed wild type E4orf6/E1b55k proteins using the mRNA/AAV co-delivery protocol by including their respective mRNAs with Cas9 in the electroporation step, followed by transduction of the cells with an AAV vector encoding both a TCRα guide RNA and a promoter/GFP expression cassette. To gain information on the influence of specific biochemical activities attributed to E4orf6/E1b55k complexes on gene editing outcome, we also expressed the H373A and H354 mutants, and compared the TCR knock-out efficiency among the various contexts (**Figure 3.5**).

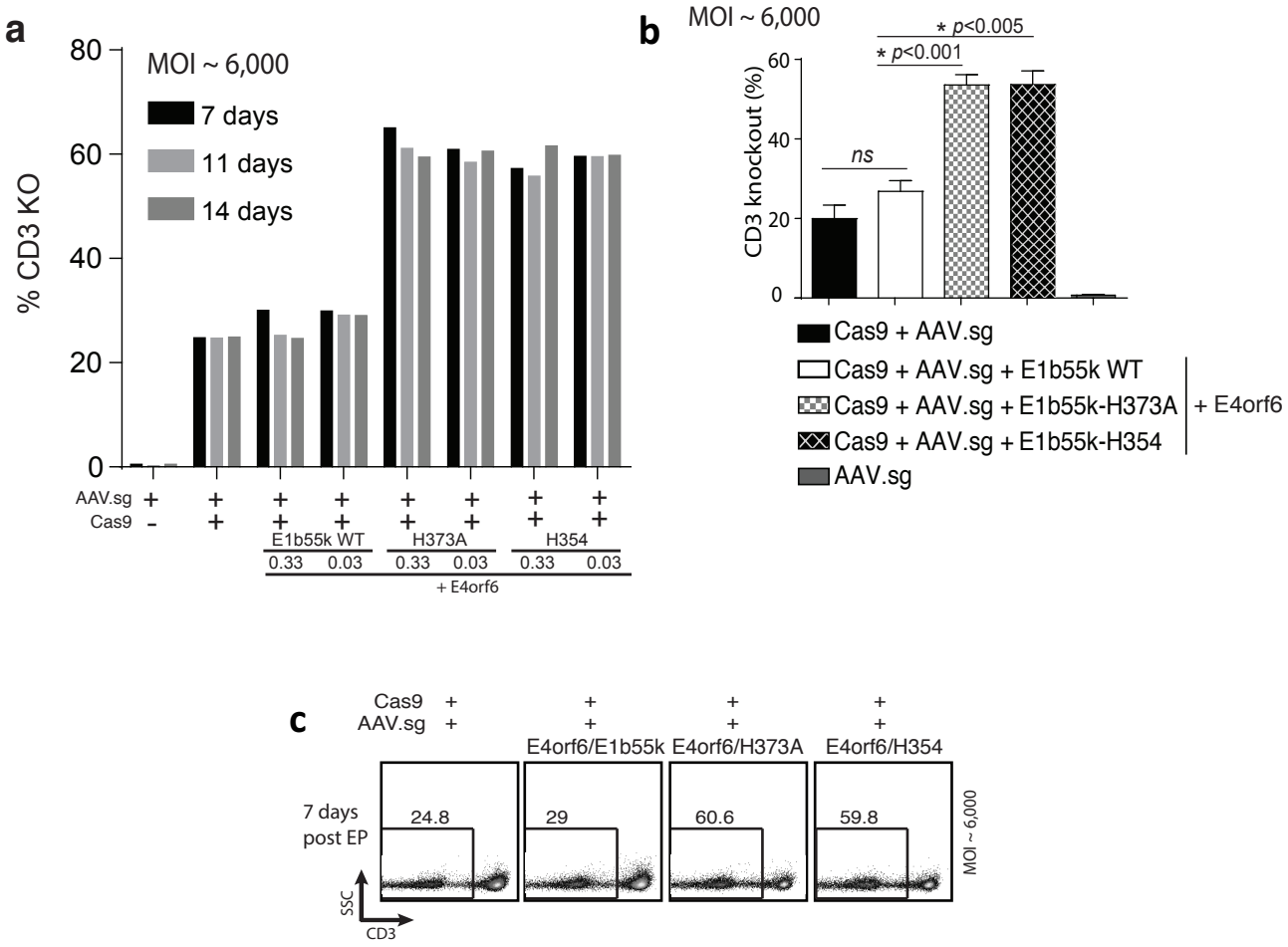


**Figure 3.5. Enhanced CRISPR-mediated gene knock-out in primary human T-cells through use of adenoviral E4orf6/E1b55k proteins. a and c).** Representative experiment indicating primary CD4+ T-cells electroporated with mRNA encoding Cas9-T2A-mCherry (1μg), E4orf6/E1b55k (WT), or the indicated mutants (at 0.33μg or 0.03μg each), rested for 2-4 hours, and transduced with AAV driving TCRα guide expression. Cells were placed in culture, following which the cells were collected and analyzed for CD3 expression by flow cytometry at the indicated time-points following EP/transduction. **a)** quantification of CD3 knock-out; **c)** representative flow plots from a subset of the experiment at seven days post EP/transduction. **b)** Quantification of n=3-4 independent experiments at AAV MOI 6000 indicating that both E1b55k H373A and H354 mutants significantly increase CRISPR-mediated TCRα knock-out, quantified by CD3 staining at seven days post EP/transduction. Primary human CD4+ or CD3+ T-cells were used.

Despite the marked increase in AAV-based GFP expression we observed earlier, we observed only a moderately increased level of TCRα knock-out with expression of wildtype Ad5 helper protein (**Figure 3.5**). However, while expression of E4orf6 with E1b55k-H373A and H354 mutants produced the expected much smaller effects on GFP expression (i.e. **Figure 3.4**), unexpectedly, substantial increases in TCRα knock-out efficiency were also observed (**Figure 3.5**). This suggests that despite their inability to fully relieve post-transduction restrictions on AAV gene expression, these E1b55k mutants retained residual biochemical activities that were sufficient to markedly enhance the overall efficiency of gene knock-out achievable with the mRNA/AAV delivery approach.

To evaluate whether expression of the E4orf6/E1b55k H373A mutant was detrimentally influencing T-cell phenotype or signaling properties over the course of the editing process, we assessed expression of a panel of surface markers and measured PHA-induced calcium signaling at two weeks post-editing. Flow cytometric assessment of cell surface markers that define naïve and memory T-cell populations showed no differences between edited vs. unedited populations (**Figure 3.6a**). Though this particular donor has high levels of $CD45RA^{+}CD45RO^{+}$ double positive cells, this was seen consistently throughout the engineering process. It did not vary in different experimental conditions, and is therefore most likely due to the donor's cellular composition rather than the genomic editing. Similarly, the signaling properties of edited T-cells were as expected, with those cells exhibiting a loss of surface TCR following TCRα gene editing showing a loss of capacity to mobilize $Ca^{2+}$ in response to stimulation with PHA relative to cells retaining surface TCR (**Figure 3.6b**).

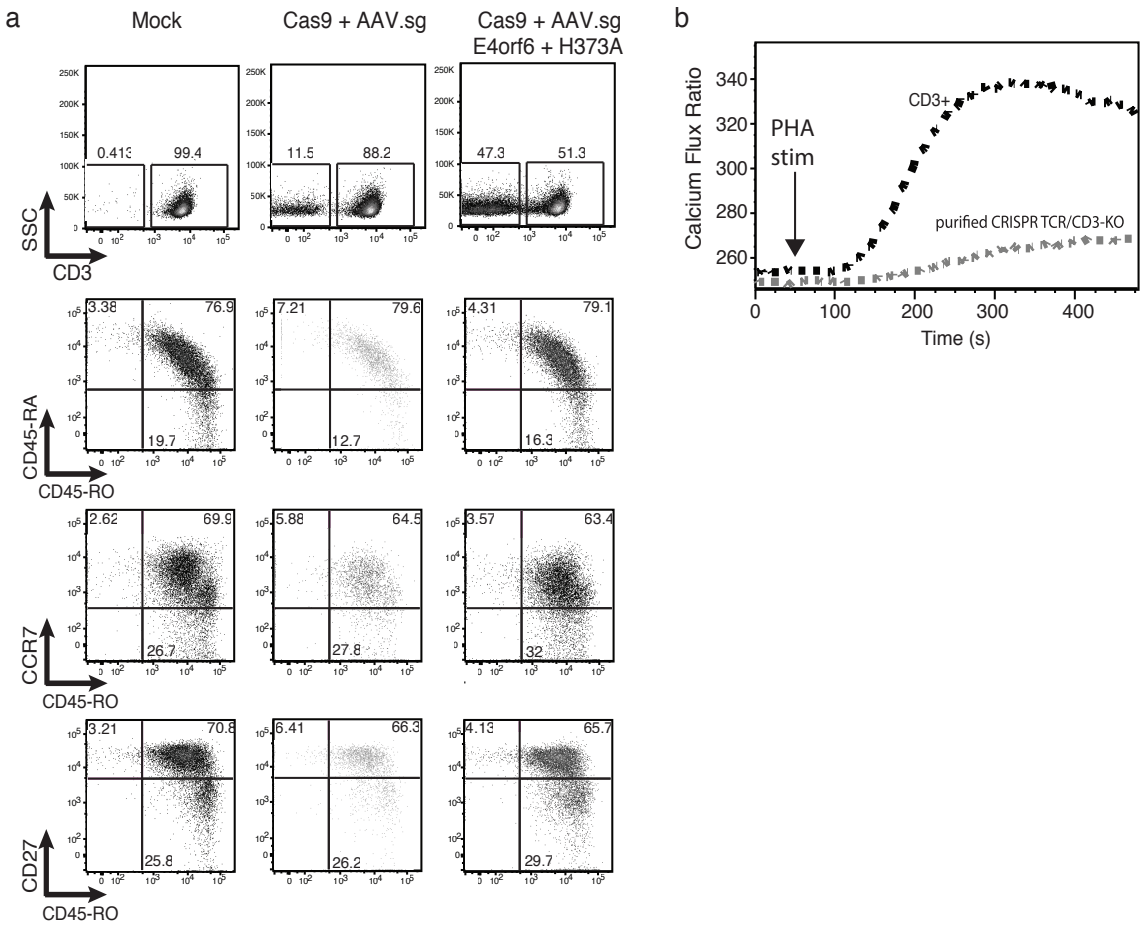


**Figure 3.6: Edited primary T-cells with E4orf6/E1b55k H373A exhibit normal surface marker phenotype and expected $Ca^{2+}$ signaling. (a)** T-cells edited using mRNA/AAV co-delivery exhibit normal surface marker phenotype. Representative flow plots of primary CD4+ T-cells that were electroporated with mRNA encoding Cas9-2A-mCherry proteins (1μg) along with E4orf6/E1b55k H373A proteins (0.03μg each) and transduced with AAV driving TCRα guide expression. Cells were placed in culture and assessed for surface protein markers 16-20 days following EP/transduction by flow cytometry. n=2 independent experiments. **(b).** Human T-cells rendered TCR-deficient via mRNA/AAV co-delivery are deficient in TCR signaling**.** Primary CD4+ T-cells were electroporated with mRNA encoding Cas9-T2A-mCherry proteins (1μg) along with E4orf6/E1b55k H373A (0.03μg each), rested for 2 hours, and transduced with AAV driving TCRα guide expression. Nine days following EP/transduction, CD3**-** cells were purified using CD3 microbeads and placed back in culture. Cells were allowed to expand for ten days, following which they were collected, and analyzed for anti-CD3-stimulated calcium signaling by flow cytometry. 200μg/mL PHA was used to stimulate the cells. Five million cells per condition were used. KO, knock-out.

### 3.6 Materials and Methods

*Cloning of CRISPR associated protein 9 (Cas9) and TCRα guides:*

Cas9 expression construct was obtained from Addgene (plasmid #41815). To ensure nuclear expression of Cas9 in primary human T-cells, Nuclear Localization Signals (NLS's) were added at both 5' and 3' ends (2X-NLS). To track transfection efficiency, Cas9 was fused in-frame with T2A-mCherry and cloned into an in-house modified version of pUC57 with a T7 promoter called pWNY to obtain pWNY-2X-NLS-Cas9-T2A-mCherry. Subsequently, 2X-NLS-Cas9-T2A-mCherry was spliced from pWNY and cloned into pEVL-200.

Guides targeting the constant region of TCRα were designed using an online CRISPR design tool (http://crispr.mit.edu). Guides were designed with a U6 promoter and ordered as gblocks (IDT, San Jose, CA). Subsequently, the gblock comprising U6 promoter and sgRNA (crRNA+tracrRNA) was cloned into a self-complementary (sc) AAV vector backbone, and checked for maintenance of intact ITRs. Four different G-block-guide constructs generated in this way were used for AAV6 synthesis, and following a series of pilot experiments, a best-performing guide was chosen for further comparative analyses. The sequence of this guide is TCAAGAGCAACAGTGCTG.

*Production of IVT mRNA:*

For the TCRα constant region TALEN constructs, inserts containing a T7 promoter, Kozak sequence, and the TALEN ORF were cloned into pEVL-300 through pEVL-500. The target site for the TCRα constant region TALEN is tTGTCCCACAGATATCCagaaccctgaccctgCCGTGTACCAGCTGAGa.[144] The TALEN and Cas9 pEVL

constructs were digested with BsaI (NEB or Thermo Scientific) to create a template with a terminal poly(A) tail. Templates were simultaneously digested with at a site upstream of the T7 (XbaI or SpeI, NEB or Thermo Scientific) to reduce the overall size of the template-containing fragment and enhance purification. After checking the completeness of the digest on a 1% agarose gel, the digested DNA was purified on a silica column and eluted in water or 10 mM Tris. IVT with ARCA capping was carried out using the mMessage mMachine T7 Ultra kit (Life Technologies, Carlsbad, CA) per the manufacturer's directions with 200-1 000 ng of the T7 to poly(A) template fragment; IVT reactions were routinely extended to 150 min. Additional DNAse and/or incubation time was used to counterbalance any increased amount of template DNA in the reaction (e.g. double DNAse or double incubation time for double template). The reaction was cleaned up after DNAse treatment using the RNeasy Mini kit (Qiagen) following the manufacturer's directions. RNA quality was determined by NanoDrop spectrophotometry (Thermo Scientific) and gel analysis with the FlashGel RNA system (Lonza). All mRNA was aliquoted in single use aliquots and stored at -80°C.

*Production of Recombinant AAV6 vectors:*

AAV stocks were produced by triple transfection of AAV vector, serotype helper and Adenoviral helper (HGT1-Adeno) plasmids in HEK293T cells. Transfected cells were collected 48 hrs later, lysed by freeze-thaw, benzonase treated and purified over iodixanol density gradient as previously described.[145] Titers of the viral stocks were determined by qPCR of AAV genomes and ranged from $10^{10}$-$10^{12}$/ml.[146]

*mRNA electroporation of primary human T-cells:*

Freshly isolated primary human T-cells were stimulated with αCD3/αCD28 microbeads (Dynal, Thermo Scientific) in RPMI with 10-20% FBS, 2.5% HEPES, and 1% L-glut or Glutamax (Thermo Scientific). For isolated pan T-cells, IL-2 (Chiron, Emeryville, CA) and IL-15 (Miltenyi, San Diego, CA) at final concentrations of 5 ng/mL IL-2 and 1 ng/mL IL-15 were added. For isolated CD4+ T-cells, IL-2, IL-7 (Peprotech, Rocky Hill, NJ), and IL-15 were added at final concentrations of 50 ng/mL IL-2, 5 ng/mL IL-7, 5 ng/mL IL-15, and 2-mercaptoethanol (Sigma-Aldrich, St. Louis, MO) was added at a final concentration of 55 µM. After 48-72 hours, the stimulation beads were removed, and the T-cells were rested for 1-16 hours in complete media with cytokines. If the initial stimulation was carried out for more than 48 hours, half of the media was replaced with fresh media with cytokines at 48 hours post-stimulation. After resting, the T-cells were washed in PBS and resuspended at $3x10^7$ cells/mL in Neon Electroporation system Buffer T (Life Technologies) with 0.25-2 µg mRNA per 300,000 cells. Electroporation was carried out in a 10 µl tip on the Neon electroporation system (Life Technologies) at 1400V, 10ms, and 3 pulses. Immediately following electroporation, cells were resuspended in complete T-cell media with cytokines (as above). Cells were either placed in a 37°C incubator or in a 30°C incubator for 24 hrs and then moved to a 37°C incubator. A cold-shock step of this nature has been observed to increase the amount of protein per cell for the period when the mRNA is present and in turn, the gene editing efficiency. [116–119] [147] For CRISPR-Cas9 experiments, cells were rested for 3 hours after electroporation and then transduced with AAV containing the CRISPR guide at a constant 10% culture volume, equating to an MOI of approximately $1.33x10^4$.

*Analysis of calcium signaling:*

$5x10^6$ cells were used per sample. Cells were washed in HBSS (with $Ca^{2+}$ and $Mg^{2+}$) (Thermofisher), loaded with 30uM Indo-1 AM (Molecular Probes, Life Technologies) in HBSS and incubated at 37 $^oC$ for 30 min, washed twice, and re-suspended in buffer. Baseline flow was obtained for 30sec, after which cells were stimulated with 200ug/mL PHA to stimulate T-cells, and data was collected for 5min.

*Flow Cytometry:*

Expression of the encoded protein was assayed by flow cytometry at 24-168 hours post-electroporation on an LSRII flow cytometer (BD Biosciences, San Jose, CA). TCR knock-out by TALEN or CRISPR was assayed by loss of TCR expression 3-7 days post-electroporation after staining with anti-CD3 (clone HIT3a, direct Alexa-488 or PerCP-Cy5.5 conjugate, BioLegend, San Diego, CA). Data was analyzed using FlowJo software (Treestar, Ashland, OR). Cells were gated on live singlet cells based on the forward and side scatter.

*Statistical Analysis:*

Statistical analyses were performed with Prism 6 (GraphPad Software). Data is shown as mean +/- SEM unless otherwise noted. Tests of statistical significance were performed using an unpaired two-tailed Student's *t*-test with Welsh's correction for unequal standard deviations when appropriate.

# 4. Functional effects of endogenous TCR knock-out on CD19 CAR T-cells

## 4.1 Introduction

After developing both TALEN- and AAV-mediated systems to delete the TCR in individual and multiplex T-cell editing applications, our next step was to incorporate this knock-out into the lentiviral transduction process used to create CAR T-cells for clinical use. Our goals included minimizing the total culture time needed to make a product, keeping the hands-on/open-system steps to a minimum, and reducing overall cell divisions to have the least-differentiated cells possible for patient infusion.

Previously, Torikai et al. reported TCR knock-out via zinc finger nucleases in CD19 CAR T-cells containing the CD28 costimulation domain, and showed that the $TCR^-$ CAR T-cells were able to proliferate in response to their target antigen, but not in response to CD3 stimulation.[148] They went on to show that the $TCR^-$ CAR T-cells performed as well as their $TCR^+$ counterparts in an *in vitro* cytotoxicity assay.[148] However, they did not test their cells *in vivo*. We chose to carry out our own *in vitro* analyses, and then test our TALEN-mediated TCR-deficient CAR T-cells alongside TCR-sufficient ones *in vivo* in an orthotopic murine tumor model, since tonic signaling through the TCR may be important for CAR T-cell engraftment. In addition, seemingly small details in the design or manufacturing process can lead to differences in the phenotype, differentiation state, homogeneity, expansion potential, survival, and tumor eradication potential of the resulting CAR T-cells. Studying the phenotype, function, and signaling of $TCR^-$ CAR T-cells will lead to a better understanding of CAR function and whether there is any interaction between the CAR and the endogenous TCR or its related structures.

## 4.2 Lentiviral CAR transduction can be combined with TALEN-mediated TCR knock-out in primary human T-cells

CD4 and CD8 T-cells (central memory or total) were isolated from healthy donors, stimulated, and transduced with a lentivirus encoding an $\alpha$CD19 CAR with an IgG4 hinge spacer

and a 4-1-BB costimulatory domain (as shown in **Figure 1.1c**), and then transfected by mRNA electroporation with the TALEN pair targeting the TCRα chain constant region. This resulted in up to 60% of CD4 and CD8 T-cells expressing the CAR but lacking the endogenous TCR **(Figure 4.1)**. Overall transduction rates were 65-70% and overall knock-out rates were 80-88% **(Figure 4.1)**.

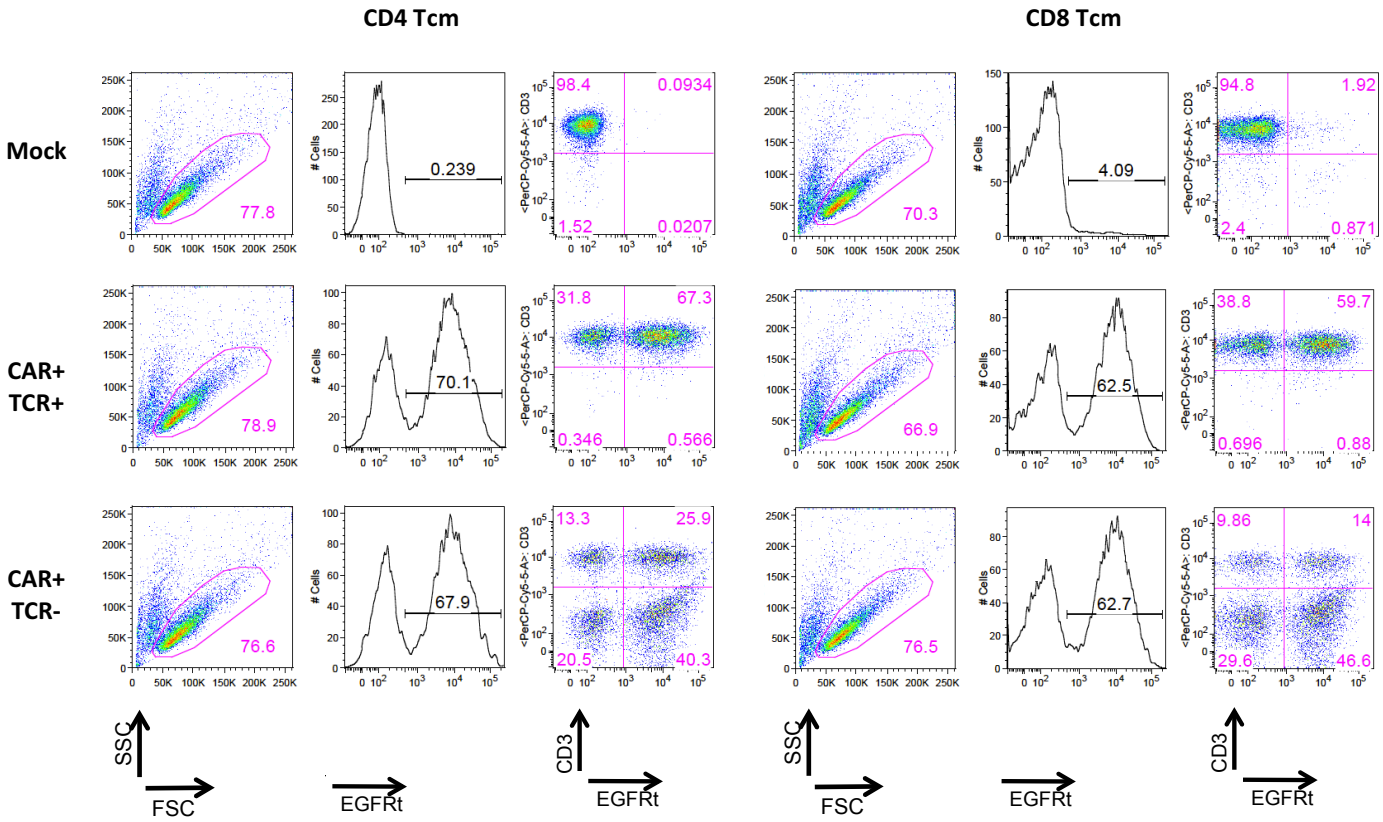


**Figure 4.1**. **Generation of TCR- and TCR+ CD19 CAR T-cells.** Central memory (CD45RA-, $CD62L^+$) CD4 and CD8 T-cells were isolated from a healthy donor and stimulated with αCD3/αCD28 beads on D0. On D1, CD4 and CD8 the cells were separately transduced with a lentivirus expressing an αCD19 CAR with an IgG4 hinge spacer and 4-1BB costimulatory domain, as well as a truncated EGFRt molecule for selection and ablation if necessary. On D3, the cells were separately transfected via mRNA electroporation with both halves of a TALEN targeting the TCRα constant region. On D7, up to 60% of both CD4 and CD8 T-cells were $CAR^+$ ($EGFRt^+$) and $TCR^-$.

### 4.2 Endogenous TCR knock-out does not impact *in vitro* CAR T-cell growth, cytokine production, or cytotoxicity.

To determine whether TCR knock-out negatively impacts CAR T-cell viability or proliferation potential, TCR- and TCR+ CAR T-cells were co-cultured with CD19+ target cells for 14 days. Over this time, both TCR+ and TCR- CAR T-cells expanded >400-fold **(Figure 4.2)**.

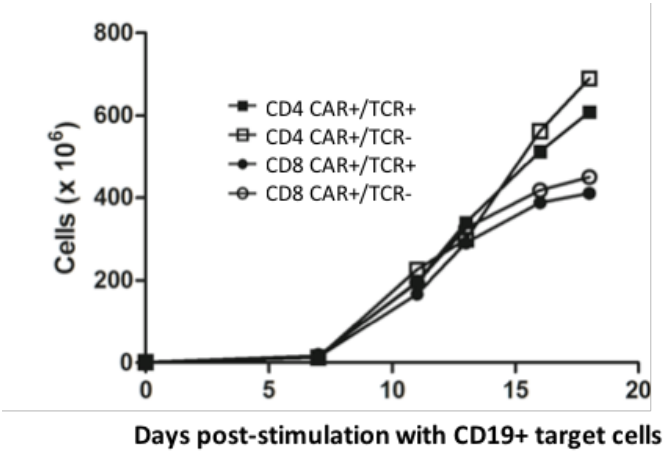


**Figure 4.2. TCR-deficient CAR T-cells expand well *in vitro*.** After the initial bead-based expansion, CD4 and CD8 TCR+ and TCR- CAR T-cells were sorted and each cultured separately with CD19+ target cells (TM-LCL) in IL-2/IL-15. Over 18 days, each population expanded at least 400-fold and there were no major differences seen between TCR+ and TCR- CAR T-cells.

Next, TCR+ and TCR- CAR T-cells were stimulated with various target cells to examine whether TCR knock-out affects cytokine release. There were no major differences in cytokine production between TCR+ and TCR- cells when stimulated with TM-LCL cells (positive control), K562 parental cells (negative control), Raji cells (B-cell lymphoma cell line), or K562+CD19 cells (target cell expressing CD19) (**Figure 4.3**).

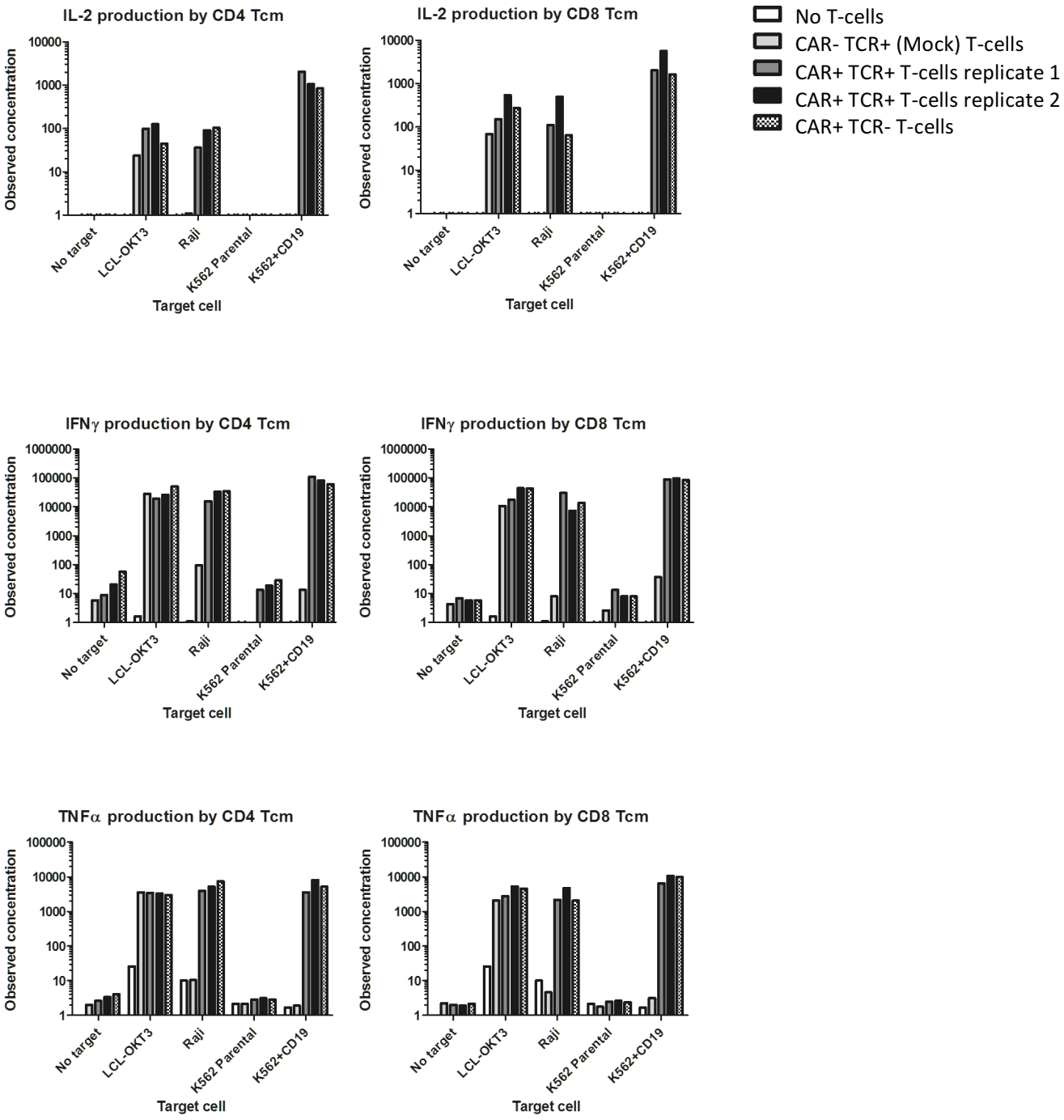


**Figure 4.3: TCR$^-$ and TCR$^+$ CD4 and CD8 Tcm CAR T-cells produce cytokines equally in response to stimulation by target cells.** TCR+ and TCR- CD4 and CD8 Tcm CAR T-cells were cultured with various target cells for 24 hours. The supernatant was then collected and cytokine production was measured using a cytometric bead array. Target cells either expressed CD19 (LCL-OKT3, Raji, and K562 + CD19) or did not express CD19 (K562 Parental). Rates of IL-2, IFNγ, and TNFα production were similar between TCR+ and TCR- cells.

Finally, we assessed whether knock-out of the endogenous TCR would have any effect on the *in vitro* cytotoxicity of CAR T-cells. Over four hours, there were no differences in cytotoxicity between TCR-sufficient and TCR-deficient CD19 CAR T-cells, both CD4 and CD8, across a variety of CD19+ target cells **(Figure 4.4)**. The CD4 T-cells do exhibit cytotoxicity, although at lower levels than the CD8 T-cells, which is in line with the growing number of reports that human CD4 CTLs exist both *in vitro* and *in vivo*.[149,150]

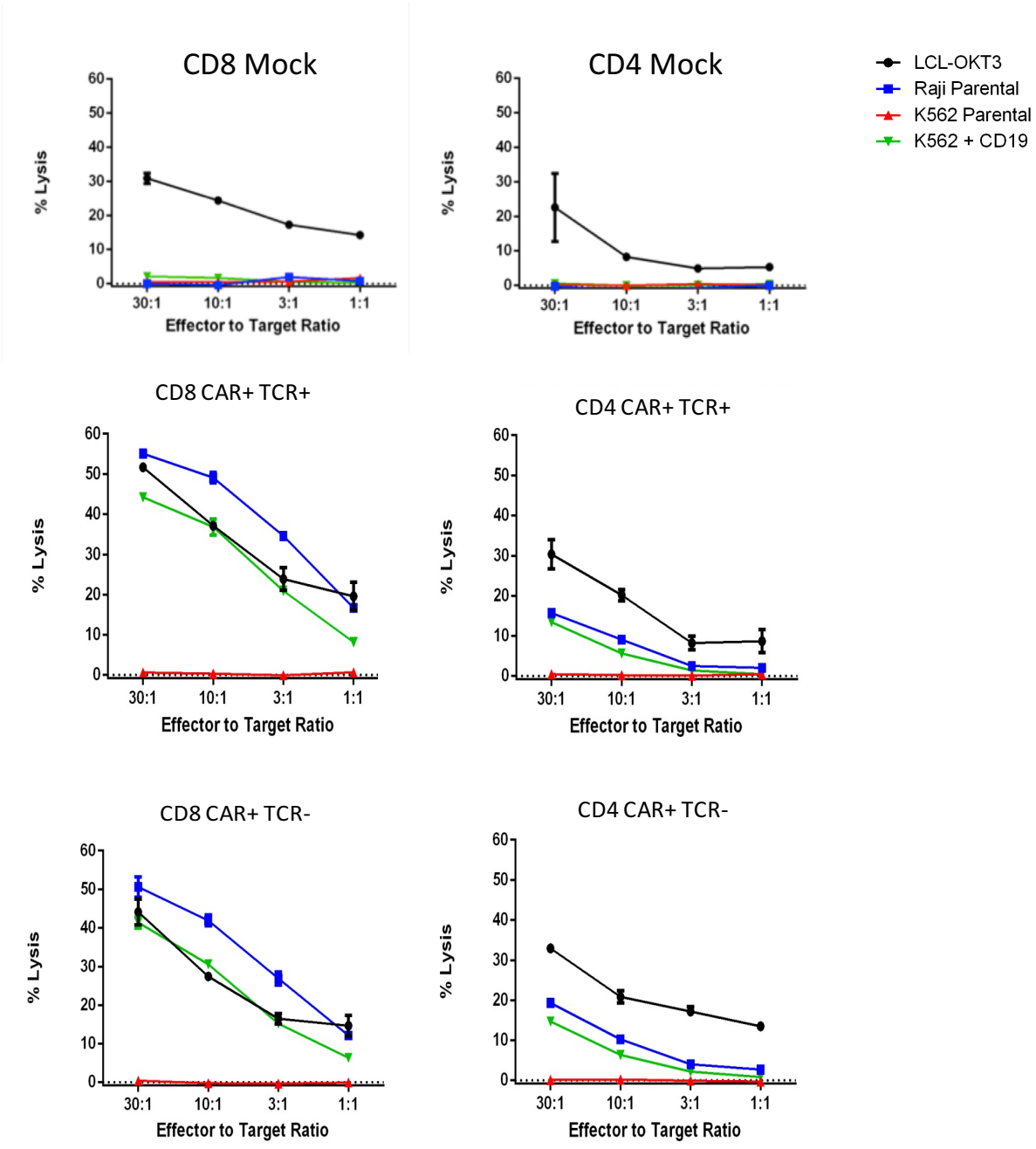

**Figure 4.4. TCR- and TCR+ CD4 and CD8 Tcm CAR T-cells kill target cells equally well *in vitro*.** TCR+ and TCR- CD4 and CD8 Tcm CAR T-cells were cultured with Chromium-51 labeled target cells for 4 hours. Target cells either expressed CD19 (LCL-OKT3, Raji, and K562+CD19) or did not express CD19 (K562 Parental). Across multiple effector:target ratios, there was no difference between TCR+ and TCR- CAR+ T-cells in the percent of target cells that were lysed.

### 4.3 Endogenous TCR knock-out does not impair CD19 CAR T-cell tumor eradication *in vivo*.

Tumor eradication *in vivo* requires many activities of CAR T-cells, both CD4s and CD8s. They must engraft in the mouse model or patient, traffic to the site(s) of the tumor, expand to very high numbers, kill the tumor cells, and survive long enough to eradicate all of the tumor cells. Removal of the endogenous TCR could potentially inhibit many of these activities. CAR T-cell function *in vivo* is dependent on the presence and function of both CD4 and CD8 T-cells,[4] and alterations in one or both of these subsets due to TCR knock-out could disrupt this cooperation. In addition, signaling downstream of the CAR is similar to that downstream of the TCR, and it is not known whether there are interactions between the two that may be disrupted by removal of the TCR.

To test the effect of TCR gene disruption on CAR T-cell function *in vivo*, we injected purified CD4 and CD8 CD19 CAR T-cells in a 1:1 ratio into NSG mice that had been previously injected with Raji tumor cells to establish a disseminated tumor. In a preliminary study, TCR-sufficient and TCR-deficient CAR T-cells eradicated the tumor equally, while mock T-cells did not **(Figure 4.5)**.

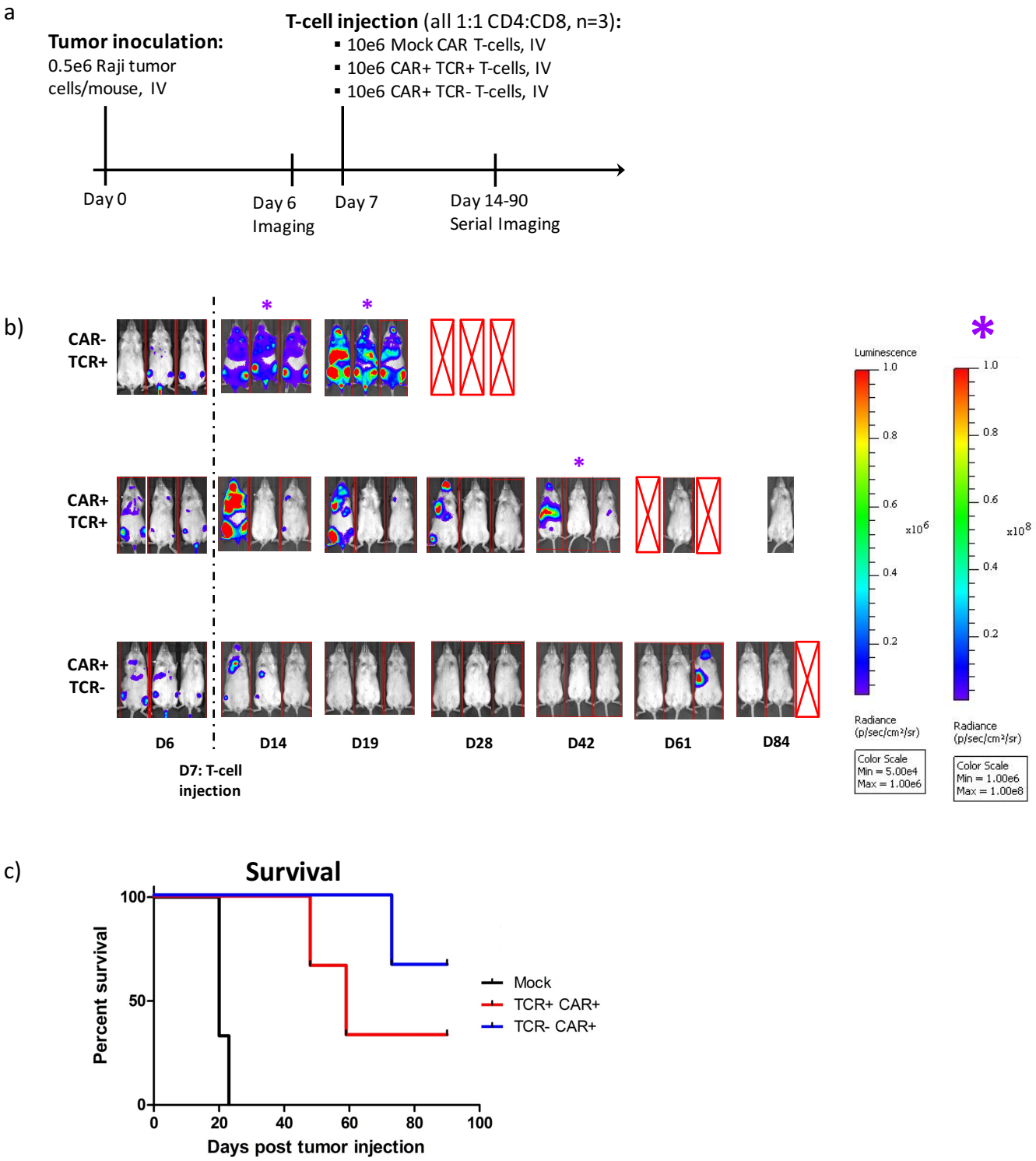


**Fig 4.5. TCR$^-$ and TCR$^+$ CD19 CAR T-cells kill target cells equally well *in vivo*.** Raji tumor cells expressing firefly luciferase (ffluc) were injected IV into NSG mice to establish disseminated tumor. One week later, mice were injected with luciferin, the substrate for ffluc, and imaged to verify tumor engraftment. Mock T-cells, TCR-deficient CAR T-cells, and TCR-sufficient CAR T-cells were then injected into different groups of mice with similar tumor engraftment in a 1:1 ratio of CD4 to CD8 T-cells. Mice were then injected

with luciferin and imaged serially on a biophotonic imaging system to determine tumor progression or regression. **a)** Schematic of experimental procedure. **b)** Biophotonic images of tumor progression/regression. Asterisk denotes images taken with a wider scale due to image saturation. **c)** Kaplan-Meier survival plot comparing each group. While mice receiving mock T-cells succumbed to disease within 3 weeks, survival rates for mice receiving TCR-sufficient CAR T-cells or TCR-deficient CAR T-cells were equal and greatly increased over those receiving mock T-cells.

## 4.4 Materials and Methods

*Cell lines:*

Raji and K562 cell lines were obtained from the ATCC. TM-LCL is a $CD19^+$ EBV-transformed lymphoblastoid cell line (LCL) that has been optimized for use as a feeder cell for T-cell culture. Cell lines were cultured in RPMI-1640 medium containing 10% FBS, 1% L-glutamine, 2.5% HEPES. K562 cells were transduced with retroviruses that encode CD19, and selected to purity by cell sorting for expression of CD19.

*Collection and separation of healthy donor T-cells:*

Blood samples were obtained from healthy donors under protocols approved by the Fred Hutchinson Cancer Research Center Institutional Review Board or the Seattle Children's Hospital Institutional Review Board. PBMCs were isolated by centrifugation of whole blood using Histopaque-1077 (Sigma-Aldrich), and washed in PBS. $CD4^+$ and $CD8^+$ cell fractions were purified using human CD4 or CD8 T-cell isolation kits (Miltenyi Biotec) on the AutoMACS mAbs conjugated to paramagnetic beads (Miltenyi Biotec).

*Production of IVT mRNA:*

For TALEN constructs, inserts containing a T7 promoter, Kozak sequence, and the TALEN ORF were cloned pEVL-300. The sequence of the T7 promoter/spacer/Kozak sequence is: TAATACGACTCACTATAGGGAGAgcggccgctttttcagcaagattaaGCCGCCACCATGGCG. The target site for the TCR$\alpha$ constant region TALEN is tTGTCCCACAGATATCCagaaccctgaccctgCCGTGTACCAGCTGAGa.[144] TALEN constructs were digested with BsaI (NEB or Thermo Scientific) to create a template with a terminal poly(A) tail. Templates were simultaneously digested at the SpeI (NEB or Thermo Scientific) site upstream of the T7 to reduce the overall size of the template-containing fragment and enhance purification. After checking the completeness of the digest on a 1% agarose gel, the digested DNA was purified on a silica column and eluted in water or 10 mM Tris. IVT with ARCA capping was carried out using the mMessage mMachine T7 Ultra kit (Life Technologies, Carlsbad, CA) per the manufacturer's directions with 200-1,000 ng of the T7 to poly(A) template fragment; IVT reactions were routinely extended to 150 min. Additional DNAse and/or incubation time was used to counterbalance any increased amount of template DNA in the reaction (e.g. double DNAse or double incubation time for double template). The reaction was cleaned up after DNAse treatment using the RNeasy Mini kit (Qiagen) following the manufacturer's directions. RNA quality was determined by NanoDrop spectrophotometry (Thermo Scientific) and gel analysis with the FlashGel RNA system (Lonza). All mRNA was aliquoted in single use aliquots and stored at -80°C.

*mRNA electroporation of primary human T-cells:*

Freshly isolated primary human T-cells were stimulated with αCD3/αCD28 microbeads (Dynal, Thermo Scientific) in RPMI with 10% FBS, 2.5% HEPES, and 1% L-glutamine (Thermo Scientific). For isolated pan T-cells, IL-2 (Chiron, Emeryville, CA) and IL-15 (Miltenyi, San Diego, CA) at final concentrations of 5 ng/mL IL-2 and 1 ng/mL IL-15 were added. After 48 hours, the stimulation beads were removed, and the T-cells were rested overnight in complete media with cytokines. After resting, the T-cells were washed in PBS and resuspended at $3x10^7$ cells/mL in Neon Electroporation system Buffer T (Life Technologies) with 0.5 μg mRNA for each TALEN half. Electroporation was carried out in a 10 μl tip on the Neon electroporation system (Life Technologies) at 1400V, 10ms, and 3 pulses. Immediately following electroporation, cells were resuspended in complete T-cell media with cytokines (as above). Cells were either placed in a 37°C incubator or in a 30°C incubator for 24 hrs and then moved to a 37°C incubator. A cold-shock step of this nature has been observed to increase the amount of protein per cell for the period when the mRNA is present and in turn, the gene editing efficiency.[116–119,147]

*Lentiviral CAR construct:*

We used a CAR comprising an FMC63-derived CD19-specific scFv fused to a modified IgG4-hinge spacer, a CD28 transmembrane domain, a 4-1BB costimulatory domain, a CD3ζ signaling domain, and a truncated EGFRt separated from the CAR by a T2A ribosomal skip sequence.[12,16,151] This allows staining, sorting, and ablation of the cells (if necessary) using cetuximab, an anti-EGFR mAb.[151] The construct was cloned into an EpHIV7 lentiviral backbone and CD19 CAR lentiviruses were produced in 293T cells.

*Lentiviral CAR transduction:*

The enriched $CD4^+$ and $CD8^+$ T-cell subsets were separately stimulated with αCD3/αCD28 human T-cell activator beads (Dynal) for 24 hr, transduced with the lentivirus encoding the CD19-specific CAR at an MOI of 1 with spinoculation at 32°C, and then cultured in complete T-cell media. If electroporation of the cells was also required, this was done 2 days after transduction.

*Cytotoxicity assay by chromium release:*

Target cells were labeled overnight with $^{51}Cr$ (Perkin Elmer), washed twice, and incubated in triplicate at $5 \times 10^3$ cells/well with effector T-cells at various effector-to-target (E:T) ratios. Supernatants were harvested after a 4-hour incubation at 37°C for γ-counting using Top Count NTX (Perkin Elmer), and specific lysis was calculated.

*Cytokine multiplexed bead assay:*

For analyses of cytokine secretion, target and effector cells were plated at an E:T ratio of 1:1, and IFN-γ, TNF-α, and IL-2 were measured by Luminex assay (Invitrogen) in the supernatant after 24 hours of incubation.

*Mouse studies:*

Murine studies were performed in a specific pathogen-free facility accredited by the Association for Assessment and Accreditation of Laboratory Animal Care, in accordance with the NIH Guide for the Care and Use of Laboratory Animals, and the Seattle Children's Research

Institute's Institutional Animal Care and Use Committee. NOD-Scid-IL2Rγ$^{NULL}$ (NSG) (The Jackson Laboratory, Bar Harbor, ME) mice at six to ten weeks old were injected intravenously (IV) with 5×10$^5$ Raji-FFLuc cells via the tail vein. The tumor load was measured by *in vivo* imaging described below 6 days after tumor injection. Mock transduced T-cells, TCR-sufficient CD19 CAR T-cells, or TCR-deficient CD19 CAR T-cells (in a 1:1 ratio of 5×10$^6$ each CD4$^+$ and CD8$^+$ CAR T-cells per mouse) were injected IV on day 7 following tumor injection. Mice were imaged serially until day 90 or until euthanization due to an IACUC-defined end-point (onset of hind limb paralysis, general malaise, or loss of >20% body weight).

*Bioluminescent imaging of mouse tumor burden:*

*In vivo* bioluminescence imaging of Raji-ffluc cells was performed following subcutaneous injection of 150 µL D-Luciferin monopotassium salt (28.57 mg/mL in sterile saline; Pierce) in sealed anesthesia box that allowed simultaneous imaging of five mice while under isoflurane sedation. Mice were imaged at the signal plateau (approximately 10 min post-D-Luciferin injection) using an IVIS Spectrum imager (PerkinElmer). The tumor burden was quantified as the total photon flux per second within a region of interest (ROI) that encompassed the head through pelvic region of the mouse; the ROIs were identically sized for all measurements.

*Flow Cytometry:*

Expression of the encoded protein was assayed by flow cytometry at 24 hours and days 7-21 post-electroporation on an LSRII flow cytometer (BD Biosciences, San Jose, CA). TCR

knock-out by TALEN was assayed by loss of TCR expression 3-7 days post-electroporation after staining with anti-CD3 (clone HIT3a, direct Alexa-488 or PerCP-Cy5.5 conjugate, BioLegend, San Diego, CA). Data was analyzed using FlowJo software (Treestar, Ashland, OR). Cells were gated on live singlet cells based on the forward and side scatter.

# 5. CRISPR/Cas9-mediated knock-out of T-cell inhibitory checkpoint proteins

## 5.1 Introduction

As discussed in the introductory chapter, while CAR T-cell therapies have been highly effective against leukemia and lymphoma, their efficacy against solid tumors is drastically reduced. A major reason for this is the immunosuppressive microenvironment created by solid tumors.[19,20,22–28] A number of mouse studies and human clinical trials of monoclonal antibodies that block the PD-1/PD-L1 pathway, as well as other pathways involving checkpoint proteins such as Tim3, Lag3, and TIGIT, have shown that blockade of these T-cell inhibitory proteins increases tumor eradication and can increase the survival of patients with multiple types of solid tumors, an effect that has been linked to enhanced anti-tumor immunosurveillance.[29–31,37,38,50,54,55,57,58,63,64] Mounting evidence indicates that these blockades work synergistically when combined.[33,62]

However, these monoclonal antibody (mAb) treatments are not without risk, and these risks also synergize as multiple mAbs are combined. These same T-cell inhibitory checkpoints protect healthy cells from autoimmune attack, and when they are released through mAb therapy, patients can develop autoimmune diseases affecting the thyroid, liver, skin, gastrointestinal, endocrine, and nervous systems, some of which have been fatal.[72,74,152] Using molecular genome engineering approaches, rather than mAbs, to disable these checkpoints would preclude this autoimmunity, and as such would be safer for patients. By combining checkpoint blockade with endogenous TCR knock-out, we hope to create a high potency CAR T-cell that could not cause off-target autoimmunity.

## 5.2 Ad5 helper proteins augment CRISPR/Cas9-mediated knock-out beyond the TCR locus: Immune checkpoints

Adapted from Gwiazda KS *et al.* 2016. *Mol Ther*.

Our initial approaches for T-cell inhibitory checkpoint knock-out using TALENs were only modestly successful. We presumed this was due to the highly-methylated nature of these loci, so we decided to switch to CRISPR/Cas9, which is not affected by methylation of targets. With the success of the E4orf6/E1b55k H373A and H354 mutant complexes on the efficiency of CRISPR/Cas9 gene disruption at the TCR$\alpha$ locus, we chose to apply them here as well. We generated and validated guide RNAs targeting four T-cell inhibitory T-cell checkpoint proteins: PD-1, TIGIT, LAG-3, and Tim3. These guide RNAs were incorporated into U6-guide expression cassettes in AAV vector backbones upstream of the MND-GFP cassette to provide for tracking of transduction/expression, and packaged into AAV vectors. Use of these AAV vectors with the E4orf6/E1b55k H373A mutant in a scaled-up expansion/manufacturing protocol based on the MaxCyte GT electroporation system resulted in generation of human T-cell populations with approximate targeted gene disruption efficiencies of 71.6±2.7%, 59.1±14.8%, 59.2±8.5%, and 66.1±14.3% of mutations at the intended cleavage sites of PD-1, TIGIT, LAG-3, and Tim3, respectively, as derived from sequence analysis (PD-1, TIGIT, Tim3) or flow cytometry (Lag-3). The representative flow cytometry data in presented in **Figure 5.1a**, and quantitated summary data in **Figure 5.1b**. An important secondary observation that emerged from these experiments was that the influence of E4orf6/E1b55k H373A mutant complexes on gene disruption efficiency was particularly prominent when the activity of a particular guide RNA was relatively low – e.g. approximately doubling the knock-out rates at the PD-1 and TIGIT loci, for which

knock-out rates with the chosen guides in the absence of E4orf6/E1b55k expression were only 36.4±10.9% and 40.4±3.6%, respectively (rates assessed by sequencing). This is a particularly salient feature of E4orf6/E1b55k H373A expression, in that it can 'rescue' poor guide activity, while guides that are already highly active are not as effectively potentiated by E4orf6/E1b55k protein expression.

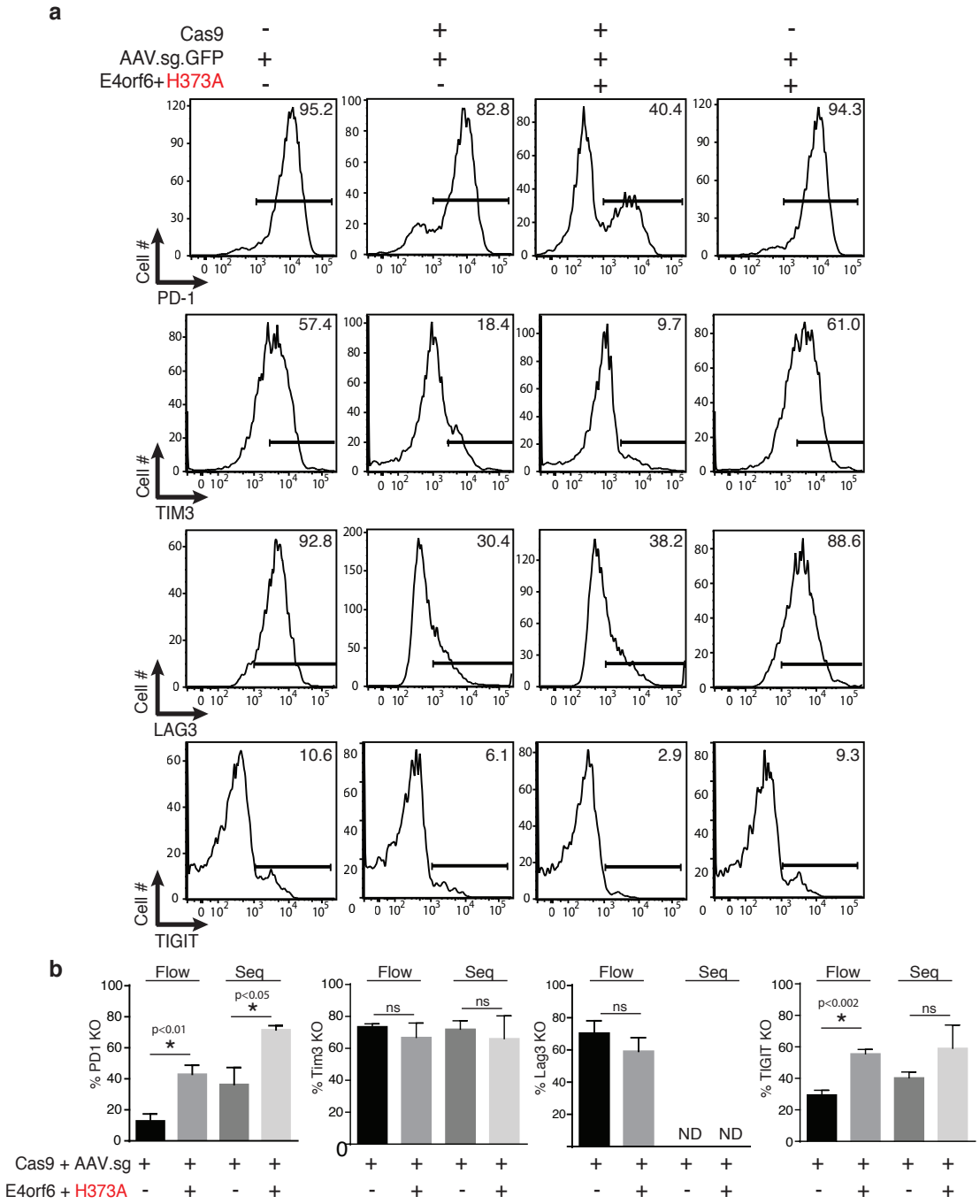

**Figure 5.1. Implementation of CRISPR/Cas9 with mRNA/AAV delivery is able to achieve efficient knock-out at multiple genomic sites. a)** Primary human CD3+ T-cells were electroporated using the MaxCyte GT system with mRNA encoding Cas9-2A-mCherry proteins (1ug) along with E4orf6/E1b55k-H373A proteins (0.03µg each), rested for 2-4 hours, and transduced with AAV driving guide expression against the indicated surface proteins. Cells were cultured for 2 weeks, then collected and analyzed for expression of the indicated surface proteins by flow cytometry. Data represent n=3-5 independent editing experiments. **b)** Quantification and summary data from flow cytometry analysis of gene knock-out and sequencing analysis of amplicons from genomic target sites. Analysis of knock-out by flow cytometry is assessed by percent loss of induction of surface protein expression. Data represent n=3-5 independent editing experiments. ND, not determined.

### 5.3 H373A mutant E4orf6/E1b55k expression enhance CRISPR/Cas9-mediated multiplex knock-out in primary human T-cells

Adapted from Gwiazda KS *et al.* 2016. *Mol Ther*.

Based on our analyses above, we hypothesized we could successfully achieve efficient levels of multiplex knock-out, using a single AAV vector to deliver multiple guides. Using the same architecture as our single AAV guide vectors, we built a dual-guide Tim3/TCRα vector, with both guides driven by individual U6 promoters (**Figure 5.2**).

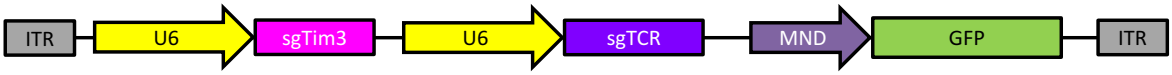


**Figure 5.2.** Schematic of the multiplex AAV vector expressing guide RNAs against Tim3 and TCRα, with individual U6 promoters, followed by a GFP trackable marker.

Following MaxCyte electroporation with Cas9 or E4orf6/E1b55k-H373A and AAV transduction with either the single Tim3 guide AAV or the AAV containing dual Tim3/ TCRα guides, TCRα and Tim3 knock-out was analyzed (**Figure 5.3**). We observed successful knock-out of both targeted genes using a single AAV, along with an increased efficiency of knock-out when E4orf6/E1b55k-H373A were co-transfected with Cas9. Importantly, we did not observe

significant differences in knock-out efficiency between the single Tim3 guide AAV and the dual Tim3 guide/TCRα guide AAV. In addition, the majority of Tim3$^-$ cells were also CD3$^-$ cells (thus TCRα$^-$), consistent with the expected outcome that any cell sufficiently well-transduced to drive guide expression to cleave one target gene also experienced a high level of guide expression for the other target gene. As translocations are a potential consequence of simultaneous induction of multiple double strand breaks, we performed karyotyping as an unbiased approach to detect cell engineering-associated translocations, and did not observe any gross abnormalities in any of twenty metaphase spreads from each condition (**Figure 5.4**).

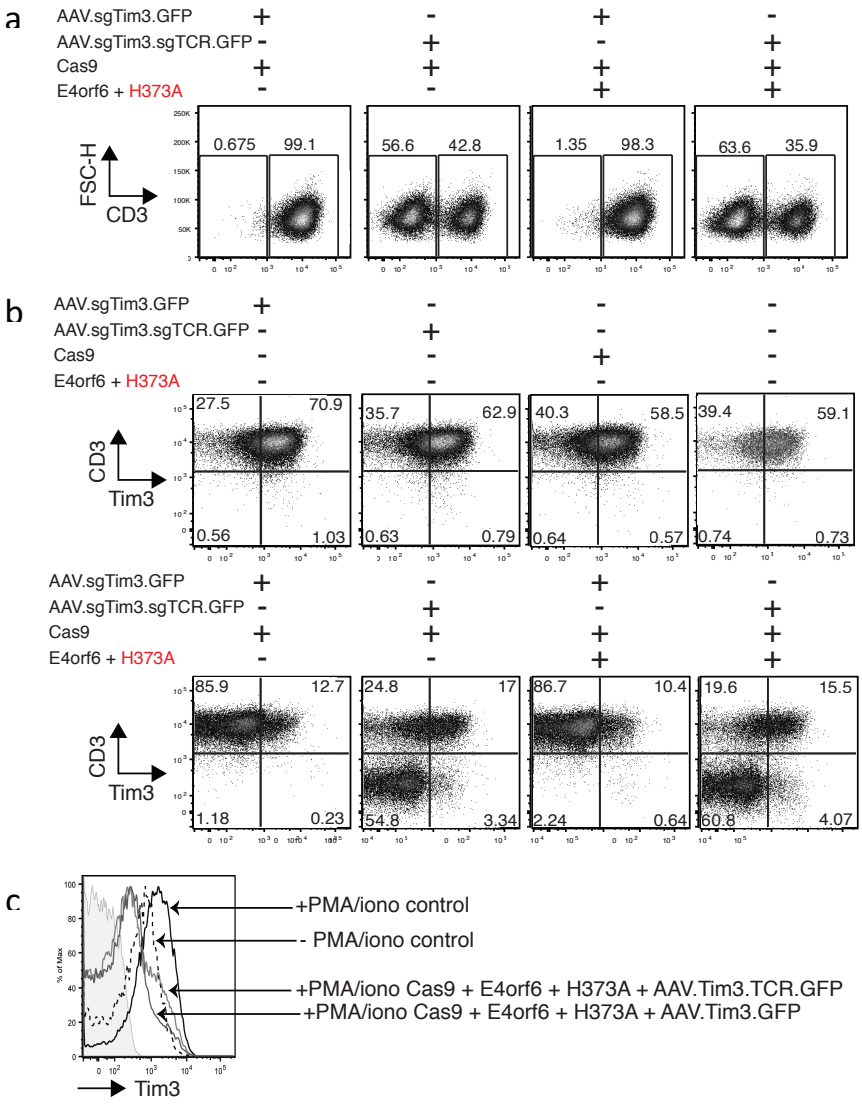

**Figure 5.3. Cas9 mRNA/AAV guide delivery achieves efficient CRISPR/Cas9-mediated multiplex knock-out in primary human T-cells with E4orf6/E1b55k H373A expression. a)** Representative flow cytometry analysis of TCRα knock-out by CD3 staining, seven days after electroporation and transduction. **b)** Representative flow cytometry analysis of TCRα knock-out and Tim3 knock-out, three weeks after initial stimulation. To upregulate Tim3 surface expression independently of TCR, cells were stimulated using PMA/ionomycin (10ng/mL and 1µg/mL, respectively), for 3-4 hours and rested for 48 hours. **c)** Upregulation of Tim3 with and without PMA/ionomycin stimulation. Shown are control cells (AAV treatment only) with and without PMA/ionomycin treatment, and stimulated cells with Tim3 knock-out compared to stimulated cells missing both Tim3 and TCRα. There were no differences between cells proficient and deficient in TCRα signaling, suggesting that PMA/ionomycin stimulation is independent of this pathway. In shaded grey are unstained cells. These flow cytometry plots are representative of n=2 or 3 experiments.

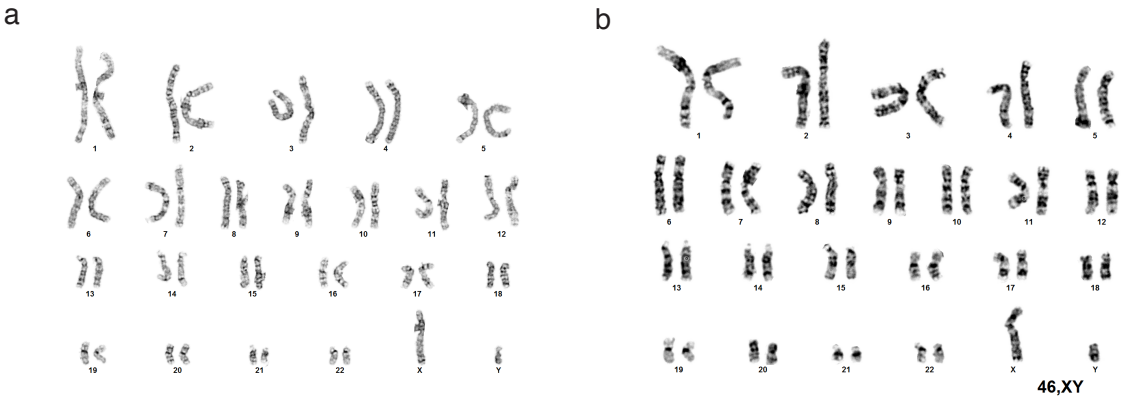


c Table 1. Summary data of karyotype results

| Sample | Band Level | Metaphase cells analyzed | Abnormalities detected (Y/N) |
|---|---|---|---|
| Untreated | 400-450 | 20 | N |
| AAV.sgTim3.GFP | 300-450 | 20 | N |
| AAV.sgTim3.sgTCRa.GFP | 300-400 | 20 | N |
| Cas9 alone | 300-550 | 20 | N |
| Cas9 + AAV.sgTim3.GFP | 300-450 | 20 | N |
| Cas9 + AAV.sgTim3.sgTCRa.GFP | 450-650 | 20 | N |
| Cas9 + E4orf6/E1b55k-H373A + AAV.sgTim3.GFP | 300-400 | 20 | N |
| Cas9 + E4orf6/E1b55k-H373A + AAV.sgTim3.sgTCRa.GFP | 300-450 | 20 | N |

**Figure 5.4. Cells exhibit normal karyotype following multiplex CRISPR/Cas9 editing.** Representative G-banding analysis following GTW staining indicating normal phenotype in cells that have undergone CRISPR/Cas9 editing with E4orf6/E1b55k-H373A. $20x10^6$ cells per sample were stimulated using PMA/ionomycin for 3-4 hours, and left to recover for 72 hours. All samples achieved metaphase spreads. Per sample, 20 metaphase spreads were created and analyzed using G-banding karyotype analysis, and no abnormalities were detected in any

sample. **a)** Representative image shows normal karyotype in cells treated with Cas9 (1μg) with AAV expressing guides against Tim3 and TCRα. Knock-out frequencies can be seen in Figure 3.9. **b)** Representative image shows normal karyotype in cells treated with Cas9 (1μg) with AAV expressing guides against Tim3 and TCRα, and E4orf6/E1b55k-H373A (0.03μg) RNAs. Knock-out frequencies can be seen in Figure 5.3. **c)** Summary Table of karyotype results. No abnormalities were detected at the band resolutions indicated, suggesting a translocation rate of less than 5%.

### 5.4 CRISPR/Cas9-mediated 5-way multiplex knock-out of the TCR and T-cell inhibitory checkpoint proteins in primary human T-cells

Based on the success of the dual Tim3/TCR knock-out using CRISPR/Cas9 enhanced by the H373A mutant of E4orf6/E1b55k using a single AAV to deliver the guides, we sought to extend this methodology to a five-way knock-out. The development of the dual guide AAV demonstrated that the order of the guides does not influence the knock-out efficiency, and that each guide should have its own U6 promoter. Using this information, we designed a single AAV vector that contained guides for PD-1, TCRα, TIGIT, Tim3, and Lag3 **(Figure 5.5)**.

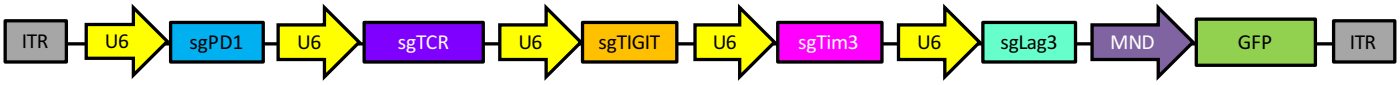


**Figure 5.5.** Schematic of the 5x multiplex AAV vector expressing guide RNAs against PD-1, TCRα, TIGIT, Tim3, and Lag3, with individual U6 promoters, followed by a GFP trackable marker.

Following MaxCyte electroporation with Cas9 with or without E4orf6/E1b55k-H373A and transduction with the AAV containing all 5 guides, PD-1, TCRα, TIGIT, Tim3 and Lag3 knock-out were analyzed (**Figure 5.6**). We observed successful knock-out of all targeted genes using a single AAV (**Figure 5.6a**), along with an increased efficiency of knock-out when E4orf6/E1b55k-H373A were co-transfected with Cas9 (**Figure 5.6b**). When we gated on $CD3^-$ cells rather than all live cells, the rates of knock-out at the other 4 loci were substantially increased, consistent

with the expected outcome that any cell sufficiently well-transduced to drive guide expression to cleave one target gene also experienced a high level of guide expression for the other target genes.

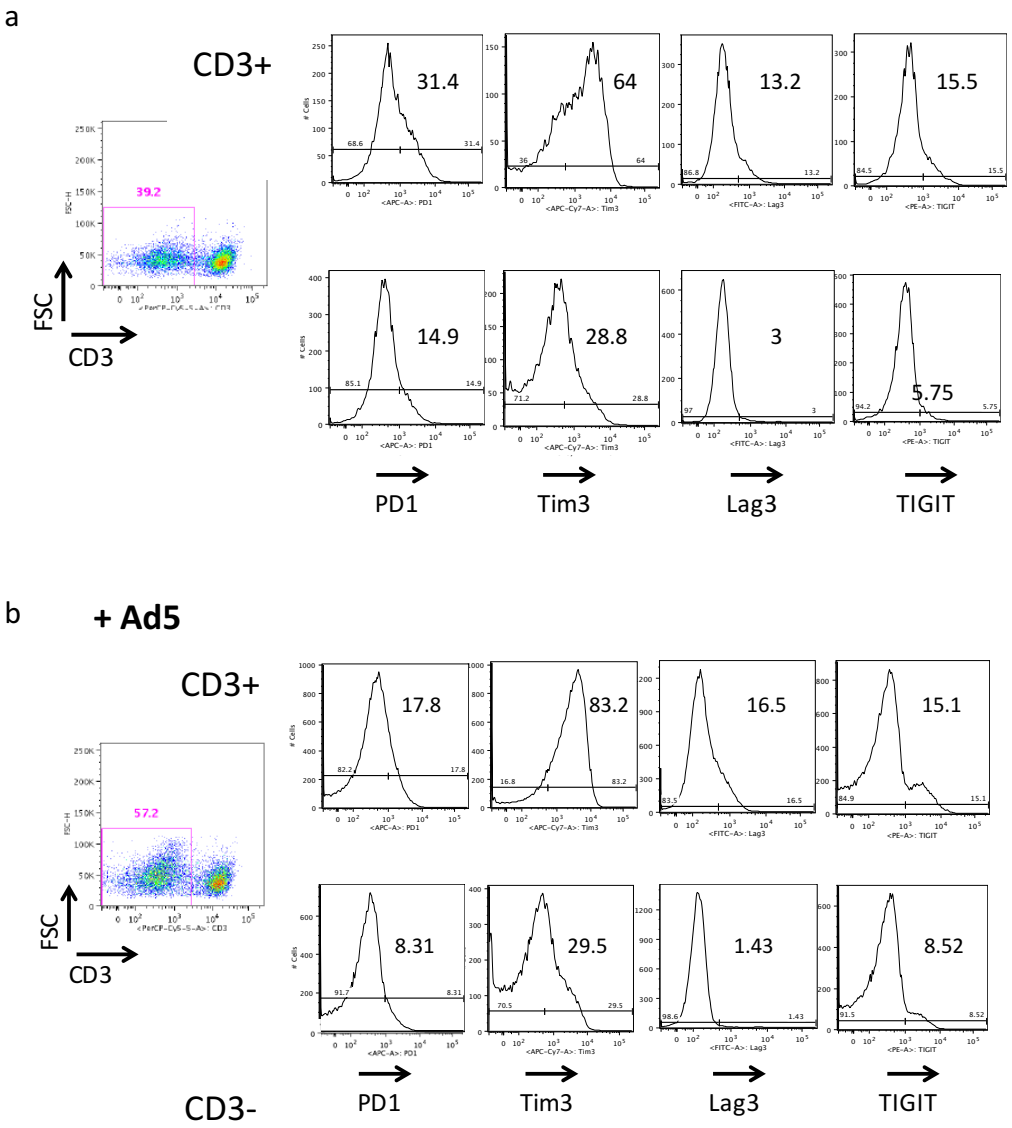


**Figure 5.6. Cas9 mRNA/5x AAV guide delivery achieves efficient multiplex knock-out in primary human T-cells, especially when combined with E4orf6/E1b55k H373A expression. a)** Representative flow cytometry analysis of TCRα knock-out by CD3 staining (left panel), with representative flow cytometry histograms of PD-1, Tim3, Lag3, and TIGIT expression (right panel). Cells were restimulated on day 18 after electroporation and transduction, and flow cytometry was then performed on day 20, gating cells into $TCR^+$ (top row) and $TCR^-$ (bottom row). To upregulate checkpoint protein expression

independently of the TCR, the stimulation on day 18 was performed with PMA/ionomycin (10ng/mL and 1μg/mL, respectively), for 3-4 hours. **b)** Same as (a) but with the addition of E4orf6/E1b55k-H373A mRNA during the electroporation with Cas9.

## 5.5 Materials and Methods

*Cloning of Cas9, E4orf6, E1b55k, and CRISPR guides:*

Cas9 expression construct was obtained from Addgene (plasmid #41815). To ensure nuclear expression of Cas9 in primary human T-cells, Nuclear Localization Signals (NLS's) were added at both 5' and 3' ends (2X-NLS). To track transfection efficiency, Cas9 was fused in-frame with T2A-mCherry and cloned into an in-house modified version of pUC57 with a T7 promoter called pWNY to obtain pWNY-2X-NLS-Cas9-T2A-mCherry. Subsequently, 2X-NLS-Cas9-T2A-mCherry was spliced from pWNY and cloned into pEVL-200. E4orf6 and E1b55k genes were gene synthesized (Integrated DNA Technologies, IDT) and cloned into an mRNA production vector. E1b55k mutants were generated using site-directed mutagenesis (QuikChange II XL Site-Directed Mutagenesis Kit, Agilent).

Guides targeting the constant region of TCRα were designed using an online CRISPR design tool (http://crispr.mit.edu). Guides were designed with a U6 promoter and ordered as gblocks (IDT, San Jose, CA). Subsequently, the gblock comprising U6 promoter and sgRNA (crRNA+tracrRNA) was cloned into a self-complementary (sc) AAV vector backbone, and checked for maintenance of intact ITRs. Four different G-block-guide constructs generated in this way were used for AAV6 synthesis, and following a series of pilot experiments, a best-performing guide was chosen for further comparative analyses. The sequence of this guide's

target is TCAAGAGCAACAGTGCTG. Guides targeting the PD-1, Tim3, Lag3, and TIGIT loci were designed in the same way as the TCRα guide. PD-1's guide target sequence is GCCCACGACACCAACCACCA, TIGIT's is TCTTCCCTAGGAATGATGAC, Lag3's is GCGGTCCCTGAGGTGCACCG, and Tim3's guide target sequence is AGAAGTGGAATACAGAGCGG.

*Production of IVT mRNA:*

mRNA expression constructs encoding Cas9, E4orf6, and E1b55k construct DNA was digested with BsaI (NEB or Thermo Scientific) to create a template with a terminal poly(A) tail. The DNA was simultaneously digested at a site upstream of the T7 (XbaI or SpeI, NEB or Thermo Scientific) to reduce the overall size of the template-containing fragment and enhance purification. After checking the completeness of the digest on a 1% agarose gel, the digested DNA was purified on a silica column and eluted in water or 10 mM Tris. IVT with ARCA capping was carried out using the mMessage mMachine T7 Ultra kit (Life Technologies, Carlsbad, CA) per the manufacturer's directions with 200-1,000 ng of the T7 to poly(A) template fragment; IVT reactions were routinely extended to 150 min. Additional DNAse and/or incubation time was used to counterbalance any increased amount of template DNA in the reaction (e.g. double DNAse or double incubation time for double template). The reaction was cleaned up after DNAse treatment using the RNeasy Mini kit (Qiagen) following the manufacturer's directions. RNA quality was determined by NanoDrop spectrophotometry (Thermo Scientific) and gel analysis with the FlashGel RNA system (Lonza). All mRNA was aliquoted in single use aliquots and stored at -80°C.

*Production of Recombinant AAV6 vectors:*

AAV stocks were produced by triple transfection of AAV vector, serotype helper and Adenoviral helper (HGT1-Adeno) plasmids in HEK293T cells. Transfected cells were collected 48 hrs later, lysed by freeze-thaw, benzonase treated and purified over iodixanol density gradient as previously described.[145] Titers of the viral stocks were determined by qPCR of AAV genomes and ranged from $10^{10}$-$10^{12}$/ml.[146]

*mRNA electroporation of primary human T-cells:*

Freshly isolated primary human T-cells were stimulated with αCD3/αCD28 human T-cell activator microbeads (Dynal, Thermo Scientific) in RPMI with 20% FBS, 2.5% HEPES, and 1% L-glutamine (Thermo Scientific). IL-2 (Chiron, Emeryville, CA) and IL-15 (Miltenyi, San Diego, CA) at final concentrations of 5 ng/mL and 1 ng/mL, respectively, were added. After 48 hours, the stimulation beads were removed, and the T-cells were rested overnight in complete media with cytokines. After resting, the T-cells were washed in PBS and resuspended at $1x10^8$ cells/mL in MaxCyte electroporation buffer T (MaxCyte Inc, Gaithersburg, MD). $5x10^6$ cells were combined with 16 μg Cas9 mRNA $\pm$ 0.5 μg each E4orf6 and E1b55k-373A in a total volume of 50 μL in an OC-100 cuvette (MaxCyte Inc, Gaithersburg, MD). Electroporation was carried out on the MaxCyte GT (MaxCyte Inc, Gaithersburg, MD) using the proprietary T-cell program. Immediately following electroporation, cells were resuspended in complete T-cell media with cytokines (as above). Cells were either placed in a 37°C incubator or in a 30°C incubator for 24 hours and then moved to a 37°C incubator. A cold-shock step of this nature has been observed

to increase the amount of protein per cell for the period when the mRNA is present and in turn, the gene editing efficiency.[116–119,147] Cells were rested for 2 hours after electroporation and then transduced with AAV containing the CRISPR guides at a constant 10% culture volume, equating to an MOI of approximately $1x10^4$.

*Stimulation with PMA/ionomycin:*

Cells were plated at a density of $1x10^6$ in a 48 or 24 well plate. 10ng/mL PMA (Sigma) and 1μg/mL of ionomycin (Sigma) was added to the media for 3-4 hours, cells were washed 3-4 times with PBS with 2% FBS, and then re-plated with fresh media. Cells were allowed to recover for 48 hours before flow cytometry, or for 72 hours for karyotype analysis.

*Karyotype analysis:*

Cells were grown in T-25 flasks at a density of $1x10^6$-$1.5x10^6$ per sample. Each sample was stimulated with PMA/ionomycin for 3-4 hours, and then allowed to rest for 72 hours in full media and cytokines. Karyotype analysis was done by the University of Washington Cytogenetics and Genomics Laboratory as Research Testing. Standard G-banding (GTW stain) chromosome analysis was performed, on 20 cells per sample.

*Flow Cytometry:*

Analysis of knock-out (TCRα, PD-1, TIGIT, Lag3, and Tim3) was performed using the LSRII flow cytometer (BD Biosciences) and data was analyzed using FlowJo software (Treestar). All antibodies were from Biolegend, unless otherwise indicated. To assess knock-out of surface

markers, cells were labeled with fluorophore-conjugated antibodies, as follows: CD3-Alexa 488, CD3-PerCPCy5.5, or CD3-APC clone HIT3a; PD1-APC clone eh12.2H7; TIGIT-Alexa 700 clone 741182 (Novus Biologicals); Tim3-APC-Cy7 clone F38-2E2; and Lag3-FITC clone 3DS223H (eBioscience). CD4 or CD8 staining was done using CD4-BFP (clone OKT4) or CD8-BFP (RPA-T8).

*Statistical Analysis*

Statistical analyses were performed with Prism 6 (GraphPad Software). Data is shown as mean +/- SEM unless otherwise noted. Tests of statistical significance were performed using an unpaired two-tailed Student's *t*-test with Welsh's correction for unequal standard deviations when appropriate.

# 6. Summary and future directions

## 6.1 Summary of thesis project

We have developed a robust tool set for gene editing of CAR T-cells and other adoptive T-cell therapies, and we have applied it to address multiple challenges currently facing the immunotherapy field. This research will help to bring the advances in immunotherapy to more patients with a wider variety of cancers.

We anticipate that one of the challenges to delivering these promising therapeutic advances is ensuring maximally efficient protein expression in the target cells. To this end, we developed a linear plasmid vector system that allows for generation of mRNA by in vitro transcription (IVT) with standard length poly(A) tails of up to approximately 500 nucleotides, and showed that this IVT mRNA has high potency when used in conjunction with electroporation of primary human T-cells. We found a significant benefit of the uniform poly(A) tail lengths of pEVL mRNA over the enzymatically tailed mRNA in both expression and mRNA stability, though beyond a tail length of 200 nucleotides there was no noted benefit to additional adenosine residues, as measured by knock-out efficiency. We predict that one of the most important uses of pEVL will be for large-scale generation of mRNA for therapeutic applications, such as genome modification reagents, mRNA-based CARs, enzyme/protein replacement or supplementation, and mRNA-based pharmaceuticals. pEVL is easily scaled up for large-scale GMP plasmid production using kanamycin selection, and allows for generation of uniformly sized, capped, and polyadenylated mRNAs in a single reaction using standard T7 RNA polymerase chemistry. As validating examples for the utility of pEVL at scale, we have been able to use pEVL-300 to generate extremely high quality and high potency mRNAs encoding

multiple TALEN pairs, BFP, Sleeping Beauty and PiggyBac transposases, and Cas9 at a 10 mg scale using standard mRNA IVT methods. pEVL is an advance toward simple, efficient, and consistent large scale synthesis of highly potent mRNAs for a wide range of therapeutic applications.

With this new tool for increased protein expression, we next sought to explore a promising expansion of CAR T-cell therapy: if the endogenous TCR can be knocked out in CAR T-cells, can patients not eligible for autologous CAR T-cell therapy receive allogeneic therapy instead? To investigate this question, we used pEVL to express TALEN as well as CRISPR/Cas9 components to eliminate expression of the endogenous TCR. These knockout CAR T-cells demonstrated no detrimental effects on function either *in vitro,* as measured by cytotoxicity, cytokine release, and expansion assays, or *in vivo,* using an established murine xenograft tumor model. We believe that this TCR knock out strategy, used for generation of allogeneic CAR T-cells, will allow patients who are not candidates for autologous CAR T-cell therapy to receive allogeneic therapy as a bridge to HSCT or to prevent relapse after HSCT. Excitingly, since we began working on TCR knock-out, two other research groups have published successes using similar strategies,[153,154] validating its usefulness and feasibility as a therapeutic approach. We also anticipate that TCR knock out may decrease the risk of autoimmunity, usually mediated through the endogenous TCR, and thus allow for the development of more aggressive CAR T-cells.

One approach to generating CAR T-cells with increased activity involves knocking out T-cell inhibitory checkpoint proteins. After designing and validating CRISPR guides against four major T-cell checkpoints (PD-1, Tim3, Lag3, and TIGIT), we established a clinically translatable

method to create multiplex knock-outs using pEVL-encoded Cas9 and viral helper proteins from Ad5, with AAV-mediated CRISPR guide delivery. We found that simultaneous transient expression of Ad5 E1b55k and E4orf6 proteins increases the effective guide dosage when the guides are encoded on AAV vectors and creates a cellular environment that promotes mutagenesis by transiently downregulating key DNA damage response/repair proteins.[89] With the above protocol, we successfully and reproducibly created a population of T-cells with deletions of the four targeted checkpoint proteins as well as the TCR. Current checkpoint blockade therapy with monoclonal antibodies can cause serious, even fatal, immune-related side effects. By using genome engineering to eliminate these inhibitory checkpoints solely in T-cells that are also engineered to attack tumors, we have designed a system that preserves the recent treatment advances made with checkpoint blockade while circumventing the need for systemic antibody therapy.

Slight alterations in methodology can lead to substantial differences in the phenotype and performance of these cell-based therapies. We and others in the field have noted that varying the T-cell subset composition, culturing conditions, CAR design, and delivery vector can all create substantial differences in the phenotype and performance of the final cellular product. Therefore, the development work described above was performed in primary human T-cells utilizing clinically applicable and scalable reagents. Consequently, all the procedures described herein can be directly implemented into current translational manufacturing processes. In summary, this project has developed and demonstrated tools to facilitate advances in immunotherapy that can be quickly and feasibly scaled up and moved into the clinic to meet the ever-changing and immediate needs of patients.

### 6.2 Future directions for mRNA technology

Although pEVL has been adopted as a workhorse of the lab for mRNA production, we are also adapting and diversifying pEVL for easier cloning of many different types of ORFs. We have created multiple versions: a destination vector for Golden Gate TALEN cloning, a set of multipurpose mRNA production vectors with a greatly expanded MCS ± a T7 promoter ± a Kozak sequence, and a version that is nearly 3kb shorter for easier handling and production, especially when using large ORFs. It is currently being tested by our collaborators for use in making HIV-resistant HSCs for a potential clinical trial, as well as for tethering mRNA to nanoparticles for drug delivery via liver-directed lipid nanoparticles. Another collaborator is investigating pEVL-derived mRNA for diseases in which enzyme replacement therapy has not been successful because intracellular protein expression is required to reverse the disease pathology. Specifically, this collaborator is tethering the mRNA to lipid nanoparticles for drug delivery via the liver. Ideally, high potency mRNA with a long poly(A) tail from pEVL may allow sufficient and sustained expression of intracellular proteins to provide for a therapeutic level and duration of protein expression within a patient's target cells.

### 6.3 Future directions for clinical trial applications

One of the most promising clinical applications of TCR-deficient CAR T-cells is the possible use of allogeneic CAR T-cells as a bridge to HSCT for patients, such as those with too few T-cells or unhealthy T-cells, for whom an autologous product cannot be produced. Although the allogeneic CAR T-cells would eventually be rejected by the host, our current data

indicates that the CAR T-cells would have sufficient time (approximately 10-14 days) to eradicate the cancerous cells before being rejected.

Another possible clinical application of TCR-deficient CAR T-cells is in the prevention of post-transplant relapse in hematopoietic cancers. Relapsed ALL is a leading contributor to pediatric cancer mortality. The 2-year disease-free survival for children with relapsed ALL who achieve a complete remission prior to transplant is 70%, whereas those who have minimal residual disease (MRD) at the time of transplant do much worse, with a 2-year disease-free survival of approximately 20%.[4] With intensification of front line therapeutic regimens, salvage rates of relapsed ALL have declined and novel therapeutic modalities that target chemotherapy resistant ALL are needed. TCR-deficient CAR T-cells could be used to augment the graft vs leukemia (GvL) effect. The level of immunologic activity against the leukemia is often matched by the severity of GVHD. TCR-deficient CAR T-cells would abrogate the risk of GVHD caused by alloreactivity.

Given the difference in survival among patients with complete remission vs those with MRD, we hypothesize that relapse can be prevented by preemptive targeting of residual leukemia early after transplant. To accomplish this, we plan to engineer TCR-deficient CAR T-cells with increased activity and drug resistance, by using donor-derived T-cells with both TALEN-mediated endogenous TCR knockout and lentiviral transduction with a vector that co-expresses a CD19 CAR and drug resistance genes. The engineered drug resistance constructs render T-cells resistant to cyclosporine (CSA) and mycophenolate mofetil (MMF), immunosuppressive drugs that post-transplant patients are routinely given. This is currently

slated to be part of the Pediatric Leukemia Adoptive Therapy (PLAT)-06 clinical trial at Seattle Children's Hospital in the near future.

### 6.4 Future directions for combination knock-out and knock-in at the TCRα locus

Another exciting extension of this work is the combination of TCR knockout via TALENs or CRISPR/Cas9 with a knock-in strategy using homology-directed repair via a donor template delivered by AAV to integrate desired gene(s) at the locus. These integrated gene cassettes can be under the control of their own promoter, or alternatively, gene trapped into the TCR〈 locus to keep expression of the integrated gene(s) under the control of the endogenous promoter and regulatory elements.

These dually edited cells are highly desirable clinically, in that universal T-cell products can be made (TCR-deficient cells) that also stably express transgenes of interest (for example, CARs, drug resistance genes, engineered receptors or ligands, and autocrine cytokine signaling components). Additionally, a built-in safety feature of this system is that a successful knock-in of the transgene guarantees knock-out of TCRα, since insertion of a large DNA cassette at exon 1 of the constant region of TCRα - where our guides and TALENs target - will always disrupt the endogenous coding sequence.

In preliminary experiments, we have found that we can successfully and reproducibly produce primary human T-cells that have high levels of both $TCR^-$ and $transgene^+$ populations (**Figure 6.1**).

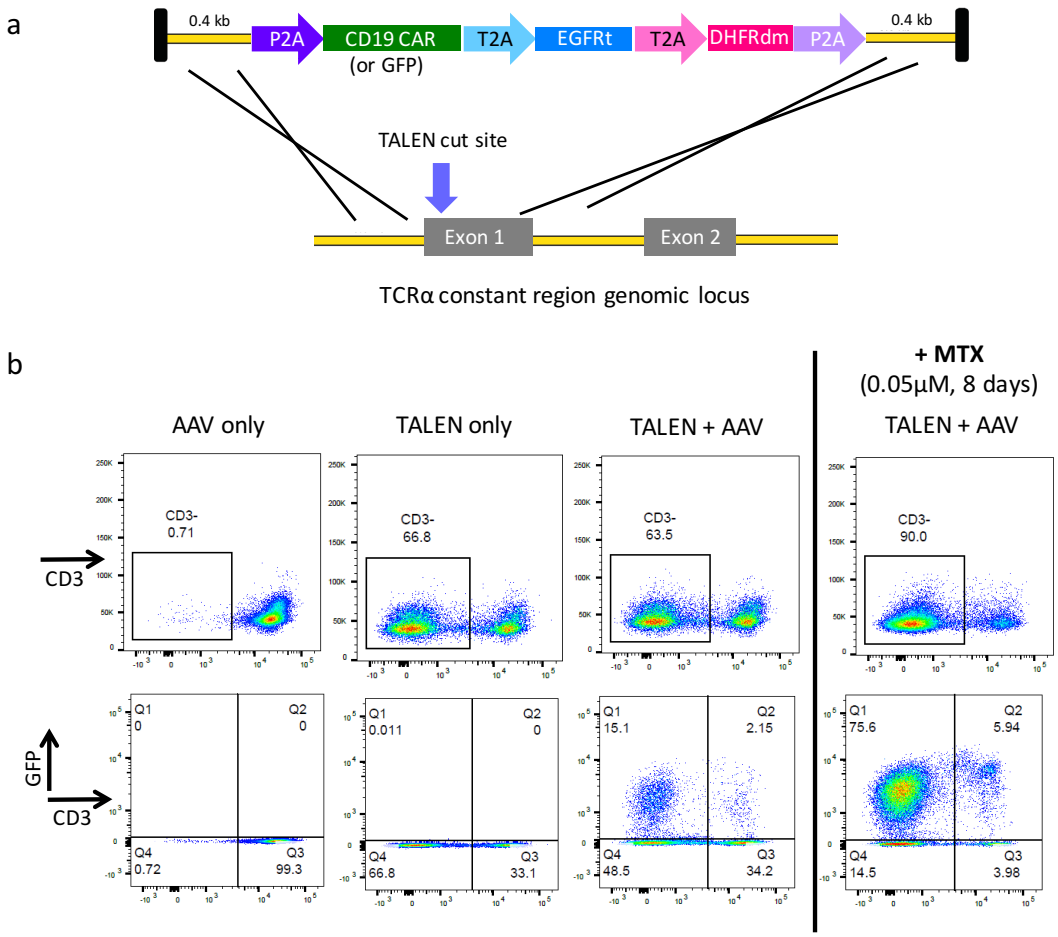


**Figure 6.1. Simultaneous knock-out and knock-in into the TCRα locus**. **a)** Schematic of the gene integration cassette used for knock in at the TALEN target site in exon 1 of the constant region of the human TCRα locus delivered by AAV vector at the indicated location in exon 1 of the TCRα constant region. **b)** Primary human T-cells electroporated with TALENs (CD3, creating a knock-out only) or TALENs with AAV (CD3 and GFP, creating both knock-out and knock-in.) Following two weeks of culture, 0.05μM methotrexate was added for 8 days to selectively expand cells that contained the integrated cassette ($GFP^+$, and thus $DHFRdm^+$). Cells were then assessed by flow cytometry.

In our studies, we found that constructs integrated into the TCRα locus and regulated by the endogenous TCRα machinery (gene trap) are able to express the transgene, albeit at lower levels than when regulated by a strong exogenous promoter. However, another group that has been examining similar constructs has found that lower and more regulated expression levels

from integrated constructs may be advantageous, especially when expressing CARs or other stimulatory molecules.[154]

### 6.5 Future directions for *in vivo* assessment of multiplex checkpoint knock-out CAR T-cells

We are interested in studying our promising T-cell populations *in vivo*, to determine whether the T-cells that contain multiple checkpoint knock-outs have increased tumor eradication potential compared to conventional CAR T-cells. Because we are able to create a population of cells with various combinations of PD-1, Tim3, Lag3, TIGIT, and TCR knock-outs, we have a means to assay which checkpoint knock-out or combination of knock-outs are advantageous for tumor eradication.

We would like to evaluate these checkpoint-deficient CAR T-cells in two *in vivo* models: a flank tumor model and an intracranial tumor model. Both models are based on injection of the Be2 neuroblastoma tumor cell line into NSG mice. Be2 cells express the cellular adhesion molecule L1CAM (CD171), which is highly expressed on neuroblastoma cells as well as on many other solid tumors, and participates in regulating tumor cell differentiation, proliferation, migration and invasion. L1CAM expression correlates with tumor progression and metastasis. The CE7 CAR (2$^{nd}$ generation CAR with 41BB co-stimulatory domain and short IgG4 hinge spacer) is being used in the ENCIT-01 neuroblastoma trial at Seattle Children's Hospital, but so far has not resulted in tumor regression. The flank tumor model is made by injecting Be2 cells mixed with a gelatinous matrix subcutaneously in the flank of NSG mice, and allowing the tumor to form, while the intracranial model is created by stereotactically injecting Be2 cells to allow an orthotopic tumor to engraft in the brain and/or spinal column of NSG mice.

Following engraftment of tumor cells, CAR T-cells would then be injected intracranially or intravenously into the mice, and T-cell trafficking, survival, tumor progression or eradication, and relapse would be measured by bioluminescent imaging. In the flank tumor model, CAR T-cells can be recovered from the tumor bed after ~2 weeks and assessed by *ex vivo* cytotoxicity and cytokine release assays, FACS analysis, ddPCR, and single-cell RNA sequencing to determine phenotype, levels of T-cell activation or exhaustion, and changes in checkpoint knockout frequency compared to the starting CAR T-cell population.

The intracranial Be2 tumor model is an especially interesting setting in which to study checkpoint knockout. At the time of disease relapse in this model (~90 days), there are numerous T-cells present in the tumor bed, though they are not able to kill the tumor cells (see Fig.2, Künkele et al. *Cancer Immunol Res*. 2015), making it a prime site to study T-cell exhaustion.[6] The tumor burden will be assessed by bioluminescent imaging while the survival of each group is measured. At the end of the study, the brain can be sectioned to study the T-cells and tumor cells by IHC, laser capture microdissection, ddPCR, and RNA seq. Finally, we also have Be2 cells transduced with CD19, allowing performance of the CE7 CAR to be compared to that of the gold standard CD19 CAR to see whether checkpoint knockout has different effects based on the affinity of the CAR, density of the tumor antigen, and strength of the co-stimulation signal (comparing 41BB-containing CARs to CD28-containing CARs). I hope to carry out these experiments during my year-long post-doctoral position in Dr. Michael Jensen's lab at Seattle Children's Research Institute.

**References**


1. Restifo, N. P., Dudley, M. E. & Rosenberg, S. A. Adoptive immunotherapy for cancer: harnessing the T cell response. *Nat. Rev. Immunol.* **12,** 269–281 (2012).
2. Fesnak, A. D., June, C. H. & Levine, B. L. Engineered T cells: the promise and challenges of cancer immunotherapy. *Nat. Rev. Cancer* **16,** 566–581 (2016).
3. June, C. H. *et al.* Engineered T cells for cancer therapy. *Cancer Immunol. Immunother. CII* **63,** 969–975 (2014).
4. Hunder, N. N. *et al.* Treatment of metastatic melanoma with autologous CD4+ T cells against NY-ESO-1. *N. Engl. J. Med.* **358,** 2698–2703 (2008).
5. Yee, C. *et al.* Adoptive T cell therapy using antigen-specific CD8+ T cell clones for the treatment of patients with metastatic melanoma: In vivo persistence, migration, and antitumor effect of transferred T cells. *Proc. Natl. Acad. Sci. U. S. A.* **99,** 16168–16173 (2002).
6. Morgan, R. A. *et al.* Cancer regression in patients after transfer of genetically engineered lymphocytes. *Science* **314,** 126–129 (2006).
7. Kalos, M. *et al.* T cells with chimeric antigen receptors have potent antitumor effects and can establish memory in patients with advanced leukemia. *Sci. Transl. Med.* **3,** 95ra73 (2011).
8. Porter, D. L., Levine, B. L., Kalos, M., Bagg, A. & June, C. H. Chimeric Antigen Receptor–Modified T Cells in Chronic Lymphoid Leukemia. *N. Engl. J. Med.* **365,** 725–733 (2011).
9. Kochenderfer, J. N. *et al.* Chemotherapy-Refractory Diffuse Large B-Cell Lymphoma and Indolent B-Cell Malignancies Can Be Effectively Treated With Autologous T Cells Expressing an Anti-CD19 Chimeric Antigen Receptor. *J. Clin. Oncol.* **33,** 540–549 (2015).
10. Zola, H. *et al.* Preparation and characterization of a chimeric CD19 monoclonal antibody. *Immunol. Cell Biol.* **69 ( Pt 6),** 411–422 (1991).
11. Jensen, M. C. & Riddell, S. R. Designing chimeric antigen receptors to effectively and safely target tumors. *Curr. Opin. Immunol.* **33,** 9–15 (2015).
12. Hudecek, M. *et al.* The nonsignaling extracellular spacer domain of chimeric antigen receptors is decisive for in vivo antitumor activity. *Cancer Immunol. Res.* **3,** 125–135 (2015).
13. Terakura, S. *et al.* Generation of CD19-chimeric antigen receptor modified CD8+ T cells derived from virus-specific central memory T cells. *Blood* **119,** 72–82 (2012).
14. Turtle, C. J., Hudecek, M., Jensen, M. C. & Riddell, S. R. Engineered T cells for anti-cancer therapy. *Curr. Opin. Immunol.* **24,** 633–639 (2012).
15. Künkele, A. *et al.* Functional Tuning of CARs Reveals Signaling Threshold above Which CD8+ CTL Antitumor Potency Is Attenuated due to Cell Fas-FasL-Dependent AICD. *Cancer Immunol. Res.* **3,** 368–379 (2015).
16. Turtle, C. J. *et al.* CD19 CAR-T cells of defined CD4+:CD8+ composition in adult B cell ALL patients. *J. Clin. Invest.* **126,** 2123–2138 (2016).
17. Barrett, D. M., Singh, N., Porter, D. L., Grupp, S. A. & June, C. H. Chimeric Antigen Receptor Therapy for Cancer. *Annu. Rev. Med.* **65,** 333–347 (2014).

18. Brentjens, R. J. *et al.* CD19-Targeted T Cells Rapidly Induce Molecular Remissions in Adults with Chemotherapy-Refractory Acute Lymphoblastic Leukemia. *Sci. Transl. Med.* **5,** 177ra38-177ra38 (2013).
19. Motz, G. T. *et al.* Tumor endothelium FasL establishes a selective immune barrier promoting tolerance in tumors. *Nat. Med.* **20,** 607–615 (2014).
20. Newick, K., Moon, E. & Albelda, S. M. Chimeric antigen receptor T-cell therapy for solid tumors. *Mol. Ther. - Oncolytics* **3,** Article 16006 (2016).
21. Maude, S. L., Teachey, D. T., Porter, D. L. & Grupp, S. A. CD19-targeted chimeric antigen receptor T-cell therapy for acute lymphoblastic leukemia. *Blood* **125,** 4017–4023 (2015).
22. Dranoff, G. Cytokines in cancer pathogenesis and cancer therapy. *Nat. Rev. Cancer* **4,** 11–22 (2004).
23. Landskron, G., De la Fuente, M., Thuwajit, P., Thuwajit, C. & Hermoso, M. A. Chronic Inflammation and Cytokines in the Tumor Microenvironment. *J. Immunol. Res.* **2014,** e149185 (2014).
24. Śledzińska, A., Menger, L., Bergerhoff, K., Peggs, K. S. & Quezada, S. A. Negative immune checkpoints on T lymphocytes and their relevance to cancer immunotherapy. *Mol. Oncol.* **9,** 1936–1965 (2015).
25. Thaventhiran, T. T Cell Co-inhibitory Receptors-Functions and Signalling Mechanisms. *J. Clin. Cell. Immunol.* **01,** (2013).
26. Anderson, A. C., Joller, N. & Kuchroo, V. K. Lag-3, Tim-3, and TIGIT: Co-inhibitory Receptors with Specialized Functions in Immune Regulation. *Immunity* **44,** 989–1004 (2016).
27. Fourcade, J. *et al.* Upregulation of Tim-3 and PD-1 expression is associated with tumor antigen-specific CD8+ T cell dysfunction in melanoma patients. *J. Exp. Med.* **207,** 2175–2186 (2010).
28. Dong, Y. *et al.* PD-1 and its ligands are important immune checkpoints in cancer. *Oncotarget* **8,** 2171–2186 (2016).
29. F. Stephen Hodi. Durable, long-term survival in previously treated patients with advanced melanoma (MEL) who received nivolumab (NIVO) monotherapy in a phase I trial. (2016).
30. Jazirehi, A. R., Lim, A. & Dinh, T. PD-1 inhibition and treatment of advanced melanoma-role of pembrolizumab. *Am. J. Cancer Res.* **6,** 2117 (2016).
31. Ribas, A. *et al.* Association of Pembrolizumab With Tumor Response and Survival Among Patients With Advanced Melanoma. *JAMA* **315,** 1600–1609 (2016).
32. Shu, C. A. & Rizvi, N. A. Into the Clinic With Nivolumab and Pembrolizumab. *The Oncologist* **21,** 527–528 (2016).
33. Larkin, J. *et al.* Combined Nivolumab and Ipilimumab or Monotherapy in Untreated Melanoma. *N. Engl. J. Med.* **373,** 23–34 (2015).
34. Boutros, C. *et al.* Safety profiles of anti-CTLA-4 and anti-PD-1 antibodies alone and in combination. *Nat. Rev. Clin. Oncol.* **13,** 473–486 (2016).
35. Le, D. T. *et al.* PD-1 Blockade in Tumors with Mismatch-Repair Deficiency. *N. Engl. J. Med.* **372,** 2509–2520 (2015).
36. Kinter, A. L. *et al.* The common gamma-chain cytokines IL-2, IL-7, IL-15, and IL-21 induce the expression of programmed death-1 and its ligands. *J. Immunol. Baltim. Md 1950* **181,** 6738–6746 (2008).

37. Chen, D. S., Irving, B. A. & Hodi, F. S. Molecular pathways: next-generation immunotherapy--inhibiting programmed death-ligand 1 and programmed death-1. *Clin. Cancer Res. Off. J. Am. Assoc. Cancer Res.* **18,** 6580–6587 (2012).
38. Pardoll, D. M. The blockade of immune checkpoints in cancer immunotherapy. *Nat. Rev. Cancer* **12,** 252–264 (2012).
39. Parsa, A. T. *et al.* Loss of tumor suppressor PTEN function increases B7-H1 expression and immunoresistance in glioma. *Nat. Med.* **13,** 84–88 (2007).
40. Latchman, Y. *et al.* PD-L2 is a second ligand for PD-1 and inhibits T cell activation. *Nat. Immunol.* **2,** 261–268 (2001).
41. Riley, J. L. PD-1 signaling in primary T cells. *Immunol. Rev.* **229,** 114–125 (2009).
42. Wherry, E. J. *et al.* Molecular Signature of CD8+ T Cell Exhaustion during Chronic Viral Infection. *Immunity* **27,** 670–684 (2007).
43. Crespo, J., Sun, H., Welling, T. H., Tian, Z. & Zou, W. T cell anergy, exhaustion, senescence, and stemness in the tumor microenvironment. *Curr. Opin. Immunol.* **25,** 214–221 (2013).
44. Strome, S. E. *et al.* B7-H1 blockade augments adoptive T-cell immunotherapy for squamous cell carcinoma. *Cancer Res.* **63,** 6501–6505 (2003).
45. Dong, H. *et al.* Tumor-associated B7-H1 promotes T-cell apoptosis: a potential mechanism of immune evasion. *Nat. Med.* **8,** 793–800 (2002).
46. Topalian, S. L. *et al.* Safety, Activity, and Immune Correlates of Anti–PD-1 Antibody in Cancer. *N. Engl. J. Med.* **366,** 2443–2454 (2012).
47. Robert, C. *et al.* Pembrolizumab versus Ipilimumab in Advanced Melanoma. *N. Engl. J. Med.* **372,** 2521–2532 (2015).
48. Zak, K. M. *et al.* Structure of the Complex of Human Programmed Death 1, PD-1, and Its Ligand PD-L1. *Structure* **23,** 2341–2348 (2015).
49. Lázár-Molnár, E. *et al.* Crystal structure of the complex between programmed death-1 (PD-1) and its ligand PD-L2. *Proc. Natl. Acad. Sci. U. S. A.* **105,** 10483–10488 (2008).
50. Chong, E. A. *et al.* PD-1 Blockade Modulates Chimeric Antigen Receptor (CAR) Modified T Cells and Induces Tumor Regression: Refueling the CAR. *Blood* blood-2016-09-738245 (2016). doi:10.1182/blood-2016-09-738245
51. Boles, K. S. *et al.* A novel molecular interaction for the adhesion of follicular CD4 T cells to follicular DC. *Eur. J. Immunol.* **39,** 695–703 (2009).
52. Levin, S. D. *et al.* Vstm3 is a member of the CD28 family and an important modulator of T-cell function. *Eur. J. Immunol.* **41,** 902–915 (2011).
53. Stanietsky, N. *et al.* The interaction of TIGIT with PVR and PVRL2 inhibits human NK cell cytotoxicity. *Proc. Natl. Acad. Sci. U. S. A.* **106,** 17858–17863 (2009).
54. Yu, X. *et al.* The surface protein TIGIT suppresses T cell activation by promoting the generation of mature immunoregulatory dendritic cells. *Nat. Immunol.* **10,** 48–57 (2009).
55. Joller, N. *et al.* Cutting edge: TIGIT has T cell-intrinsic inhibitory functions. *J. Immunol. Baltim. Md 1950* **186,** 1338–1342 (2011).
56. Goding, S. R. *et al.* Restoring immune function of tumor-specific CD4+ T cells during recurrence of melanoma. *J. Immunol. Baltim. Md 1950* **190,** 4899–4909 (2013).
57. Johnston, R. J. *et al.* The Immunoreceptor TIGIT Regulates Antitumor and Antiviral CD8+ T Cell Effector Function. *Cancer Cell* **26,** 923–937 (2014).

58. Workman, C. J. & Vignali, D. A. A. The CD4-related molecule, LAG-3 (CD223), regulates the expansion of activated T cells. *Eur. J. Immunol.* **33,** 970–979 (2003).
59. Kouo, T. *et al.* Galectin-3 Shapes Antitumor Immune Responses by Suppressing CD8+ T Cells via LAG-3 and Inhibiting Expansion of Plasmacytoid Dendritic Cells. *Cancer Immunol. Res.* **3,** 412–423 (2015).
60. Grosso, J. F. *et al.* LAG-3 regulates CD8+ T cell accumulation and effector function in murine self- and tumor-tolerance systems. *J. Clin. Invest.* **117,** 3383–3392 (2007).
61. Workman, C. J. & Vignali, D. A. A. Negative regulation of T cell homeostasis by lymphocyte activation gene-3 (CD223). *J. Immunol. Baltim. Md 1950* **174,** 688–695 (2005).
62. Matsuzaki, J. *et al.* Tumor-infiltrating NY-ESO-1–specific CD8+ T cells are negatively regulated by LAG-3 and PD-1 in human ovarian cancer. *Proc. Natl. Acad. Sci.* **107,** 7875–7880 (2010).
63. Hastings, W. D. *et al.* TIM-3 is Expressed on Activated Human CD4+ T Cells and Regulates Th1 and Th17 Cytokines. *Eur. J. Immunol.* **39,** 2492–2501 (2009).
64. Mujib, S. *et al.* Antigen-independent induction of Tim-3 expression on human T cells by the common γ-chain cytokines IL-2, IL-7, IL-15, and IL-21 is associated with proliferation and is dependent on the phosphoinositide 3-kinase pathway. *J. Immunol. Baltim. Md 1950* **188,** 3745–3756 (2012).
65. Zhu, C. *et al.* The Tim-3 ligand galectin-9 negatively regulates T helper type 1 immunity. *Nat. Immunol.* **6,** 1245–1252 (2005).
66. Dardalhon, V. *et al.* Tim-3/galectin-9 pathway: regulation of Th1 immunity through promotion of CD11b+Ly-6G+ myeloid cells. *J. Immunol. Baltim. Md 1950* **185,** 1383–1392 (2010).
67. Leitner, J. *et al.* TIM-3 does not act as a receptor for galectin-9. *PLoS Pathog.* **9,** e1003253 (2013).
68. Elahi, S., Niki, T., Hirashima, M. & Horton, H. Galectin-9 binding to Tim-3 renders activated human CD4+ T cells less susceptible to HIV-1 infection. *Blood* **119,** 4192–4204 (2012).
69. Kikushige, Y. *et al.* A TIM-3/Gal-9 Autocrine Stimulatory Loop Drives Self-Renewal of Human Myeloid Leukemia Stem Cells and Leukemic Progression. *Cell Stem Cell* **17,** 341–352 (2015).
70. Sakuishi, K. *et al.* TIM3 $^{+}$ FOXP3 $^{+}$ regulatory T cells are tissue-specific promoters of T-cell dysfunction in cancer. *OncoImmunology* **2,** e23849 (2013).
71. Romero, D. Immunotherapy: PD-1 says goodbye, TIM-3 says hello. *Nat. Rev. Clin. Oncol.* **13,** 202–203 (2016).
72. Hughes, J. *et al.* Precipitation of autoimmune diabetes with anti-PD-1 immunotherapy. *Diabetes Care* **38,** e55-57 (2015).
73. A. Postow, M. & MD. Managing Immune Checkpoint-Blocking Antibody Side Effects. *J. Clin. Oncol.*
74. Singh, A. K. *et al.* Fatal GvHD induced by PD-1 inhibitor pembrolizumab in a patient with Hodgkin's lymphoma. *Bone Marrow Transplant.* **51,** 1268–1270 (2016).
75. Christian, M. *et al.* Targeting DNA Double-Strand Breaks with TAL Effector Nucleases. *Genetics* **186,** 757–761 (2010).
76. Jinek, M. *et al.* A Programmable Dual-RNA–Guided DNA Endonuclease in Adaptive Bacterial Immunity. *Science* **337,** 816–821 (2012).

77. Tsai, S. Q. & Joung, J. K. Defining and improving the genome-wide specificities of CRISPR-Cas9 nucleases. *Nat. Rev. Genet.* **17,** 300–312 (2016).
78. Carlson, D. F., Fahrenkrug, S. C. & Hackett, P. B. Targeting DNA With Fingers and TALENs. *Mol. Ther. — Nucleic Acids* **1,** e3 (2012).
79. Bibikova, M., Beumer, K., Trautman, J. K. & Carroll, D. Enhancing gene targeting with designed zinc finger nucleases. *Science* **300,** 764 (2003).
80. Mani, M., Kandavelou, K., Dy, F. J., Durai, S. & Chandrasegaran, S. Design, engineering, and characterization of zinc finger nucleases. *Biochem Biophys Res Commun* **335,** 447–57 (2005).
81. Boissel, S. *et al.* megaTALs: a rare-cleaving nuclease architecture for therapeutic genome engineering. *Nucleic Acids Res.* **42,** 2591–2601 (2014).
82. Stoddard, B. L. Homing Endonucleases: From Microbial Genetic Invaders to Reagents for Targeted DNA Modification. *Structure* **19,** 7–15 (2011).
83. Gaj, T., Gersbach, C. A. & Barbas, C. F. ZFN, TALEN, and CRISPR/Cas-based methods for genome engineering. *Trends Biotechnol.* **31,** 397–405 (2013).
84. Iyama, T. & Wilson, D. M. DNA repair mechanisms in dividing and non-dividing cells. *DNA Repair* **12,** 620–636 (2013).
85. Mansour, W. Y. *et al.* Hierarchy of nonhomologous end-joining, single-strand annealing and gene conversion at site-directed DNA double-strand breaks. *Nucleic Acids Res.* **36,** 4088–4098 (2008).
86. Kuhar, R. *et al.* Novel fluorescent genome editing reporters for monitoring DNA repair pathway utilization at endonuclease-induced breaks. *Nucleic Acids Res.* **42,** e4 (2014).
87. Shrivastav, M., De Haro, L. P. & Nickoloff, J. A. Regulation of DNA double-strand break repair pathway choice. *Cell Res.* **18,** 134–147 (2008).
88. Delacôte, F. *et al.* High Frequency Targeted Mutagenesis Using Engineered Endonucleases and DNA-End Processing Enzymes. *PLOS ONE* **8,** e53217 (2013).
89. Gwiazda, K. S. *et al.* High Efficiency CRISPR/Cas9-mediated Gene Editing in Primary Human T-cells Using Mutant Adenoviral E4orf6/E1b55k 'Helper' Proteins. *Mol. Ther. J. Am. Soc. Gene Ther.* **24,** 1570–1580 (2016).
90. Paquet, D. *et al.* Efficient introduction of specific homozygous and heterozygous mutations using CRISPR/Cas9. *Nature* **533,** 125–129 (2016).
91. Sather, B. D. *et al.* Efficient modification of CCR5 in primary human hematopoietic cells using a megaTAL nuclease and AAV donor template. *Sci. Transl. Med.* **7,** 307ra156-307ra156 (2015).
92. Bothmer, A. *et al.* Characterization of the interplay between DNA repair and CRISPR/Cas9-induced DNA lesions at an endogenous locus. *Nat. Commun.* **8,** 13905 (2017).
93. Morgan, R. A. & Kakarla, S. Genetic modification of T cells. *Cancer J. Sudbury Mass* **20,** 145–150 (2014).
94. Zhao, Y. *et al.* High-efficiency transfection of primary human and mouse T lymphocytes using RNA electroporation. *Mol. Ther. J. Am. Soc. Gene Ther.* **13,** 151–159 (2006).
95. Knudsen, M. L., Ljungberg, K., Liljeström, P. & Johansson, D. X. Intradermal electroporation of RNA. *Methods Mol. Biol. Clifton NJ* **1121,** 147–154 (2014).
96. Smits, E. *et al.* RNA-based gene transfer for adult stem cells and T cells. *Leukemia* **18,** 1898–1902 (2004).

97. Holtkamp, S. *et al.* Modification of antigen-encoding RNA increases stability, translational efficacy, and T-cell stimulatory capacity of dendritic cells. *Blood* **108,** 4009–4017 (2006).
98. Shindo, Y. *et al.* Adoptive immunotherapy with MUC1-mRNA transfected dendritic cells and cytotoxic lymphocytes plus gemcitabine for unresectable pancreatic cancer. *J. Transl. Med.* **12,** 175 (2014).
99. Benencia, F. Antigen-specific mRNA transfection of autologous dendritic cells. *Methods Mol. Biol. Clifton NJ* **1139,** 77–86 (2014).
100. Coosemans, A. *et al.* Immunological response after WT1 mRNA-loaded dendritic cell immunotherapy in ovarian carcinoma and carcinosarcoma. *Anticancer Res.* **33,** 3855–3859 (2013).
101. Benteyn, D., Van Nuffel, A. M. T., Wilgenhof, S. & Bonehill, A. Single-step antigen loading and maturation of dendritic cells through mRNA electroporation of a tumor-associated antigen and a TriMix of costimulatory molecules. *Methods Mol. Biol. Clifton NJ* **1139,** 3–15 (2014).
102. Pfeiffer, I. A. *et al.* Triggering of NF-κB in cytokine-matured human DCs generates superior DCs for T-cell priming in cancer immunotherapy. *Eur. J. Immunol.* **44,** 3413–3428 (2014).
103. Coosemans, A. *et al.* Wilms' Tumor Gene 1 (WT1)--loaded dendritic cell immunotherapy in patients with uterine tumors: a phase I/II clinical trial. *Anticancer Res.* **33,** 5495–5500 (2013).
104. Berdien, B., Mock, U., Atanackovic, D. & Fehse, B. TALEN-mediated editing of endogenous T-cell receptors facilitates efficient reprogramming of T lymphocytes by lentiviral gene transfer. *Gene Ther.* **21,** 539–548 (2014).
105. Holt, N. *et al.* Human hematopoietic stem/progenitor cells modified by zinc-finger nucleases targeted to CCR5 control HIV-1 in vivo. *Nat. Biotechnol.* **28,** 839–847 (2010).
106. Li, L. *et al.* Genomic editing of the HIV-1 coreceptor CCR5 in adult hematopoietic stem and progenitor cells using zinc finger nucleases. *Mol. Ther. J. Am. Soc. Gene Ther.* **21,** 1259–1269 (2013).
107. Sahin, U., Karikó, K. & Türeci, Ö. mRNA-based therapeutics--developing a new class of drugs. *Nat. Rev. Drug Discov.* **13,** 759–780 (2014).
108. Gallie, D. R. The cap and poly(A) tail function synergistically to regulate mRNA translational efficiency. *Genes Dev.* **5,** 2108–2116 (1991).
109. Munroe, D. & Jacobson, A. mRNA poly(A) tail, a 3' enhancer of translational initiation. *Mol. Cell. Biol.* **10,** 3441 (1990).
110. Kühn, U. & Wahle, E. Structure and function of poly(A) binding proteins. *Biochim. Biophys. Acta BBA - Gene Struct. Expr.* **1678,** 67–84 (2004).
111. Godiska, R. *et al.* Linear plasmid vector for cloning of repetitive or unstable sequences in Escherichia coli. *Nucleic Acids Res.* **38,** e88–e88 (2010).
112. Zheng, D. & Tian, B. Sizing up the poly(A) tail: insights from deep sequencing. *Trends Biochem. Sci.* **39,** 255–257 (2014).
113. Chang, H., Lim, J., Ha, M. & Kim, V. N. TAIL-seq: Genome-wide Determination of Poly(A) Tail Length and 3' End Modifications. *Mol. Cell* **53,** 1044–1052 (2014).
114. Subtelny, A. O., Eichhorn, S. W., Chen, G. R., Sive, H. & Bartel, D. P. Poly(A)-tail profiling reveals an embryonic switch in translational control. *Nature* **508,** 66–71 (2014).

115. Subach, O. M., Cranfill, P. J., Davidson, M. W. & Verkhusha, V. V. An enhanced monomeric blue fluorescent protein with the high chemical stability of the chromophore. *PloS One* **6,** e28674 (2011).
116. Kumar, N., Gammell, P., Meleady, P., Henry, M. & Clynes, M. Differential protein expression following low temperature culture of suspension CHO-K1 cells. *BMC Biotechnol.* **8,** 42 (2008).
117. Kumar, N., Gammell, P. & Clynes, M. Proliferation control strategies to improve productivity and survival during CHO based production culture : A summary of recent methods employed and the effects of proliferation control in product secreting CHO cell lines. *Cytotechnology* **53,** 33–46 (2007).
118. Kaufmann, H., Mazur, X., Marone, R., Bailey, J. E. & Fussenegger, M. Comparative analysis of two controlled proliferation strategies regarding product quality, influence on tetracycline-regulated gene expression, and productivity. *Biotechnol. Bioeng.* **72,** 592–602 (2001).
119. Kaufmann, H., Mazur, X., Fussenegger, M. & Bailey, J. E. Influence of low temperature on productivity, proteome and protein phosphorylation of CHO cells. *Biotechnol. Bioeng.* **63,** 573–582 (1999).
120. Grupp, S. A. *et al.* Chimeric Antigen Receptor–Modified T Cells for Acute Lymphoid Leukemia. *N. Engl. J. Med.* **368,** 1509–1518 (2013).
121. Kochenderfer, J. N. *et al.* B-cell depletion and remissions of malignancy along with cytokine-associated toxicity in a clinical trial of anti-CD19 chimeric-antigen-receptor-transduced T cells. *Blood* **119,** 2709–2720 (2012).
122. Kochenderfer, J. N. *et al.* Eradication of B-lineage cells and regression of lymphoma in a patient treated with autologous T cells genetically engineered to recognize CD19. *Blood* **116,** 4099–4102 (2010).
123. Brentjens, R. J. *et al.* CD19-targeted T cells rapidly induce molecular remissions in adults with chemotherapy-refractory acute lymphoblastic leukemia. *Sci. Transl. Med.* **5,** 177ra38 (2013).
124. Riddell, S. R., Jensen, M. C. & June, C. H. Chimeric Antigen Receptor–Modified T Cells: Clinical Translation in Stem Cell Transplantation and Beyond. *Biol. Blood Marrow Transplant.* **19,** S2–S5 (2013).
125. Provasi, E. *et al.* Editing T cell specificity towards leukemia by zinc finger nucleases and lentiviral gene transfer. *Nat. Med.* **18,** 807–815 (2012).
126. Certo, M. T. *et al.* Tracking genome engineering outcome at individual DNA breakpoints. *Nat. Methods* **8,** 671–676 (2011).
127. Doyon, Y. *et al.* Transient cold shock enhances zinc-finger nuclease–mediated gene disruption. *Nat. Methods* **7,** 459–460 (2010).
128. Valton, J. *et al.* Overcoming Transcription Activator-like Effector (TALE) DNA Binding Domain Sensitivity to Cytosine Methylation♦. *J. Biol. Chem.* **287,** 38427–38432 (2012).
129. Hsu, P. D. *et al.* DNA targeting specificity of RNA-guided Cas9 nucleases. *Nat. Biotechnol.* **31,** 827–832 (2013).
130. Ryan, M. D., King, A. M. & Thomas, G. P. Cleavage of foot-and-mouth disease virus polyprotein is mediated by residues located within a 19 amino acid sequence. *J. Gen. Virol.* **72 ( Pt 11),** 2727–2732 (1991).

131. Kim, J. H. *et al.* High Cleavage Efficiency of a 2A Peptide Derived from Porcine Teschovirus-1 in Human Cell Lines, Zebrafish and Mice. *PLoS ONE* **6,** e18556 (2011).
132. Sather, B.D. *et al.* Efficient modification of CCR5 in primary human hematopoietic cells using a megaTAL nuclease and AAV donor template. *Sci. Transl. Med.* **7,** 1–12 (2015).
133. Lisowski, L., Tay, S. S. & Alexander, I. E. Adeno-associated virus serotypes for gene therapeutics. *Curr. Opin. Pharmacol.* **24,** 59–67 (2015).
134. Kotterman, M. A. & Schaffer, D. V. Engineering adeno-associated viruses for clinical gene therapy. *Nat. Rev. Genet.* **15,** 445–451 (2014).
135. Zinn, E. & Vandenberghe, L. H. Adeno-associated virus: fit to serve. *Curr. Opin. Virol.* **8,** 90–97 (2014).
136. Baker, A., Rohleder, K. J., Hanakahi, L. A. & Ketner, G. Adenovirus E4 34k and E1b 55k oncoproteins target host DNA ligase IV for proteasomal degradation. *J. Virol.* **81,** 7034–7040 (2007).
137. Boyer, J., Rohleder, K. & Ketner, G. Adenovirus E4 34k and E4 11k inhibit double strand break repair and are physically associated with the cellular DNA-dependent protein kinase. *Virology* **263,** 307–312 (1999).
138. Stracker, T. H., Carson, C. T. & Weitzman, M. D. Adenovirus oncoproteins inactivate the Mre11-Rad50-NBS1 DNA repair complex. *Nature* **418,** 348–352 (2002).
139. Lentz, T. B. & Samulski, R. J. Insight into the mechanism of inhibition of adeno-associated virus by the Mre11/Rad50/Nbs1 complex. *J. Virol.* **89,** 181–194 (2015).
140. Sanlioglu, S., Duan, D. & Engelhardt, J. F. Two independent molecular pathways for recombinant adeno-associated virus genome conversion occur after UV-C and E4orf6 augmentation of transduction. *Hum. Gene Ther.* **10,** 591–602 (1999).
141. Stracker, T. H., Carson, C. T. & Weitzman, M. D. Adenovirus oncoproteins inactivate the Mre11-Rad50-NBS1 DNA repair complex. *Nature* **418,** 348–352 (2002).
142. Schwartz, R. A. *et al.* The Mre11/Rad50/Nbs1 Complex Limits Adeno-Associated Virus Transduction and Replication. *J. Virol.* **81,** 12936–12945 (2007).
143. Schwartz, R. A. *et al.* Distinct requirements of adenovirus E1b55K protein for degradation of cellular substrates. *J. Virol.* **82,** 9043–9055 (2008).
144. Poirot, L. *et al.* Multiplex genome edited T-cell manufacturing platform for 'off-the-shelf' adoptive T-cell immunotherapies. *Cancer Res.* (2015). doi:10.1158/0008-5472.CAN-14-3321
145. Khan, I. F., Hirata, R. K. & Russell, D. W. AAV-mediated gene targeting methods for human cells. *Nat. Protoc.* **6,** 482–501 (2011).
146. Aurnhammer, C. *et al.* Universal real-time PCR for the detection and quantification of adeno-associated virus serotype 2-derived inverted terminal repeat sequences. *Hum. Gene Ther. Methods* **23,** 18–28 (2012).
147. Doyon, Y. *et al.* Transient cold shock enhances zinc-finger nuclease-mediated gene disruption. *Nat. Methods* **7,** 459–460 (2010).
148. Torikai, H. *et al.* A foundation for universal T-cell based immunotherapy: T cells engineered to express a CD19-specific chimeric-antigen-receptor and eliminate expression of endogenous TCR. *Blood* **119,** 5697–5705 (2012).
149. Appay, V. *et al.* Characterization of CD4+ CTLs Ex Vivo. *J. Immunol.* **168,** 5954–5958 (2002).

150. Takeuchi, A. & Saito, T. CD4 CTL, a Cytotoxic Subset of CD4+ T Cells, Their Differentiation and Function. *Front. Immunol.* **8,** (2017).
151. Wang, X. *et al.* A transgene-encoded cell surface polypeptide for selection, in vivo tracking, and ablation of engineered cells. *Blood* **118,** 1255–1263 (2011).
152. Postow, L. & Funabiki, H. An SCF complex containing Fbxl12 mediates DNA damage-induced Ku80 ubiquitylation. *Cell Cycle* **12,** 587–595 (2013).
153. Qasim, W. *et al.* Molecular remission of infant B-ALL after infusion of universal TALEN gene-edited CAR T cells. *Sci. Transl. Med.* **9,** eaaj2013 (2017).
154. Eyquem, J. *et al.* Targeting a CAR to the TRAC locus with CRISPR/Cas9 enhances tumour rejection. *Nature* **543,** 113–117 (2017).
155. Paganin, M. *et al.* Minimal residual disease is an important predictive factor of outcome in children with relapsed 'high-risk' acute lymphoblastic leukemia. *Leukemia* **22,** 2193–2200 (2008).
156. Hong, H. *et al.* Diverse Solid Tumors Expressing a Restricted Epitope of L1-cam Can Be Targeted by Chimeric Antigen Receptor Redirected T Lymphocytes. *J. Immunother.* **37,** 93–104 (2014).